MASTER

Study of a diffusion flamelet model

a first step in the development of a reduction technique based on a non-premixed flamelet model

Delhaye, S.

Award date:
2004

Study of a diffusion flamelet model

A first step in the development of a reduction technique based on a non-premixed flamelet model

Stanley Delhaye

July 5, 2004

Contents

Abstract

This report is part of a research of which the main goal is to reduce the necessary computation time to simulate combustion processes, but without losing too much accuracy. Besides the detailed numerical simulations, there are traditionally two different methods to model flames. The first are the chemical reduction techniques, which are based on the observation that during combustion most of the time-scales corresponding to chemistry, are often much smaller than time-scales associated with transport phenomena. The second are the flamelet models, which describe the internal flame structure, and which are based on the assumption that in a flame, gradients in the direction perpendicular to the flame are much larger than gradients along flame. This means that a multi-dimensional flame can be accurately described by a set of quasi one-dimensional flame structures.

Both the aforementioned methods can be used to construct a database in a pre-processing step, in which the mixture composition is stored as a function of so-called controlling variables. The number of controlling variables is one of the factors that limit the accuracy when a database is used to retrieve the flame structure. As said before, the reduced mechanism is constructed by assuming steady-state conditions for a portion of the species. This is where reduction techniques essentially differ from the flamelet approach.

Therefore, the Combustion Technology Group at the Eindhoven University of Technology has been investigating ways to 'bridge the gap' between reduction techniques and flamelet models. Until now, this research has been concentrated on (partially) premixed systems, which resulted in the Flamelet Generated Manifolds (FGM) method and the Phase-Space Intrinsic Low-Dimensional Manifolds (PS-ILDM) method. It is desirable to develop such a hybrid method for non-premixed flames as well.

The ultimate challenge is to develop a reduction technique that is based on a universal flamelet model, which describes both premixed and non-premixed flames with the same set of equations. When this has been achieved, it may be possible to apply an automated time-scale analysis to this flamelet model, analogous to the PS-ILDM method.

Before this can be done, however, an existing non-premixed flamelet model, and the assumptions that have been made, will have to be studied, which has been done in this graduation thesis. Therefore, the goal of this thesis was to gain insight in a non-premixed flamelet model and to estimate the effect of the assumptions that were made in the derivation of this flamelet model.

In this thesis, an existing, standard non-premixed flamelet method [14] has been discussed in more detail. This non-premixed flamelet method is based on the assumption that there are no preferential diffusion effects, i.e. $Le_i = 1$. To investigate the effects of this assumption, the derivation without assuming that there is no preferential diffusion was done. First, a coordinate transformation was applied to the conservation equation for species, which leads to a description of conservation equation for species in mixture fraction space. Using the

assumption that perturbations in the directions along the flame surface are small, led to a 1D flamelet model describing species conservation in mixture fraction space. Using a 1D solver, a numerical analysis was carried out, where it was shown that these effects cannot be neglected for non-premixed flames, when using more realistic Lewis numbers. The preferential diffusion terms were scaled with the maximum value of the chemical source terms, and it was observed that this ratio was up to 10% for several species when a strain rate of $a = 100\ s^{-1}$ was chosen. For a strain rate of 400 s^{-1}, this ratio was even larger, i.e. 20% for CH_3O and 21.5% for CO_2.

The diffusion flamelet method can also be used to construct a flamelet database, where commonly the flame structure is stored as a function of the mixture fraction Z and the stoichiometric value of the scalar dissipation rate χ_{st}. An analytical model is needed that relates the stoichiometric value of the scalar dissipation rate to the local value of the scalar dissipation rate that is found during the simulation of a combustion process. It seems that the accuracy of the analytical model for the scalar dissipation rate influences the results when the flame structure is retrieved from the database. It was shown that the assumption,which was made during the derivation of the analytical model, that the density is constant, results in errors when predicting the stoichiometric value of the scalar dissipation rate.

Samenvatting

Dit afstudeerverslag is een deel van een onderzoek waarvan het doel is om de rekentijd, die nodig is om verbrandingsprocessen te beschrijven, terug te brengen, zonder dat de nauwkeurigheid daar te veel onder leidt. Naast de gedetailleerde numerieke simulaties, zijn er twee andere veel gebruikte methodes, die beide de rekentijd drastisch verlagen. Allereerst zijn er de zogenaamde chemische reductie technieken. Deze zijn gebaseerd op de observatie dat bij verbrandingsprocessen het merendeel van de chemische tijd-schalen veel kleiner is dan de tijd-schalen die horen bij transport verschijnselen. Daarnaast zijn er de zogeheten flamelet modellen, die de interne structuur van een vlam beschrijven en waarbij wordt aangenomen dat in een vlam, gradiënten loodrecht op de vlam veel groter zijn dan gradiënten in de richting langs de vlam. Met andere woorden, een multi-dimensionale vlam kan nauwkeurig beschreven worden met een set van quasi-1D vlam structuren.

Beide bovengenoemde methodes kunnen gebruikt worden om, in een pre-processing stap, een database aan te maken waarin de compositie van het mengsel is opgeslagen als functie van zogeheten controle-variabelen. Het aantal controle-variabelen bepaalt ondermeer de maximale nauwkeurigheid die haalbaar is wanneer een database gebruikt wordt. Een gereduceerd mechanisme wordt gevonden door aan te nemen dat het merendeel van de chemische componenten zich in steady-state bevindt. Dat wil zeggen dat de chemische bronterm van deze chemische componenten 0 is.

Daarom wordt op de Technische Universiteit Eindhoven door de Combustion Technology Group onderzoek verricht naar manieren om de chemische reductie technieken en de flamelet modellen dichter naar elkaar te brengen. Tot nog toe is het onderzoek gericht geweest op (deels) voorgemengde systemen. Dit heeft geleid tot de Flamelet Generated Manifolds (FGM) methode en de Phase-Space Intrinsic Low-Dimensional Manifolds (PS-ILDM) methode. Het is dan ook gewenst om een soortgelijke methode te ontwikkelen voor niet-voorgemengde systemen.

De ultieme uitdaging is om een reductie methode te ontwikkelen die gebaseerd is op een universeel flamelet model. Hiermee wordt bedoeld een flamelet model dat zowel voorgemengde als niet-voorgemengde vlammen kan beschrijven. Wanneer dit is bereikt, is het wellicht mogelijk om een geautomatiseerde tijd-schaal analyse toe te passen op dit universeel flamelet model, analoog aan de PS-ILDM methode.

Voordat het echter zover is, zal een bestaande, veelgebruikte niet-voorgemengd flamelet model en de aannames die in de afleiding van dit model gemaakt zijn, moeten worden onderzocht. Dat is in dit afstudeerverslag gedaan. Het doel van dit verslag is dan ook om inzicht te krijgen in een niet-voorgemengd flamelet model en om een afschatting te maken van de invloed van aannames die gedaan zijn tijdens de afleiding van dit model.

Daarom zal in dit verslag een bestaande, veelgebruikte niet-voorgemengd flamelet methode [14] in meer detail worden bestudeerd. Dit niet-voorgemengd flamelet model is gebaseerd op

de aanname dat er geen preferentiële diffusie is, m.a.w. $Le_i = 1$. Om de invloed van deze aanname te toetsen, is de afleiding van dit flamelet model herhaald, maar nu zonder de aanname dat er geen preferentiële diffusie is. Allereerst is er een coördinaten transformatie toegepast om de behoudsvergelijking voor chemische componenten in termen van de mengsel fractie Z te schijven. Wanneer wordt aangenomen dat gradiënten in de richting langs het vlam oppervlak mogen worden verwaarloosd, leidt dit tot een 1D beschrijving van het flamelet model in de mengsel fractie ruimte. Een numerieke analyse is uitgevoerd met behulp van een 1D rekenprogramma. Hierbij is aangetoond dat effecten die worden veroorzaakt door preferentiële diffusie niet altijd kunnen worden verwaarloosd wanneer Lewis getallen worden gekozen die realistischer zijn dan $Le_i = 1$. De preferentiële diffusie termen zijn geschaald met de maximum waarde van de chemische bron term en het blijkt dat voor sommige chemische componenten deze verhouding meer dan 10% was. De 'strain rate' die hierbij hoort is $a = 100\ s^{-1}$. Voor een 'strain rate' van $400\ s^{-1}$, was deze verhouding voor sommige componenten nog groter, nl. 20% voor CH_3O en 21.5% voor CO_2.

De niet-voorgemengde flamelet methode kan ook worden gebruikt om een flamelet database te construeren. Het is dan gebruikelijk om de vlam structuur op te slaan als functie van de mengel fractie Z en de stoichiometrische waarde van de scalaire dissipatie snelheid χ_{st}. Hierbij is een analytisch model nodig om de lokale waarde van de scalaire dissipatie snelheid, die uit de vlam simulatie volgt, te relateren aan de stoichiometrische waarde van de scalaire dissipatie snelheid. Het lijkt erop dat de nauwkeurigheid van het gebruikte analytisch model voor de scalaire dissipatie snelheid invloed heeft op de resultaten wanneer de compositie van het mengsel wordt opgezocht in de flamelet database. Het blijkt dat de aanname bij de afleiding van het analytisch model, dat de dichtheid constant is, resulteert in afwijkingen bij de voorspelling van de stoichiometrische waarde van de scalaire dissipatie snelheid.

Chapter 1

Introduction

1.1 General introduction

In recent years, it has become increasingly important to accurately model combustion systems. The reason behind this is twofold: to use the models to improve the efficiency of burner systems and to reduce the amount of pollutants that are produced during a combustion process.

The accuracy of the calculations is mainly determined by the chosen chemical model. Unfortunately, not only the number of equations can be very large, but they are also strongly coupled. The wide range of time-scales implies that the set of equations is stiff. These facts amount to large computation times, which is undesirable. Generally, there are two approaches that lead to a considerable decrease in calculation times: chemical reduction techniques and flamelet models.

Reduction techniques reduce the number of equations that has to be solved during flame calculations, but without losing too much accuracy. These reduction techniques are based on fact that most of the chemical processes are much faster than transport phenomena, i.e. most of the chemical time-scale are much smaller than the physical time-scales. This leads to steady-state assumptions for species corresponding with the fast chemical time-scales.

Flamelet models are based on the assumption that changes along the flame are much smaller than changes perpendicular to the flame, which results in a quasi one-dimensional description of the flame structure. Reduction techniques on the other hand, are generally based purely on chemistry, which makes them applicable to both premixed and non-premixed flames. However, as transport processes are not included during the construction of the reduced mechanism, they can be inaccurate in regions where transport phenomena become more important, i.e. the colder regions in the flame. To solve this problem, new approaches were developed at the Eindhoven University of Technology, the Flamelet Generated Manifolds (FGM) method and the Phase-Space Intrinsic Low-Dimensional Manifolds (PS-ILDM) method. Both these methods, amongst others, will be discussed in more detail later on.

Because the FGM and PS-ILDM methods were developed for (partially) premixed flames, it remains to be seen if they are applicable to non-premixed combustion. The ultimate goal of this research is to develop a reduction technique that is based on universal flame equations, applicable to both premixed and non-premixed flames. In the long run it may be possible to develop a reduction method based on a *unifying flamelet theory*. The idea behind this is that the equations that describe premixed flamelets [6] may also be used to describe non-premixed

flamelets. This could be used as a starting point to develop a reduction method based on a truly unifying flamelet theory. However, this method still has to be developed and tested, which goes beyond the scope of this report.

In this report, the standard, often used flamelet model, introduced by Peters [14], is studied in detail. The main focus of this study is to investigate which assumptions are made and what the effects of these assumptions are on the accuracy of this flamelet model.

This chapter starts with a historical background on combustion in section 1.1.1, followed by an introduction to combustion in general in section 1.1.2. Then, in section 1.2 the equations that will be used throughout this report will be presented. An overview of this thesis and a description of the main goals of this thesis are given in section 1.3.

1.1.1 Historical background

Even today combustion is still essential to humankind, as it was in the past and as it will be in the foreseeable future. It still is the major energy-release process, as nearly 80 percent of the world primary energy is generated through combustion. Unfortunately combustion generates pollutants, which have several unwanted effects on the environment. Furthermore, the resources of fossil fuels are not unlimited and it is obvious that they have to be used as efficiently as possible. Even when renewable energy sources are considered, fossil fuels will remain an important energy source for the next 100 years [1]. Besides that, combustion of biomass is also an example of a renewable energy source. With this in mind, it is clear that studying combustion is very relevant.

Since early history man has used fire as a source for heat and light. The nature of combustion was not always clearly understood. For instance, the ancient Greeks believed fire to be a basic element of the universe and in 1697 the German physician and chemist Georg Ernst Stahl proposed the existence of phlogiston, derived from the Latin word phlegma, which means fire spirit. The idea of phlogiston was discarded by Lavoisier [7]. Although it was clear that combustion required a fuel and an igniter. It was not until the 17^{th} century that it was learnt that air was also needed. In 1663 Boyle discovered that, under vacuum, sulphur could not be ignited by concentrated light, but the first to realise that oxygen was the key was Lavoisier, which was in 1777.

Since then combustion science has advanced a lot. Deeper understanding in fundamental aspects of combustion has been gained, with numerous ways to accurately model combustion processes as a result. With the introduction of modern computers, it became possible to perform detailed studies of combustion phenomena. However, due to the complexity of the models, simulation times can become very large and are still restricted to simple configurations.

1.1.2 Introduction to combustion

Combustion can be described as a self-sustaining oxidative chemical reaction characterised by a thermal runaway, i.e. it is a quick exothermal oxidation producing light, heat, smoke and gases near the so-called flame front.

Chemistry is very important for combustion, as it not only determines at what rate the fuel and oxidiser are consumed but it also indicates which reactions and chemical components are important to the reaction progress. Furthermore, the reaction rates determine which combustion products are formed and at which rate. The global reaction mechanism for combustion is

Fuel + Oxidiser → Products.

In reality these products are not formed in just one step, but there are a lot of elementary reactions, describing the conversion of fuel and oxidiser into intermediates and finally into products. In order to accurately describe a combustion process, these elementary reactions have to be included as well.

1.1.3 Premixed and non-premixed combustion

Depending on the initial state of the mixing of fuel and oxidiser, a combustion process can be identified as (partially) premixed or non-premixed. In premixed combustion, the unburnt gas is already a mixture of fuel and air, and the rate of reaction is only limited by the chemical kinetics of the reactions involved and heat diffusion towards the unburnt mixture. Figure 1.1 (left) shows an example of a premixed flame geometry. The unburnt mixture is at the left side of a tube, while the burnt gasses are at the other side. The unburnt mixture is separated from the burnt gasses by the flame front, which moves from right to left through the tube, consuming the unburnt mixture. The velocity of the flame front is the so-called burning velocity, denoted by S_L. Due to the rise in temperature, the burnt gasses expand, causing an outflow of burnt gasses.

In non-premixed combustion there is no characteristic burning velocity, and diffusion of fuel towards the oxidiser and vice versa, is the limiting process. The mass burning rate is fixed by the rate at which fuel and oxidiser approach the flame by diffusion from each side. An example of the non-premixed geometry is a counterflow diffusion flame, which can be seen in figure 1.1 (right). This configuration will be considered throughout this report. The fuel and the oxidiser flow in opposite directions and the two flows are separated by a stagnation surface. This causes the flows to diverge outward in y-direction. On the stagnation surface the overall velocity in x-direction is equal to zero. Individual molecules can diffuse beyond the stagnation plane to keep the chemical reaction going.

In figure 1.2 (l) the structure of a premixed flame can be seen. Note that only a few species are shown. The unburnt mixture containing both fuel and oxidiser, is present in a large amount at the left side of the flame, and is consumed at the flame front. The combustion products, consisting of CO_2 and H_2O amongst others, are produced at the flame front. The intermediate species are produced and consumed almost immediately at the flame front. In this figure one of the intermediates, OH, is shown. Because the mass fraction for OH is very small, it is scaled with $0.25 \times Y_{\mathrm{OH,max}}$ for convenience. The temperature T rises from its minimum value at the unburnt side of the flame to its maximum value at the burnt side.

Figure 1.2 (r) shows the structure of a non-premixed flame in a counterflow geometry. Combustion can only take place when mixing on a molecular scale is accomplished which is the result of diffusion. As can be seen, both the fuel and the oxidiser are consumed at the flame front, while products like CO_2 and H_2O are produced there. The intermediate species, of which OH is one, are produced and consumed at the flame front. Here, the mass fraction for OH is again scaled with $0.25 \times Y_{\mathrm{OH,max}}$. The temperature T has its maximum value at the flame front, and decreases to both the fuel side and the oxidiser side.

In both figures 1.2, (l) and (r), the species mass fractions are shown as a function of the spatial position x. With non-premixed combustion however another coordinate is often used, i.e. the mixture fraction Z, which is a measure for the mixing of the gas-streams. One of the benefits of using the mixture fraction is that it is not influenced by chemistry.

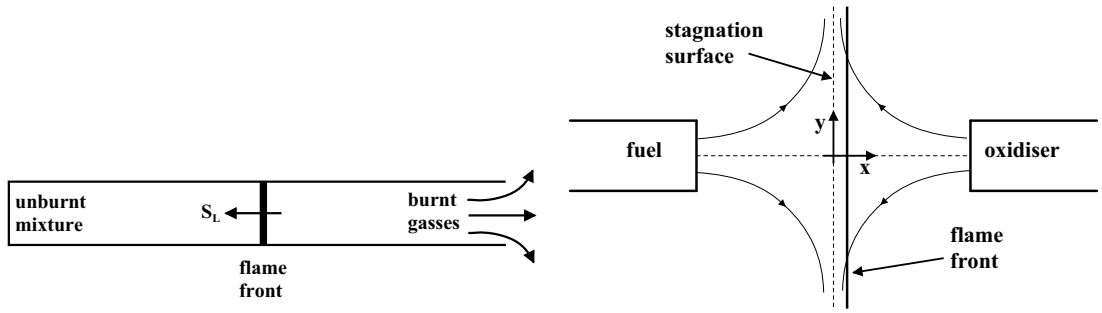

Fig. 1.1: Schematic representation of a premixed flame in a tube (left) and a counterflow diffusion flame (right).

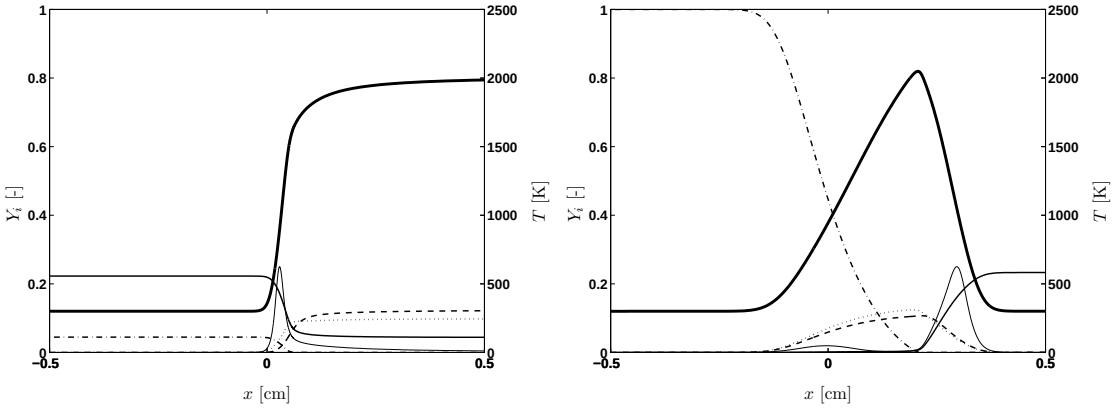

Fig. 1.2: The internal structure of a premixed flame (l) and a non-premixed flame (r). Shown are the mass fractions Y_i and the scaled temperature $\tilde{T}$. Solid: Y_{O_2}; dash-dot: Y_{CH_4}; dotted: Y_{H_2O}; dashed: Y_{CO_2}; thin solid: Y_{OH}, scaled with $10 \times Y_{OH,max}$ (l) and $2.5 \times Y_{OH,max}$ (r) for visualisation purposes; thick solid: temperature scaled with the maximum value of the temperature.

The mixture fraction Z is defined in such a way that $Z = 1$ at the fuel side and $Z = 0$ at the oxidiser side of the flame. Furthermore, it is continuously increasing, which allows the mixture fraction to be used as a coordinate describing the reaction progress in a non-premixed flame. Another quantity that is closely related to the mixture fraction is the so-called scalar dissipation rate χ, which is the inverse of a characteristic diffusion time scale. More details about Z and χ can be found in chapters 3 and 4. The scalar dissipation rate is often used in combination with the mixture fraction to characterise diffusion flames.

1.2 Governing equations

Flames can be described as thin reactive-diffusive layers embedded within an otherwise non-reacting flow field. Mathematical models based on this view are the so-called flamelet models [19]. The flow field is described by the conservation equations from fluid dynamics, i.e. conservation of mass, momentum and energy or enthalpy [11]. In addition, conservation equations for the chemical components are needed to describe the chemical behaviour of the flame. These conservation equations are presented in section 1.2.1. The conservation equations are complemented by two state equations, of which the first is the caloric equation

of state and the latter the thermal equation of state. This is done in section 1.2.2. Various other variables, such as the stress tensor, the heat flux, and the diffusion velocities require transport models. Additionally, chemical models are needed to calculate the chemical source terms. These transport and chemical models are presented in section 1.2.3.

1.2.1 Conservation laws

In a chemically reacting flow, a mass balance equation for every species has to be solved

$$\frac{\partial(\rho_i)}{\partial t} + \nabla \cdot (\rho_i \mathbf{u}_i) = \dot{\omega}_i \qquad \text{for} \qquad i = 1, \ldots, N_s, \tag{1.1}$$

with ρ_i the mass density of species i and $\mathbf{u}_i$ the particular velocity of species i. The species source term $\dot{\omega}_i$ describes the rate of change of the mass of species i due to chemical reactions. The particular velocity of species i is determined by a combination of the average flow velocity $\mathbf{u}$ and the diffusion velocity $\mathbf{V}_i$ and can be written as $\mathbf{u}_i = \mathbf{u} + \mathbf{V}_i$. The species mass fraction is defined as

$$Y_i = \rho_i / \rho \qquad \text{for} \qquad i = 1, \ldots, N_s. \tag{1.2}$$

For the species mass density the following is true

$$\sum_{i=1}^{N_s} \rho_i = \rho, \tag{1.3}$$

which means that $\sum_{i=1}^{N_s} Y_i = 1$. When the definition of $\mathbf{u}_i$ is substituted in equation (1.1), and by using the definition of the mass fraction of each species (1.2), equation (1.1) can be written as

$$\frac{\partial(\rho Y_i)}{\partial t} + \nabla \cdot (\rho \mathbf{u} Y_i) + \nabla \cdot (\rho \mathbf{V}_i Y_i) = \dot{\omega}_i \qquad \text{for} \qquad i = 1, \ldots, N_s. \tag{1.4}$$

In section 1.2.3 an approach to model the diffusion velocity $\mathbf{V}_i$ will be introduced. Taking the summation of equation (1.1) over all species, results in

$$\sum_{i=1}^{N_s} \frac{\partial(\rho_i)}{\partial t} + \sum_{i=1}^{N_s} \nabla \cdot (\rho_i \mathbf{u}_i) = \sum_{i=1}^{N_s} \dot{\omega}_i. \tag{1.5}$$

Considering that $\sum_{i=1}^{N_s} \rho_i \mathbf{u}_i = \rho \mathbf{u}$, which defines the average mixture velocity, and where ρ_i is defined by (1.3), leads to the conservation equation of mass for the mixture

$$\frac{\partial \rho}{\partial t} + \nabla \cdot (\rho \mathbf{u}) = 0, \tag{1.6}$$

with ρ the mass density and $\mathbf{u} = (u,\ v,\ w)^T$. Note that this equation does not contain a source term $\dot{\omega}_i$, contrary to the conservation equation of species (1.4).

Conservation of momentum is described by the Navier-Stokes equations

$$\frac{\partial(\rho \mathbf{u})}{\partial t} + \nabla \cdot (\rho \mathbf{u}\mathbf{u}) = \rho \mathbf{g} - \nabla \cdot \boldsymbol{\mathcal{P}}. \tag{1.7}$$

Here, $\mathbf{g}$ is the gravitational acceleration and $\boldsymbol{\mathcal{P}}$ is the stress tensor, which is defined as $\boldsymbol{\mathcal{P}} = p\boldsymbol{\mathcal{I}} - \boldsymbol{\tau}$. Here, p is the hydrostatic pressure, $\boldsymbol{\tau}$ is the viscous stress tensor, and $\boldsymbol{\mathcal{I}}$ the unit tensor.

The transport equation for the conservation of enthalpy is

$$\frac{\partial(\rho h)}{\partial t} + \nabla \cdot (\rho \mathbf{u} h) = \rho \mathbf{u} \cdot \mathbf{g} - \nabla \cdot \mathbf{q} + \boldsymbol{\tau} : (\nabla \mathbf{u}) + \frac{dp}{dt}, \tag{1.8}$$

where h is the enthalpy density and $\mathbf{q}$ is the heat flux, which is a field quantity. The last term on the r.h.s. is the material derivative for the pressure.

1.2.2 State equations

With the use of two state equations the pressure and enthalpy can be written as functions of the density, the temperature and the species mass fractions. For the enthalpy the caloric equation of state will be used and for the pressure this is the thermal equation of state.

In most common combustion problems the gas mixture and its components are considered to behave as perfect gasses. The thermal equation of state is then given by the ideal gas law, which is a relation between the pressure, the density, the temperature and the species mass fractions. The ideal gas law for the pressure for each species p_i is given by

$$p_i = n_i RT = nX_i RT \qquad \text{for} \qquad i = 1, \ldots, N_s, \tag{1.9}$$

where R is the universal gas constant and $X_i = n_i/n$ the species mole fraction, with n_i the molar concentration of species i and n the total gas mixture. The species mole fraction is related to the species mass fraction as follows

$$X_i = Y_i \frac{\bar{M}}{M_i} \qquad \text{for} \qquad i = 1, \ldots, N_s, \tag{1.10}$$

with M_i the molar mass of species i and $\bar{M}$ the mean molar mass. When $\rho = n\bar{M}$ is used in combination with (1.10), equation (1.9) becomes

$$p_i = \rho RT \frac{Y_i}{M_i} \qquad \text{for} \qquad i = 1, \ldots, N_s. \tag{1.11}$$

The sum of all the partial pressures p_i is equal to the hydrostatic pressure according to

$$p = \sum_{i=1}^{N_s} p_i = \rho RT \sum_{i=1}^{N_s} \frac{Y_i}{M_i}. \tag{1.12}$$

The enthalpy density is related to the temperature T and the species mass fractions Y_i by the caloric equation of state as follows

$$h = \sum_{i=1}^{N_s} Y_i h_i, \tag{1.13}$$

where h_i is the enthalpy density of species i. The enthalpy density h_i is related to the formation enthalpy at the reference temperature T^*

$$h_i = h_i^* + \int_{T^*}^{T} c_{p_i}(T)\, dT \qquad \text{for} \qquad i = 1, \ldots, N_s, \tag{1.14}$$

with h_i^* the species enthalpy density of formation at the reference temperature T^* and c_{p_i} the specific heat of species i at constant pressure, which is well tabulated in polynomial form [10].

1.2.3 Transport and chemistry models

In this section the transport models for the diffusion velocity, the viscous stress tensor and the heat-flux are presented. Furthermore a model is given in order to calculate the chemical source terms.

Transport models

The diffusion velocity field $\mathbf{V}_i$ can be solved by using the so-called Stefan-Maxwell equations [23]. When neglecting contributions caused by pressure and temperature gradients, the equations that have to be solved, are

$$\nabla X_i = \sum_{k=1}^{N_s} \frac{X_i X_k}{\mathcal{D}_{ik}} \left(\mathbf{V}_k - \mathbf{V}_i\right) \qquad \text{for} \qquad i = 1, \ldots, N_s, \tag{1.15}$$

with $\mathcal{D}_{ik}$ the binary mass diffusion coefficient of species i into species k. Because the computational costs to solve equation (1.15) are very high, a model that is less complex will be used. This model is based on Fick's law and it is commonly used to model the diffusion velocities [13]. The diffusion velocities are defined as

$$\mathbf{V}_i = -\frac{D_{im}}{Y_i} \nabla Y_i \qquad \text{for} \qquad i = 1, \ldots, N_s - 1, \tag{1.16}$$

where D_{im} is the diffusion coefficient of species i into the mixture m, which can be related to the overall diffusion coefficient D as follows, $D = D_{im} Le_i$. The Lewis number, which is the ratio of thermal conduction and species mass diffusion, is defined as

$$Le_i = \frac{\lambda}{\rho D_{im} c_p} \qquad \text{for} \qquad i = 1, \ldots, N_s - 1, \tag{1.17}$$

where c_p is the specific heat at constant pressure and λ the heat conductivity. Equation (1.16) assumes that there is an abundant species. For premixed methane-air flames, this is nitrogen. With non-premixed flames, however, nitrogen is only abundant at the oxidiser side. However, for the counterflow configuration that is used in this thesis, the flame is situated at the oxidiser side of the flame, see figure 1.1, meaning that this will not have a large effect on processes that occur near the flame. Using (1.17), equation (1.16) becomes

$$\mathbf{V}_i = -\frac{D}{Le_i Y_i} \nabla Y_i \qquad \text{for} \qquad i = 1, \ldots, N_s - 1, \tag{1.18}$$

where it has been assumed that the Lewis number is constant. Equation (1.18) is the diffusion model that will be used throughout the remainder of this report. Using this definition, equation (1.4) becomes

$$\frac{\partial \left(\rho Y_i\right)}{\partial t} + \nabla \cdot \left(\rho \mathbf{u} Y_i\right) - \frac{1}{Le_i} \nabla \cdot \left(\rho D \nabla Y_i\right) = \dot{\omega}_i \qquad \text{for} \qquad i = 1, \ldots, N_s - 1. \tag{1.19}$$

The transport model for the heat flux $\mathbf{q}$, is given by [23]

$$\mathbf{q} = -\lambda \nabla T + \sum_{k=1}^{N_s} \rho V_k Y_k h_k, \tag{1.20}$$

The first term of (1.20) represents heat transport through conduction and the second term represents heat transport through mass diffusion. It can be shown [20] that equation (1.20) can also be written as

$$\mathbf{q} = -\rho D \nabla h - \rho D \sum_{k=1}^{N_s} \left(\frac{1}{Le_k} - 1 \right) h_k \nabla Y_k. \tag{1.21}$$

When it is assumed that the gas mixture behaves as a Newtonian fluid, the viscous stress tensor $\boldsymbol{\tau}$ can be modeled with Stokes' law of friction, cf. [23]

$$\boldsymbol{\tau} = \mu \left(\nabla \mathbf{v} + (\nabla \mathbf{v})^T - \frac{2}{3} (\nabla \cdot \mathbf{v}) \boldsymbol{\mathcal{I}} \right), \tag{1.22}$$

where μ is the dynamic viscosity of the mixture, which is related to the kinematic viscosity ν as $\mu = \rho\nu$. Using equation (1.21), the conservation equation for the enthalpy (1.8) becomes

$$\frac{\partial (\rho h)}{\partial t} + \nabla \cdot (\rho \mathbf{u} h) - \nabla \cdot (\rho D \nabla h) = \sum_{k=1}^{N_s} \left(\frac{1}{Le_k} - 1 \right) \nabla \cdot (\rho D h_k \nabla Y_k), \tag{1.23}$$

where it has been assumed that effects caused by gravity, viscous stress and pressure can be neglected.

Chemistry model

For combustion of a methane-air flame, the global reaction can be written as

$$\mathrm{CH_4} + 2\mathrm{O_2} \rightarrow \mathrm{CO_2} + 2\mathrm{H_2O}.$$

On a molecular level, many elementary reactions take place. The general form that describes these reactions is given by

$$\sum_{i=1}^{N_s} {\nu_{ij}}' \frac{\rho Y_i}{M_i} \rightleftharpoons \sum_{i=1}^{N_s} {\nu_{ij}}'' \frac{\rho Y_i}{M_i} \qquad \text{for} \qquad j = 1, \ldots, N_r, \tag{1.24}$$

where ${\nu_{ij}}'$ and ${\nu_{ij}}''$ are the molar stoichiometric coefficients of species i in reaction j, and N_r is the number of reactions. The chemical source term for species i $\dot{\omega}_i$ contains the contribution of all chemical reactions and is given by

$$\dot{\omega}_i = M_i \sum_{j=1}^{N_r} \left({\nu_{ij}}'' - {\nu_{ij}}' \right) r_j \qquad \text{for} \qquad i = 1, \ldots, N_s, \tag{1.25}$$

where the reaction rate r_j, is defined as

$$r_j = k_j^f \prod_{i=1}^{N_s} \left(\frac{\rho Y_i}{M_i} \right)^{{\nu_{ij}}'} - k_j^b \prod_{i=1}^{N_s} \left(\frac{\rho Y_i}{M_i} \right)^{{\nu_{ij}}''} \qquad \text{for} \qquad j = 1, \ldots, N_r, \tag{1.26}$$

where k_j is the reaction rate constant of reaction j, and the superscripts f and b refer to the forward and backward reactions. This leads to the following expression for the chemical source term

$$\dot{\omega}_i = M_i \sum_{j=1}^{N_r} \left(\nu_{ij}'' - \nu_{ij}{}' \right) \left\{ k_j^f \prod_{i=1}^{N_s} \left(\frac{\rho Y_i}{M_i} \right)^{\nu_{ij}{}'} - k_j^b \prod_{i=1}^{N_s} \left(\frac{\rho Y_i}{M_i} \right)^{\nu_{ij}{}''} \right\} \quad \text{for} \quad i = 1, \ldots, N_s. \tag{1.27}$$

The reactions and the reaction constants are listed in reaction mechanisms. The reaction mechanism that has been used in this study is the mechanism from Smooke [18], which contains only 16 species and 25 reactions.

1.3 Overview of this thesis

This work is part of a research, of which the main objective is the development of a reduction method that is based on a unified flamelet model. This reduction method can be used in both premixed and non-premixed flame computations. However, the development and testing of such a method goes beyond the scope of this thesis. The goal of this work is to evaluate the existing, standard Diffusion Flamelet Method, which is based on a number of assumptions that can lead to inaccuracies.

The first assumption that will be investigated is the assumption that the Lewis numbers for all species are unity, i.e. that there are no preferential diffusion effects. In order to evaluate this, a new flamelet model will be derived, which includes preferential diffusion. The order of magnitude of preferential diffusion effects is then calculated for a one-dimensional counterflow diffusion flame, using a 1D solver.

The second assumption arises when a flamelet database is constructed and used during complex flamelet computations. When it is assumed that the chemistry is infinitely fast, which is known as the Burke-Schumann solution, the reaction takes place at the infinitely thin reaction zone. Because the chemistry is assumed to be infinitely fast, the fuel and oxidiser will be completely converted into combustion products. However, when the other time-scales become more important, which occurs if the scalar dissipation rate increases, the assumption that chemistry is infinitely fast is no longer valid. The fuel and oxidiser are no longer completely converted, which means that the flame temperature drops. It can therefore be concluded that the solution also depends on the scalar dissipation rate.

Therefore, when diffusion flamelets are computed, the composition is stored in a database as a function of the mixture fraction Z and the stoichiometric value of the scalar dissipation rate χ_{st}. This can be done in a pre-processing step. Later, during complex flame calculations, an equation for the mixture fraction is solved. Then the scalar dissipation rate, which is strongly coupled with the mixture fraction, can then also be determined. The flame structure is then found from the flamelet database. Generally, the local value of the scalar dissipation rate is not equal to its stoichiometric value. Therefore, an analytical model is used to relate the local values of the scalar dissipation rate to their corresponding stoichiometric values. The assumption that is made to derive the analytical solution and that will be studied is the assumption that the density is constant, i.e. a non-combusting system. For a combusting system, this assumption is not valid, which leads to an error in the analytical model. Therefore, numerical values of the stoichiometric scalar dissipation rate will be compared to their modeled counterparts.

This chapter started with an introduction to combustion in general. Then the equations that will be used throughout this report were derived. An overview of existing reduction methods is given in chapter 2. In chapter 3, the existing, standard diffusion flamelet model with $Le_i = 1$, that was introduced by Peters will be derived. After that, the same procedure will be repeated, but the $Le_i = 1$ assumption will not be made, which means that all species can have a different diffusivity, leading to so-called preferential diffusion. Chapter 3 will start with the introduction to the mixture fraction. After that, the quasi-1D flamelet equations will be derived, starting from the full set of 3D equations. Using a numerical approach, the order of magnitude of preferential diffusion effects is also discussed, as well as the effect of preferential diffusion on the flame structure. An analytical solution for the mixture fraction will be presented in chapter 4. This solution can be used to derive a model for the scalar dissipation rate. The scalar dissipation rate is very important to diffusion flame models as it is the inverse of a characteristic diffusion time scale. As said, the mixture fraction and the scalar dissipation rate can be used to characterise diffusion flames. There are some doubts on whether the choice for these two variables as characteristic parameters is the best [8]. Furthermore, the model for the scalar dissipation rate that was derived in the previous chapter will be compared with the numerical values in this chapter as well. In chapter 5, conclusions will be drawn and recommendations for future research will be given.

Chapter 2

Reduction of the computation time

In order to accurately predict temperature profiles and the composition of the gas mixtures, detailed combustion models have to be solved, i.e. equations (1.6), (1.7), (1.23) and (1.19). These detailed models generally involve large reaction mechanisms, which contain many chemical components and even more reactions. Generally, there are two approaches to model flames, which both reduce the amount of computation time, but without losing too much accuracy. The first are the chemical reduction techniques, which are based on the assumption that chemical time-scales are much smaller than time-scales representing transport and mixing processes. The second are the so-called laminar flamelet models, which are based on the assumption that distortions along the flame surface are small compared to distortions perpendicular to the flame. This is also an indication that the chemistry is fast compared to transport and mixing phenomena.

At the Combustion Technology Group of the Eindhoven University of Technology, these the chemical reduction technique and the flamelet approach have been combined, effectively "bridging the gap" between the two. This led to the Flamelet Generated Manifolds method and the Phase-Space Intrinsic Low-Dimensional Manifolds method.

In section 2.1, first the general concept of combustion in the composition space and so-called manifolds will be explained. The reduction methods that will be briefly discussed here are the Conventional Reduction Method introduced by Peters [15], which will be done in section 2.2 and the Intrinsic Low-Dimensional Manifolds method [12], which will be presented in section 2.3. In section 2.4 the Flamelet Generated Manifolds method [22] will be discussed and the Phase-Space Intrinsic Low-Dimensional Manifolds method [4] in section 2.5. Section 2.6 will contain a short summary of this chapter, and some conclusions will be drawn.

2.1 Composition space and manifolds

A mixture of N_s chemical species can be represented by a point in the N_s-dimensional composition space, with N_s the number of species. A combustion process can be described by a path through the reaction space, which is a lower dimensional sub-space of the composition space. The reaction space has a lower dimension than the composition space due to restrictions, i.e. species mass conservation and element mass conservation. By assuming correlations between species, the chemical composition is restricted to an even lower dimensional space within the composition space, which is also referred to as a manifold. There are various methods to find these correlations, and some of them will be discussed below.

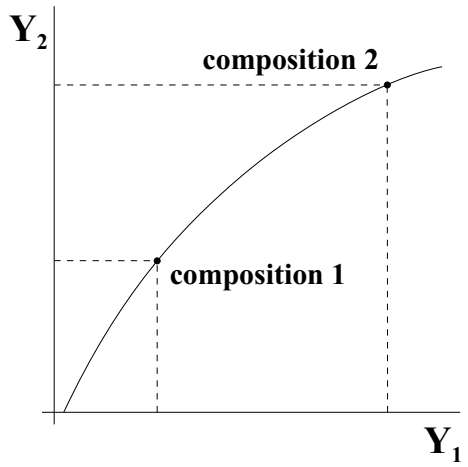

Fig. 2.1: A projection on the $Y_1 - Y_2$ plane of a two dimensional composition space with a one dimensional manifold, represented by the solid line, which is a correlation between Y_1, Y_2 and Y_3.

The vector containing the species mass fractions is defined as $\mathbf{Y} = (Y_1, ..., Y_{N_s})^T$. Each correlation between species reduces the dimension of the manifold by 1. For instance, steady-state assumptions, meaning that the chemical source term is equal to zero, can be used to derive the correlations between species. By applying steady-state assumptions for species $i = 1, \ldots, N_{ss}$, equation (1.27) can be written as follows

$$M_i \sum_{j=1}^{N_r} \left(\nu_{ij}'' - \nu_{ij}{}' \right) \left\{ k_j^f \prod_{i=1}^{N_s} \left(\frac{\rho Y_i}{M_i} \right)^{\nu_{ij}{}'} - k_j^b \prod_{i=1}^{N_s} \left(\frac{\rho Y_i}{M_i} \right)^{\nu_{ij}{}''} \right\} = 0, \qquad \text{for} \qquad i = 1, \ldots, N_{ss} \tag{2.1}$$

where N_{ss} is the number of steady-state species. Suppose that a certain mixture consists of species Y_1, Y_2 and Y_3, then $\mathbf{Y}$ becomes $(Y_1, Y_2, Y_3)^T$. In figure (2.1), a projection on the $Y_1 - Y_2$ plane can be seen. In principle any point represents a possible solution to a chemical process in this 3-dimensional solution space. However, when correlations between Y_1, Y_2 and Y_3 are known, the solution space can be reduced to a 1-dimensional manifold. Now it is possible to do calculations for only one species, for instance Y_1, because for every solution of Y_1 the mass fractions of Y_2 and Y_3 are known. In case of N_s species, the manifold can be constructed using multiple correlations.

2.2 Conventional reduction method

The Conventional Reduction Method (CRM), introduced by Peters [15], applies steady-state assumptions for intermediate species and partial equilibrium assumptions for fast reactions. This means that for species $i = 1, \ldots, N_{ss}$, which are assumed to be in steady-state, the sum of all chemical reactions equals zero. Equation (2.1) indicates that the time scales of the reactions producing or consuming a steady-state species are much shorter than the time scales concerning convection and diffusion. For the first N_{ss} species, an algebraic equation like

(2.1) is solved, instead of equation (1.19). During flame calculations equation (1.19) is solved for the remaining species, together with the algebraic equations for the steady-state species. Because the fastest time scales are removed from the differential equations, the number of differential equations as well as the stiffness of the system is significantly reduced.

Because the selection of the steady-state species is done manually, this method requires both experience and insight in the chemical kinetics, making it only suitable for simple mechanisms. Because the steady-state species are selected globally, the reduced mechanism is not accurate in the entire domain. This is due to the fact that it depends on local conditions which species can be assumed to be in steady-state. Because of this, a reduced mechanism will likely not be accurate for conditions it is not developed for. These problems can be avoided by using the Intrinsic Low-Dimensional Manifolds method, which applies such a time-scale analysis locally.

2.3 Intrinsic low-dimensional manifolds

Like the CRM, the Intrinsic Low-Dimensional Manifolds (ILDM) method is used to reduce the number of differential equations that needs to be solved during flame calculations. This method is also based on steady-state assumptions. The difference is that with ILDM this is done automatically. Furthermore, the analysis is based on a local time-scale analysis of the chemical source term. It is assumed that the fast and slow time-scales can be well separated. If that is the case, the progress of the chemical reactions can be accurately described by the slow processes. Here only a brief overview will be given, for more information the reader is referred to [12].

To decouple the fast and slow time-scales, a local eigenvalue analysis is applied to the chemical source term. In this analysis, it is assumed that both convection and diffusion may be neglected. When applying this assumption, the conservation equation for species (1.19) becomes

$$\rho \frac{\partial Y_i}{\partial t} = \dot{\omega}_i \qquad \text{for} \qquad i = 1, \ldots, N_s. \tag{2.2}$$

Linearising $\dot{\omega}_i$ around a reference composition $\mathbf{Y}^0 = \left(\mathbf{Y}_1^0, ..., \mathbf{Y}_{N_s}^0\right)$ results in

$$\rho \frac{\partial}{\partial t}\left(\mathbf{Y} - \mathbf{Y}^0\right) \cong \mathbf{J}(\mathbf{Y} - \mathbf{Y}^0), \tag{2.3}$$

where $\mathbf{J}$ is known as the Jacobian, with $J_{ij} = \frac{\partial \omega_i}{\partial Y_j}$. The Jacobian is used in an eigenvalue analysis that separates all time-scales, and the eigenvalues can be separated into three groups, see figure 2.2.

The first group represents the conserved variables, corresponding to eigenvalues equal to zero, i.e. the element mass fractions Z_j and the enthalpy h. The other eigenvalues can be separated into a fast and slow group. Depending on the size of the real part of the eigenvalues, it is decided which processes can be assumed to be in steady-state. Large negative eigenvalues represent the fast group while the slow group is identified by the positive and small negative eigenvalues. When it is assumed that species, corresponding to the small time-scales, are in steady-state, the reaction progress is restricted to a lower dimensional space within the composition space. This lower dimensional space is referred to as manifold. In figure 2.3, it is schematically shown how the reaction trajectories are rapidly attracted to the manifold.

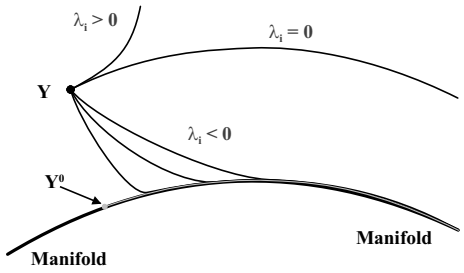

Fig. 2.2: Schematic representation of the eigenvalues. The slow group is made up of positive and small negative eigenvalues, identifying the species that span the manifold. Large negative eigenvalues represent the fast group and identify the species that are assumed to be in steady state. Eigenvalues equal to 0 correspond to conserved variables.

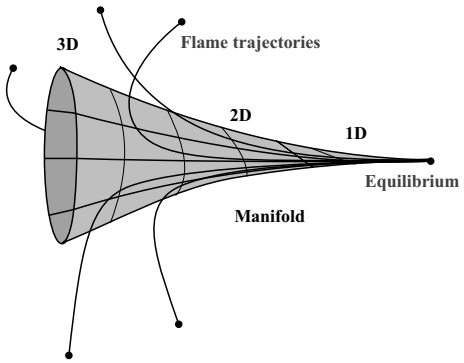

Fig. 2.3: Schematic representation of a manifold. The low-dimensional manifold is defined by the points within the composition-space, where most of the chemical source terms reach steady state very fast.

Once on the manifold, the reaction trajectory is much slower. This manifold is stored as a function of so-called controlling variables. During the flame calculations, only the equations (including convection and diffusion) for the controlling variables are solved. The values of the other species are found by using the data stored in the manifold. Note that Z_j and h are kept constant. If, however, this is not the case in the application, variations in Z_j and h have to be added to the manifold. In that case, the element mass fraction Z_j and h act as additional controlling variables, and thus add extra dimensions to the manifold.

Because the steady-state species are identified locally, the reduced mechanism truly includes only the slow reactions, prohibited that the slow and fast time-scales are well separated. However, the ILDM method applies an eigenvalue analysis to the chemical source term only. This means that it is only accurate where the chemistry is much faster than convection and diffusion. This is true in the hot regions of the flame, but in the colder regions the ILDM method becomes less accurate. For premixed combustion, the pre-heat zone plays a vital part in the combustion proces. It is near the edge of this region and the reaction zone that diffusion is very important for the heat transport from the flame to the pre-heat zone. The Flamelet Generated Manifolds method is more accurate in the colder flame regions than ILDM is for premixed flames.

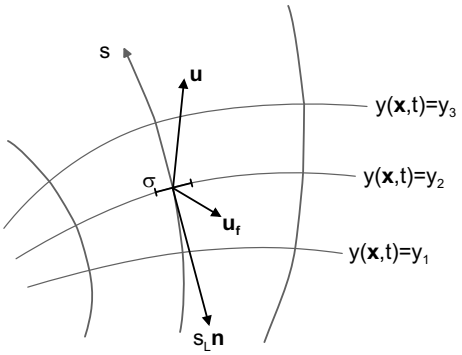

Fig. 2.4: Schematic representation of a premixed flamelet system.

2.4 Flamelet generated manifolds

The Flamelet Generated Manifolds (FGM) method [22] is the combination of two approaches, i.e. the flamelet approach and the reduced chemistry approach. FGM is based on the flamelet assumption that the gradients perpendicular to the flame surface are much larger than the gradients along the flame surface. This essentially means that a multi-dimensional flame can be considered as a set of 1D flamelets. Therefore, the compositions in 1D flames can be used to represent the compositions in 3D flames. The way that it is implemented however, is very similar to reduction techniques. In a pre-processing step, a manifold is constructed that includes the slow time-scales. The dimension of the manifold can be increased to capture more time-scales.

Figure 2.4 shows a schematic representation of a premixed flamelet system. Here, a premixed flame is defined as the area, separating the unburnt from the burnt gasses. The scalar variable $\mathcal{Y}$ defines the flame and can be a linear combination of species mass fractions. It is defined such that it is $\mathcal{Y}_u = 0$ in the unburnt gases and $\mathcal{Y}_b = 1$ in the burnt gases, while it must also be continuously increasing.

A flame surface is defined as an iso-surface of $\mathcal{Y}$, meaning that $\mathcal{Y}\ (\mathbf{x}, t) = const$ on such a surface. The motion of such a surface is described by the kinematic equation

$$\frac{d\mathcal{Y}}{dt} \equiv \frac{\partial \mathcal{Y}}{\partial t} + \mathbf{u}_f \cdot \nabla \mathcal{Y} = 0, \tag{2.4}$$

which essentially means that a point on a flame surface stays on this surface for all t. The local velocity of the flame surface $\mathbf{u}_f$ is the sum of the local fluid velocity $\mathbf{u}$ and the local burning velocity S_L

$$\mathbf{u}_f = \mathbf{u} + S_L \mathbf{n}, \tag{2.5}$$

where $\mathbf{n}$ is the normal to the iso-surface, which is defined as $\mathbf{n} = -\nabla\mathcal{Y}/|\nabla\mathcal{Y}|$.

Substitution of (2.5) in (2.4) results in

$$\frac{\partial \mathcal{Y}}{\partial t} + \mathbf{u} \cdot \nabla \mathcal{Y} = S_L |\nabla \mathcal{Y}|. \tag{2.6}$$

There is a great similarity with the well-known G-equation [23]. The difference is that the G-equation describes the motion of a single flame sheet, i.e. $\mathcal{Y} = \mathcal{Y}^0$, whereas equation (2.6) describes the motion of all flame surfaces with $\mathcal{Y}_u < \mathcal{Y} < \mathcal{Y}_b$. Furthermore, the burning

velocity S_L is a field quantity in (2.6), while in the G-equation it is defined at the flame sheet only.

With the coordinate system attached to the flame surface, see figure 2.4, described by (2.6), the full set of conservation equations (1.6), (1.7), (1.8) and (1.4) can be cast in a quasi-1D form, referred to as the flamelet equations. Introducing the arc-length perpendicular to the flame surfaces s and the variable σ, which is a measure for the area through which transport takes place, in the flame-attached system, the conservation equations become [9]

$$\frac{\partial \sigma m}{\partial s} = -\sigma \rho K, \tag{2.7}$$

$$\frac{\partial (\sigma m Y_i)}{\partial s} - \frac{\partial}{\partial s}\left(\sigma \frac{\lambda}{Le_i c_p}\frac{\partial Y_i}{\partial s}\right) = \sigma \dot{\omega}_i - \sigma \rho K Y_i + Q_i \qquad \text{for} \qquad i = 1, \ldots, N_s, \tag{2.8}$$

$$\frac{\partial (\sigma m h)}{\partial s} - \frac{\partial}{\partial s}\left(\sigma \frac{\lambda}{c_p}\frac{\partial h}{\partial s}\right) = \frac{\partial}{\partial s}\left(\sigma \frac{\lambda}{c_p}\sum_{i=1}^{N_s}\left(\frac{1}{Le_i} - 1\right) h_i \frac{\partial Y_i}{\partial s}\right) - \sigma \rho K h + Q_h, \tag{2.9}$$

where Q_i describes transport along the flame surfaces that arise because generally the iso-surfaces of Y_i and h do not lie along the iso-surfaces of $\mathcal{Y}$

When assuming that there are no perturbations from a 1D-flat flame perturbations, i.e. $K = 0$, $\sigma = 1$, $Q_i = 0$ and $Q_h = 0$, the above flamelet equations can be written as

$$\frac{\partial m}{\partial s} = 0, \tag{2.10}$$

$$\frac{\partial (m Y_i)}{\partial s} - \frac{\partial}{\partial s}\left(\frac{\lambda}{Le_i c_p}\frac{\partial Y_i}{\partial s}\right) = \dot{\omega}_i \qquad \text{for} \qquad i = 1, \ldots, N_s, \tag{2.11}$$

$$\frac{\partial (m h)}{\partial s} - \frac{\partial}{\partial s}\left(\frac{\lambda}{c_p}\frac{\partial h}{\partial s}\right) = \frac{\partial}{\partial s}\left(\frac{\lambda}{c_p}\sum_{i=1}^{N_s}\left(\frac{1}{Le_i} - 1\right) h_i \frac{\partial Y_i}{\partial s}\right). \tag{2.12}$$

A more detailed derivation can be found in [22].

In order to construct a manifold, the set of 1D flamelet equations (2.10)-(2.12) can be solved with CHEM1D [5]. The solution of this set of equations is determined by the initial temperature and pressure of the unburnt mixture and each solution forms a curve in the composition space and can be considered as a 1D manifold. In order to capture more time-scales, i.e. increasing the dimension of the manifold, the initial composition is varied, while the enthalpy and element mass fractions are kept constant. This can be done by changing the values of the controlling variables and the temperature, so that all flamelets end up in the same chemical equilibrium.

While FGM is shown to give accurate results [19, 21], the time-scale analysis is not based on a strong mathematical fundament yet, as is the case with ILDM. It is also developed for (partially) premixed flames only and it remains to be seen if it can be applied to diffusion flames. Inclusion of more time-scales in the manifold is also not straightforward. With the Phase-Space Intrinsic Low-Dimensional Manifolds method, which is under development, a mathematic fundament is introduced for the FGM method.

2.5 Phase-space intrinsic low-dimensional manifolds

As with the ILDM method, the Phase-Space Intrinsic Low-Dimensional Manifolds (PS-ILDM) method [4] is used to create a unique manifold, but now diffusion effects are included. This is done by performing a time-scale analysis of the reactive-diffusive system, instead of the reactive system only. Subsequently, the ILDM approach is used to find a manifold in the composition phase space. The composition phase space is defined by the species mass fractions and their gradients.

Using the assumption that effects like stretch and curvature are small and that there is no transport along the flame surfaces, i.e. $K = 0$, $\sigma = 1$, $Q_i = 0$ and $Q_h = 0$, equations (2.11) and (2.12) can also be written as

$$\frac{\partial \psi_i}{\partial s} = m\frac{Le_i c_p}{\lambda}\psi_i - \dot{\omega}_i \qquad \text{for} \qquad i = 1, \ldots, N_s, \tag{2.13}$$

$$\frac{\partial \psi_h}{\partial s} = m\frac{c_p}{\lambda}\psi_h - m\sum_{i=1}^{N_s}\left(1 - Le_i\right)\frac{c_p}{\lambda}\psi_i. \tag{2.14}$$

Here, the diffusive flux for species ψ_i and the diffusive flux for enthalpy ψ_h are defined as

$$\psi_i = \frac{\lambda}{Le_i c_p}\frac{\partial Y_i}{\partial s} \qquad \text{for} \qquad i = 1, \ldots, N_s, \tag{2.15}$$

$$\psi_h = \frac{\lambda}{c_p}\frac{\partial h}{\partial s} + \frac{\lambda}{c_p}\sum_{i=1}^{N_s} h_i \left(\frac{1}{Le_i} - 1\right)\frac{\partial Y_i}{\partial s}. \tag{2.16}$$

This is done in order to transform the otherwise second order differential equations into first order differential equations. In vector form these equations read

$$\frac{d\boldsymbol{\Theta}}{ds} = \boldsymbol{\Omega}\left(\boldsymbol{\Theta}\right), \tag{2.17}$$

where $\boldsymbol{\Theta} = (Y_1, ..., Y_{N_s}, h, \psi_1, ..., \psi_{N_s}, \psi_h)^T$ is a vector in the $2(N_s+1)$-dimensional composition space and $\boldsymbol{\Omega}$ is the source of $\boldsymbol{\Theta}$, defined by equations (2.13)-(2.16). Note that the form of equation (2.17) is analogous to (2.2). Instead of the time t, the spatial coordinate s will be used to parameterise the evolution of the system. But this is irrelevant, because the evolution through phase-space domain is considered and not through the time-spatial domain.

Analogous to the ILDM method, equations (2.17) can be linearised around reference points $\boldsymbol{\Theta}^0$

$$\frac{\partial}{\partial s}\left(\boldsymbol{\Theta} - \boldsymbol{\Theta}^0\right) = \boldsymbol{A}\left(\boldsymbol{\Theta} - \boldsymbol{\Theta}^0\right), \tag{2.18}$$

where $\boldsymbol{A}$ is defined as

$$\boldsymbol{A} = \begin{pmatrix} \mathbf{0} & \boldsymbol{B} \\ -\boldsymbol{J} & m\boldsymbol{B} \end{pmatrix}. \tag{2.19}$$

Here $\mathbf{0}$ is a $((N_s + 1) \times (N_s + 1))$ null-matrix, $\boldsymbol{J}$ the Jacobian of the source term, which was defined in section 2.3. $\boldsymbol{B}$ is a $((N_s + 1) \times (N_s + 1))$ matrix containing the definitions of the fluxes ψ_i and ψ_h. The mass burning rate m is an independent variable, which introduces

an additional degree of freedom. Because it can be chosen independently, it adds an extra dimension to the manifold.

Where the Jacobian $\boldsymbol{J}$ was used to separate the fast and slow processes for the ILDM method, for the PS-ILDM method the matrix $\boldsymbol{A}$ is used. The resulting eigenvalues can be separated into three groups. The first group corresponds to eigenvalues equal to zero, which are the conserved variables. The other two groups are distinguished as a slow and fast group. These eigenvalues correspond to the eigenvalues found with the ILDM method. The difference is that the (mostly) negative eigenvalues of ILDM have, in case of PS-ILDM, a positive counterpart. The positive eigenvalues represent transport in the negative s-direction and negative eigenvalues corresponds to transport in the positive s-direction. The construction of the manifold is analogous to the construction of an ILDM.

Because of the mathematical fundament for the time-scale analysis, separating the fast and slow processes can be done automatically. Increasing the dimension of the manifold is then in theory straightforward. Unfortunately, the PS-ILDM method is not yet easy to apply to actual flame computations [3]. Furthermore, because the flamelet model is based on premixed equations, PS-ILDM will likely not be applicable to diffusion flames. One way to possibly resolve this is to combine the time-scale analysis of ILDM with the flamelet equations of the diffusion flamelet method.

2.6 Summary and conclusions

All the mentioned reduction methods have their limitations as to what they can be used for. Like CRM, the ILDM method can be used for premixed as well as non-premixed flame calculations, but because the reduced mechanisms are based on chemistry only, these methods become less accurate in the colder flame regions. It is in these regions that the convection and diffusion time-scales become of the same order as the chemistry time-scale. In premixed flames the preheat zone is essential to the combustion. Diffusion is a very important process to transport the heat from the flame to the preheat zone. Therefore, the ILDM method is less suitable to use for premixed flames. For laminar (partially) premixed flames FGM gives more accurate results, and although it has been successfully used [19, 21], its applicability to diffusion flames is questionable. Furthermore, unlike the ILDM method, the time-scale analysis of the FGM method is not based on a mathematical fundament. It is also not sure whether the manifold that is constructed with the FGM method is the intrinsic manifold, whereas the ILDM is. Increasing the dimension of the FGM is also not straightforward. Based on the same ideas as the ILDM method and having the advantages of the FGM method is the PS-ILDM method. The manifold includes both chemistry and diffusion, and should give more accurate results than the ILDM method, but because premixed flamelet equations are used, the PS-ILDM method is only applicable to (partially) premixed flames. This makes their applicability to non-premixed flames questionable. Therefore, a method that is analogous to either FGM or PS-ILDM has to be developed, but based on diffusion flamelet equations. But before that, an existing, standard diffusion flamelet model will be studied. It is important to know what assumptions are made, and what the effects are of these assumptions. This will be done in the next two chapters.

Chapter 3

Non-premixed flamelet model

Before a diffusion flamelet model based reduction technique can be developed, the flamelet model itself has to be studied. A flamelet model, introduced by Peters [14], will be derived in this chapter, and the assumptions that are made, will be reviewed. One of these assumptions will be analysed numerically. The major assumption on which flamelet models are based is that all gradients of a flame are much larger perpendicular to the flame than they are along the flame surfaces. This model of Peters is often used in turbulent flame simulations, and is regarded as a reference case.

Usually, for methane-air flames, combustion takes place near the surface of stoichiometric mixture, which is the iso-surface where the mixture fraction Z equals its stoichiometric value. Because the mixture fraction is an independent variable, it can be used as a new independent coordinate. Rearranging the set of 3D equations leads to a set of quasi-1D equations. Assuming that gradients along the flame surface are small, the resulting equations can be written in 1D form, which are called the flamelet equations. These flamelet equations describe the inner flame structure in mixture fraction space.

The mixture fraction is presented in section 3.1, and the coordinate transformation to mixture fraction space in section 3.2. First, the flamelet model as derived by Peters is given in section 3.2.2. The assumption that is made during this derivation, is that all Lewis numbers are unity. This means that preferential diffusion effects are not included in this flamelet model. To evaluate this assumption, a flamelet model including the preferential diffusion terms, is derived in section 3.2.3, followed by a comparison between this flamelet model and an alternative approach introduced by Peters and Pitsch, which will be presented in section 3.2.4. The order of magnitude of the preferential diffusion terms and the effect on the flame structure in general will be numerically studied in section 3.3. Finally, some conclusions will be drawn in section 3.4.

3.1 The mixture fraction

The mixture fraction Z is an important variable for diffusion flames. There are several definitions for Z, but all these definitions are normalised such that $Z = 1$ for pure fuel and $Z = 0$ for pure oxidiser. In this section, a conservation equation for Z will be derived.

During a reaction, species are consumed or produced, but chemical elements are conserved. The element mass fraction is defined as

$$Z_j = \sum_{k=1}^{N_s} w_{jk} Y_k \qquad \text{for} \qquad j = 1, \ldots, N_e, \tag{3.1}$$

where w_{jk} is defined as

$$w_{jk} = \frac{a_{jk} M_j}{M_k} \qquad \text{for} \quad j = 1, \ldots, N_e \quad \text{and} \quad \text{for} \quad k = 1, \ldots, N_s, \tag{3.2}$$

with a_{jk} the total number of chemical elements j in species k. Furthermore, M_j and M_k are the molar masses of element j and species k, respectively.

Since elements cannot be created or annihilated by chemical reactions, element mass is conserved during chemical reactions. This implies

$$\sum_{k=1}^{N_s} w_{jk} \dot{\omega}_k = 0. \tag{3.3}$$

Taking the sum of equation (1.19) according to (3.1), leads to the following equation for Z_j

$$\frac{\partial(\rho Z_j)}{\partial t} + \nabla \cdot (\rho \mathbf{u} Z_j) - \sum_{k=1}^{N_s} w_{jk} \frac{1}{Le_k} \nabla \cdot (\rho D \nabla Y_k) = 0 \qquad \text{for} \qquad j = 1, \ldots, N_e. \tag{3.4}$$

To regain a transport equation on the l.h.s. of the above equation in terms of Z_j, $\nabla \cdot (\rho D \nabla Z_j)$ is subtracted on both sides of equation (3.4). Using (3.1), equation (3.4) can be written as

$$\frac{\partial(\rho Z_j)}{\partial t} + \nabla \cdot (\rho \mathbf{u} Z_j) - \nabla \cdot (\rho D \nabla Z_j) = \sum_{k=1}^{N_s} w_{jk} \left(\frac{1}{Le_k} - 1 \right) \nabla \cdot (\rho D \nabla Y_k) \quad \text{for} \quad j = 1, \ldots, N_e, \tag{3.5}$$

where the terms on the r.h.s. represent element mass fraction variations caused by preferential diffusion. Note the similarity with the conservation equation for enthalpy (1.23).

In [2], Z^* is introduced according to

$$Z^* = 2 \frac{Z_C}{M_C} + \frac{1}{2} \frac{Z_H}{M_H} - \frac{Z_O}{M_O}, \tag{3.6}$$

for hydrocarbon mixtures. In more general form this reads

$$Z^* = \sum_{j=1}^{N_e} \beta_j Z_j, \tag{3.7}$$

where β_j is the specific stoichiometric coefficient of element j, being $\frac{2}{M_C}$ for C, $\frac{1}{2M_H}$ for H and $\frac{-1}{M_O}$ for O, respectively. The mixture fraction Z is defined as, c.f. [2]

$$Z = \frac{Z^* - Z^*_{ox}}{Z^*_{fu} - Z^*_{ox}}, \tag{3.8}$$

where Z^*_{ox} is defined as Z^* for pure oxidiser and Z^*_{fu} is Z^* for pure fuel.

Applying equations (3.1), (3.7) and (3.8) to the conservation equation for species, results in a conservation equation for the mixture fraction

$$\frac{\partial(\rho Z)}{\partial t} + \nabla \cdot (\rho \mathbf{u} Z) - \nabla \cdot (\rho D \nabla Z) = \sum_{j=1}^{N_e} \sum_{k=1}^{N_s} \beta'_{jk} \left(\frac{1}{Le_k} - 1 \right) \nabla \cdot (\rho D \nabla Y_k) \,, \tag{3.9}$$

where β'_{jk} is defined as

$$\beta'_{jk} = \frac{\beta_j w_{jk}}{Z^*_{fu} - Z^*_{ox}} \quad \text{for} \quad j = 1, \ldots, N_e \quad \text{and} \quad \text{for} \quad k = 1, \ldots, N_s. \tag{3.10}$$

The unsteady convection-diffusion equation can be recognised on the l.h.s. of equation (3.9), while the term on the r.h.s. represents mixture fraction variations caused by preferential diffusion. Preferential diffusion can be regarded as a source term and is the result of two different effects. The first effect is that there is the preference of mass diffusion over thermal conduction or vice versa if the Lewis numbers are not equal to 1, which leads to a non-zero r.h.s. for the enthalpy equation (1.23). And the second effect is that there is a preference in the mass diffusion of the species themselves, which occurs when all species have a different diffusion velocity, and thus all species have different Lewis numbers. This leads to a non-zero r.h.s. for the species equation (1.19) as well. Note that when all Lewis numbers are equal to 1, the r.h.s. of equation (3.9) cancels, leading to

$$\frac{\partial(\rho Z)}{\partial t} + \nabla \cdot (\rho \mathbf{u} Z) - \nabla \cdot (\rho D \nabla Z) = 0, \tag{3.11}$$

When the Lewis numbers for all species have the same value, i.e. $Le_k = Le$, it is possible to write equation (3.9) as

$$\frac{\partial(\rho Z)}{\partial t} + \nabla \cdot (\rho \mathbf{u} Z) - \frac{1}{Le} \nabla \cdot (\rho D \nabla Z) = 0. \tag{3.12}$$

This equation indicates that there is no preferential mass-diffusion between species when they all have the same Lewis number. The equation for the element mass fractions for this case is

$$\frac{\partial(\rho Z_j)}{\partial t} + \nabla \cdot (\rho \mathbf{u} Z_j) - \frac{1}{Le} \nabla \cdot (\rho D \nabla Z_j) = 0 \qquad \text{for} \qquad j = 1, \ldots, N_e, \tag{3.13}$$

which is similar to equation (3.12).

3.2 Transformation to mixture fraction space

In diffusion flames, the mixture fraction can be used as an independent variable. This allows to apply a coordinate transformation to mixture fraction space. Assuming that gradients perpendicular to the surface of stoichiometric mixture are larger than gradients along this surface, leads to a 1D flamelet model in mixture fraction space. First, the transformation rules that will be applied, are derived. After that, the coordinate transformation of the species equations to Z-space will be presented, followed by a comparison to an alternative approach to include preferential diffusion in the flamelet model.

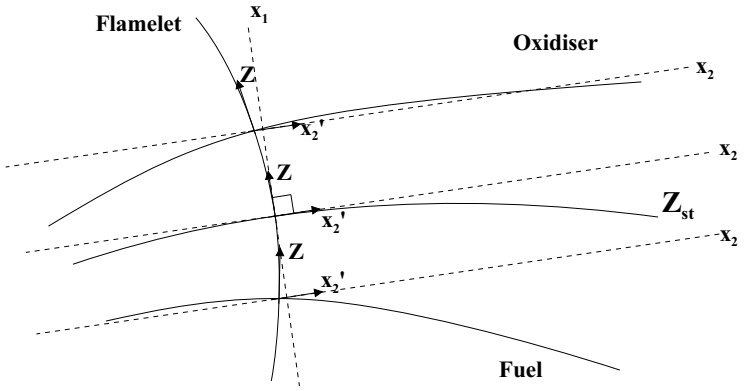

Fig. 3.1: A coordinate system attached to the surface of the stoichiometric mixture of a flame. The new coordinate Z is locally perpendicular to the iso-surfaces of the flame. This is not the case with the new coordinates x_2' and x_3'. This results in a coordinate system that is only orthogonal at the surface of the stoichiometric mixture.

3.2.1 Transformation rules

In [14], Peters considers a diffusion flame with a coordinate system, $(x_1,\ x_2,\ x_3,\ t)$, attached to the surface of the stoichiometric mixture Z_{st}. See figure 3.1 for a two-dimensional representation. The general transformation rules are as follows

$$\frac{\partial}{\partial x_1} = \frac{\partial Z}{\partial x_1}\frac{\partial}{\partial Z} + \frac{\partial x_2'}{\partial x_1}\frac{\partial}{\partial x_2'} + \frac{\partial x_3'}{\partial x_1}\frac{\partial}{\partial x_3'} + \frac{\partial t'}{\partial x_1}\frac{\partial}{\partial t'}, \tag{3.14}$$

$$\frac{\partial}{\partial x_2} = \frac{\partial Z}{\partial x_2}\frac{\partial}{\partial Z} + \frac{\partial x_2'}{\partial x_2}\frac{\partial}{\partial x_2'} + \frac{\partial x_3'}{\partial x_2}\frac{\partial}{\partial x_3'} + \frac{\partial t'}{\partial x_2}\frac{\partial}{\partial t'}, \tag{3.15}$$

$$\frac{\partial}{\partial x_3} = \frac{\partial Z}{\partial x_3}\frac{\partial}{\partial Z} + \frac{\partial x_2'}{\partial x_3}\frac{\partial}{\partial x_2'} + \frac{\partial x_3'}{\partial x_3}\frac{\partial}{\partial x_3'} + \frac{\partial t'}{\partial x_3}\frac{\partial}{\partial t'}, \tag{3.16}$$

$$\frac{\partial}{\partial t} = \frac{\partial Z}{\partial t}\frac{\partial}{\partial Z} + \frac{\partial x_2'}{\partial t}\frac{\partial}{\partial x_2'} + \frac{\partial x_3'}{\partial t}\frac{\partial}{\partial x_3'} + \frac{\partial t'}{\partial t}\frac{\partial}{\partial t'}. \tag{3.17}$$

The scale factors can be chosen arbitrarily, as long as three independent coordinates remain. With these choices for the scale factors

$$\frac{\partial x_2'}{\partial x_1} = \frac{\partial x_3'}{\partial x_1} = \frac{\partial x_3'}{\partial x_2} = \frac{\partial x_2'}{\partial x_3} = \frac{\partial x_2'}{\partial t} = \frac{\partial x_3'}{\partial t} = \frac{\partial t'}{\partial x_1} = \frac{\partial t'}{\partial x_2} = \frac{\partial t'}{\partial x_3} = 0. \tag{3.18}$$

and

$$\frac{\partial x_2'}{\partial x_2} = \frac{\partial x_3'}{\partial x_3} = \frac{\partial t'}{\partial t} = 1, \tag{3.19}$$

the transformation rules can be written as

$$\frac{\partial}{\partial x_1} = \frac{\partial Z}{\partial x_1}\frac{\partial}{\partial Z}, \tag{3.20}$$

$$\frac{\partial}{\partial x_\eta} = \frac{\partial Z}{\partial x_\eta}\frac{\partial}{\partial Z} + \frac{\partial}{\partial x'_\eta}, \tag{3.21}$$

$$\frac{\partial}{\partial t} = \frac{\partial Z}{\partial t}\frac{\partial}{\partial Z} + \frac{\partial}{\partial t'}, \tag{3.22}$$

with ($\eta = 2, 3$), indicating the two directions along the flame surfaces. The second derivatives are given by

$$\frac{\partial^2}{\partial x_1^2} = \frac{\partial^2 Z}{\partial x_1^2}\frac{\partial}{\partial Z} + \left(\frac{\partial Z}{\partial x_1}\right)^2 \frac{\partial^2}{\partial Z^2}, \tag{3.23}$$

$$\frac{\partial^2}{\partial x_\eta^2} = \frac{\partial^2 Z}{\partial x_\eta^2}\frac{\partial}{\partial Z} + \left(\frac{\partial Z}{\partial x_\eta}\right)^2 \frac{\partial^2}{\partial Z^2} + \frac{\partial Z}{\partial x_\eta}\frac{\partial^2}{\partial Z \partial x'_\eta} + \frac{\partial^2}{\partial x'^2_\eta}. \tag{3.24}$$

3.2.2 Transformation into a spatial-coordinate-free system with $Le_i = 1$

When the transformation rules (3.20)-(3.24) are applied to the species equation (1.19), this equation can be written as

$$\begin{aligned}
&\frac{\partial Y_i}{\partial Z}\left(\rho\frac{\partial Z}{\partial t} + \rho u_\alpha \frac{\partial Z}{\partial x_\alpha} - \rho D\frac{\partial^2 Z}{\partial x_\alpha^2} - \left(\frac{\partial Z}{\partial x_\alpha}\right)^2 \frac{\partial(\rho D)}{\partial Z} - \sum_{\eta=2}^{3}\left\{\frac{\partial Z}{\partial x_\eta}\frac{\partial(\rho D)}{\partial x'_\eta}\right\}\right) + \\
&\rho\frac{\partial Y_i}{\partial t'} + \sum_{\eta=2}^{3}\left(\rho u_{x'_\eta}\frac{\partial Y_i}{\partial x'_\eta}\right) - \rho D\left(\frac{\partial Z}{\partial x_\alpha}\right)^2 \frac{\partial^2 Y_i}{\partial Z^2} - \sum_{\eta=2}^{3}\left\{2\rho D\frac{\partial Z}{\partial x_\eta}\frac{\partial^2 Y_i}{\partial Z \partial x'_\eta} + \right. \\
&\left.\frac{\partial Z}{\partial x_\eta}\frac{\partial Y_i}{\partial x'_\eta}\frac{\partial(\rho D)}{\partial Z} + \rho D\frac{\partial^2 Y_i}{\partial x'^2_\eta} + \frac{\partial Y_i}{\partial x'_\eta}\frac{\partial(\rho D)}{\partial x'_\eta}\right\} = \dot{\omega}_i \qquad \text{for} \qquad i = 1, \ldots, N_s - 1,
\end{aligned} \tag{3.25}$$

where it was assumed that $Le_i = 1$, and equation (1.6) was used. In (3.25) the Einstein summation convention was used, with ($\alpha = 1, 2, 3$). Likewise, the same transformation can be applied to the conservation equation for the mixture fraction (3.9), resulting in

$$\rho\frac{\partial Z}{\partial t} + \rho u_\alpha \frac{\partial Z}{\partial x_\alpha} - \rho D\frac{\partial^2 Z}{\partial x_\alpha^2} - \left(\frac{\partial Z}{\partial x_\alpha}\right)^2 \frac{\partial(\rho D)}{\partial Z} - \sum_{\eta=2}^{3}\left\{\frac{\partial Z}{\partial x_\eta}\frac{\partial(\rho D)}{\partial x'_\eta}\right\} = 0, \tag{3.26}$$

which is used to eliminate the 5 terms between the first set of brackets. The scalar dissipation rate is defined as

$$\chi = 2D\left(\frac{\partial Z}{\partial x_\alpha}\right)^2, \tag{3.27}$$

which is the inverse of a characteristic diffusion time-scale. It can be regarded as the diffusivity in mixture fraction space. Using equations (3.26) and (3.27), the species conservation

equation can finally be written as

$$\rho\frac{\partial Y_i}{\partial t'} = \frac{\rho\chi}{2}\frac{\partial^2 Y_i}{\partial Z^2} + \dot{\omega}_i - R^i_{\parallel} \qquad \text{for} \qquad i = 1, \ldots, N_s - 1, \tag{3.28}$$

which is the flamelet model derived by Peters. In the above equation, $R^i_{\parallel}$ represents transport in the x'_2 and x'_3 directions and is defined as follows

$$R^i_{\parallel} = \sum_{\eta=2}^{3} \left\{ \rho u_{x'_\eta} \frac{\partial Y_i}{\partial x'_\eta} - \left(\frac{\partial Z}{\partial x_\eta}\frac{\partial(\rho D)}{\partial x'_\eta}\frac{\partial Y_i}{\partial x'_\eta} + 2\rho D \frac{\partial Z}{\partial x_\eta}\frac{\partial^2 Y_i}{\partial Z \partial x'_\eta} + \rho D \frac{\partial^2 Y_i}{\partial x'^2_\eta} \right) \right\} \tag{3.29}$$
$$\text{for} \qquad i = 1, \ldots, N_s - 1,$$

where the first term represents convection along the x'_2 and x'_3 directions, and the other terms represent diffusion along the x'_2 and x'_3 directions. By arranging equation (3.28) in this way, it is easy to see that when a stationary 1D flame geometry is chosen, like figure 1.1 (l), $R^i_{\parallel}$ is equal to zero and the instationary term in (3.28) vanishes. This leads to the following expression

$$\frac{\rho\chi}{2}\frac{\partial^2 Y_i}{\partial Z^2} + \dot{\omega}_i = 0 \qquad \text{for} \qquad i = 1, \ldots, N_s - 1, \tag{3.30}$$

which is the flamelet model for the case that $Le_i = 1$. If however, iso-surfaces of species mass fractions Y_i are not parallel to Z, then $R^i_{\parallel} \neq 0$. On the other hand, $R^i_{\parallel} = 0$ if the iso-surfaces are parallel. It would be interesting to study the magnitude of $R^i_{\parallel}$, compared to the source term $\dot{\omega}_i$, from a DNS of a turbulent flame to see how large these terms in practice can be.

3.2.3 Transformation into a spatial-coordinate-free system with $Le_i \neq 1$

In this section, the procedure of the previous section will be repeated, but without making the assumption that all Lewis numbers are unity. Transforming the species equation (1.19) leads to

$$\begin{aligned}
&\frac{\partial Y_i}{\partial Z}\left(\rho\frac{\partial Z}{\partial t} + \rho u_\alpha \frac{\partial Z}{\partial x_\alpha}\right) + \rho\frac{\partial Y_i}{\partial t'} + \sum_{\eta=2}^{3}\left(\rho u_{x'_\eta}\frac{\partial Y_i}{\partial x'_\eta}\right) - \\
&\frac{1}{Le_i}\left[\rho D\left(\frac{\partial Z}{\partial x_\alpha}\right)^2\frac{\partial^2 Y_i}{\partial Z^2} + \rho D\frac{\partial Y_i}{\partial Z}\frac{\partial^2 Z}{\partial x^2_\alpha} + \frac{\partial Y_i}{\partial Z}\left(\frac{\partial Z}{\partial x_\alpha}\right)^2\frac{\partial(\rho D)}{\partial Z} + \right. \\
&\sum_{\eta=2}^{3}\left\{2\rho D\frac{\partial Z}{\partial x_\eta}\frac{\partial^2 Y_i}{\partial Z \partial x'_\eta} + \frac{\partial Z}{\partial x_\eta}\frac{\partial Y_i}{\partial x'_\eta}\frac{\partial(\rho D)}{\partial Z} + \frac{\partial Y_i}{\partial Z}\frac{\partial Z}{\partial x_\eta}\frac{\partial(\rho D)}{\partial x'_\eta} + \right. \\
&\left.\left.\rho D\frac{\partial^2 Y_i}{\partial x'^2_\eta} + \frac{\partial Y_i}{\partial x'_\eta}\frac{\partial(\rho D)}{\partial x'_\eta}\right\}\right] = \dot{\omega}_i \qquad \text{for} \qquad i = 1, \ldots, N_s - 1,
\end{aligned} \tag{3.31}$$

which is similar to (3.25), except for the Lewis numbers dependence. The transport equation for Z can be used to eliminate the terms between the first set of brackets on the l.h.s. of equation (3.31). Applying the coordinate transformation to (3.9), results in

$$\rho\frac{\partial Z}{\partial t}+\rho u_\alpha\frac{\partial Z}{\partial x_\alpha}-\rho D\frac{\partial^2 Z}{\partial x_\alpha^2}-\left(\frac{\partial Z}{\partial x_\alpha}\right)^2\frac{\partial(\rho D)}{\partial Z}-\sum_{\eta=2}^{3}\left\{\frac{\partial Z}{\partial x_\eta}\frac{\partial(\rho D)}{\partial x'_\eta}\right\}=$$
$$\sum_{j=1}^{N_e}\sum_{k=1}^{N_s}\beta'_{jk}\left(\frac{1}{Le_k}-1\right)\left[\rho D\left(\frac{\partial Z}{\partial x_\alpha}\right)^2\frac{\partial^2 Y_k}{\partial Z^2}+\rho D\frac{\partial Y_k}{\partial Z}\frac{\partial^2 Z}{\partial x_\alpha^2}+\right.$$
$$\frac{\partial Y_k}{\partial Z}\left(\frac{\partial Z}{\partial x_\alpha}\right)^2\frac{\partial(\rho D)}{\partial Z}+\sum_{\eta=2}^{3}\left\{2\rho D\frac{\partial Z}{\partial x_\eta}\frac{\partial^2 Y_k}{\partial Z\partial x'_\eta}+\frac{\partial Z}{\partial x_\eta}\frac{\partial Y_k}{\partial x'_\eta}\frac{\partial(\rho D)}{\partial Z}+\right.$$
$$\left.\left.\frac{\partial Y_k}{\partial Z}\frac{\partial Z}{\partial x_\eta}\frac{\partial(\rho D)}{\partial x'_\eta}+\rho D\frac{\partial^2 Y_k}{\partial x'^2_\eta}+\frac{\partial Y_k}{\partial x'_\eta}\frac{\partial(\rho D)}{\partial x'_\eta}\right\}\right], \tag{3.32}$$

Using equation (3.32), the species conservation equation can finally be written as

$$\rho\frac{\partial Y_i}{\partial t'}=\frac{\rho\chi}{2}\frac{1}{Le_i}\frac{\partial^2 Y_i}{\partial Z^2}+\dot\omega_i-R^i_\parallel-P^i_\perp-P^i_\parallel \qquad \text{for} \qquad i=1,\ldots,N_s-1, \tag{3.33}$$

which is similar to equation (3.28), if $Le_i=1$ is chosen. As before, $R^i_\parallel$ represents transport in the x'_2 and x'_3 directions and is now defined as

$$R^i_\parallel=\sum_{\eta=2}^{3}\left\{\rho u_{x'_\eta}\frac{\partial Y_i}{\partial x'_\eta}-\frac{1}{Le_i}\left(\frac{\partial Z}{\partial x_\eta}\frac{\partial(\rho D)}{\partial x'_\eta}\frac{\partial Y_i}{\partial x'_\eta}+2\rho D\frac{\partial Z}{\partial x_\eta}\frac{\partial^2 Y_i}{\partial Z\partial x'_\eta}+\rho D\frac{\partial^2 Y_i}{\partial x'^2_\eta}\right)\right\} \tag{3.34}$$
$$\text{for} \qquad i=1,\ldots,N_s-1.$$

Furthermore, $P^i_\perp$, represents preferential diffusion perpendicular to the flame surface, and can be written as

$$P^i_\perp=-\frac{\partial Y_i}{\partial Z}\left(\frac{1}{Le_i}-1\right)\left[\frac{1}{4}\frac{\partial(\rho\chi)}{\partial Z}+\frac{1}{4}\frac{\chi}{D}\frac{\partial(\rho D)}{\partial Z}\right]+$$
$$\frac{\partial Y_i}{\partial Z}\sum_{j=1}^{N_e}\sum_{k=1}^{N_s}\beta'_{jk}\left(\frac{1}{Le_k}-1\right)\left[\frac{\rho\chi}{2}\frac{\partial^2 Y_k}{\partial Z^2}+\frac{1}{4}\frac{\partial(\rho\chi)}{\partial Z}\frac{\partial Y_k}{\partial Z}+\frac{1}{4}\frac{\chi}{D}\frac{\partial(\rho D)}{\partial Z}\frac{\partial Y_k}{\partial Z}\right] \tag{3.35}$$
$$\text{for} \qquad i=1,\ldots,N_s-1.$$

Note that the term in the double summation arises due to the source term at the r.h.s. of the mixture fraction conservation equation (3.9). In section 3.1, the mixture fraction was defined as a linear combination of element mass fractions, which is the definition on which $P^i_\perp$ is based. Preferential diffusion along the x'_2 and x'_3 directions, represented by $P^i_\parallel$, can be written as

$$P^i_\parallel=-\frac{\partial Y_i}{\partial Z}\left(\frac{1}{Le_i}-1\right)\sum_{\eta=2}^{3}\left\{\frac{\partial Z}{\partial x_\eta}\frac{\partial(\rho D)}{\partial x'_\eta}\right\}+$$
$$\frac{\partial Y_i}{\partial Z}\sum_{j=1}^{N_e}\sum_{k=1}^{N_s}\beta'_{jk}\left(\frac{1}{Le_k}-1\right)\sum_{\eta=2}^{3}\left\{\frac{\partial Z}{\partial x_\eta}\frac{\partial(\rho D)}{\partial x'_\eta}\frac{\partial Y_k}{\partial x'_\eta}+2\rho D\frac{\partial Z}{\partial x_\eta}\frac{\partial^2 Y_k}{\partial Z\partial x'_\eta}\right.$$
$$\left.+\rho D\frac{\partial^2 Y_k}{\partial x'^2_\eta}+\frac{\partial Z}{\partial x_\eta}\frac{\partial(\rho D)}{\partial x'_\eta}\frac{\partial Y_k}{\partial Z}\right\} \qquad \text{for} \qquad i=1,\ldots,N_s-1. \tag{3.36}$$

Using the flamelet assumption, i.e. that perturbations perpendicular to the flame are much larger that perturbations along the flame, both $R^i_{\parallel}$ and $P^i_{\parallel}$ vanish. This leads to the following expression

$$\frac{\rho\chi}{2}\frac{1}{Le_i}\frac{\partial^2 Y_i}{\partial Z^2} + \dot{\omega}_i - P^i_{\perp} = 0 \qquad \text{for} \qquad i = 1, \ldots, N_s - 1. \tag{3.37}$$

The same coordinate transformation can be applied to the enthalpy equation (1.23), which will result in a preferential diffusion term for the enthalpy $P^h = P^h_{\perp} + P^h_{\parallel}$. However, this has not been done in this thesis.

Note that equation (3.37) cannot always be used to construct a manifold in Z-space. This is caused by the fact that when there is preferential diffusion, Z is no longer always continuously increasing. However, it will be used to evaluate the preferential diffusion terms, which gives an indication of what is neglected if $Le_i = 1$ is chosen.

3.2.4 Alternative approach to include preferential diffusion

Because the mixture fraction of the preferential diffusion flamelet model, which was derived in the previous section, may not be always continuously increasing, another flamelet model that also includes preferential diffusion will be discussed in this section. This alternative flamelet model has been derived by Peters in Pitsch [17]. Unlike the flamelet model derived in the previous section, the mixture fraction defined in this section is still continuously increasing.

In their paper, Peters and Pitsch show that the commonly used definitions for the mixture fraction can not be used easily to derive a conservation equation without the $Le_i = 1$ assumption. Therefore, Peters and Pitsch introduced an alternative definition for the mixture fraction. As mentioned before, there are several definitions for the mixture fraction. The two most commonly used are based on a one-step overall reaction and on the local element conservation equation, respectively. Peters and Pitsch define the mixture fraction directly as a conserved scalar in a two-feed system, being fuel and oxidiser. The mixture fraction obeys the following transport equation

$$\rho\frac{\partial Z}{\partial t} + \rho\mathbf{u}\cdot\nabla Z - \frac{1}{Le_Z}\nabla\cdot(\rho D\nabla\cdot Z) = 0, \tag{3.38}$$

where Le_Z is introduced as the mixture fraction Lewis number. Furthermore, Z is defined as being zero in one feed and unity in the second feed. For this definition no assumptions about Lewis numbers have been made. The result is that the mixture fraction distribution is only determined by the conservation equation and hence it is uncoupled completely from the local composition, i.e. this definition of Z no longer has a physical meaning if $Le_i \neq Le_Z$.

If a laminar counterflow diffusion flame is considered, a 1D set of equations can be derived and the governing transport equations for species mass fractions Y_i are given by

$$\rho\frac{\partial Y_i}{\partial t} + \rho u\frac{\partial Y_i}{\partial s} + \frac{\partial}{\partial s}\left(\rho Y_i V_i\right) - \dot{\omega}_i = 0 \qquad \text{for} \qquad i = 1, \ldots, N_s. \tag{3.39}$$

The diffusion velocity V_i, is defined as a combination of the species diffusion velocity V_i^D and a correction velocity V^C, i.e. $V_i = V_i^D + V^C$. The correction velocity arises due to the mass conservation constraint $\sum_{k=1}^{N_s} Y_k V_k = 0$. These velocities are defined as follows

$$V_i^D = -\frac{D}{Le_i Y_i}\frac{\partial Y_i}{\partial s} \qquad \text{for} \qquad i = 1, \ldots, N_s, \tag{3.40}$$

$$V^C = \sum_{k=1}^{N_s} \frac{D}{Le_k}\frac{\partial Y_k}{\partial s}. \tag{3.41}$$

Assuming that the Lewis numbers are constant throughout the domain, the resulting equation becomes

$$\rho\frac{\partial Y_i}{\partial t'} = \frac{\rho\chi}{2}\frac{Le_Z}{Le_i}\frac{\partial^2 Y_i}{\partial Z^2} + \dot{\omega}_i - P_\perp^{i,alt} \qquad \text{for} \qquad i = 1, \ldots, N_s, \tag{3.42}$$

where $P_\perp^{i,alt}$ represents an alternative expression for preferential diffusion, containing both contributions of V_i^D and V^C. This expression can be written as

$$\begin{aligned} P_\perp^{i,alt} = &-\frac{\partial Y_i}{\partial Z}\left(\frac{Le_Z}{Le_i} - 1\right)\left[\frac{1}{4}\frac{\partial \rho\chi}{\partial Z} + \frac{1}{4}\rho\chi Le_Z\frac{c_p}{\lambda}\frac{\partial}{\partial Z}\left(\frac{\lambda}{c_p Le_Z}\right)\right] + \\ &\sum_{k=1}^{N_s}\left[\frac{\rho\chi}{2}\frac{Le_Z}{Le_k}Y_i\frac{\partial^2 Y_k}{\partial Z^2} + \frac{1}{4}\frac{Le_Z}{Le_k}\left(\frac{\partial}{\partial Z}\left(\rho\chi Y_i\right) + \rho\chi Le_Z\frac{c_p}{\lambda}\frac{\partial}{\partial Z}\left(\frac{\lambda}{c_p Le_Z}Y_i\right)\right)\frac{\partial Y_k}{\partial Z}\right] \\ &\text{for} \qquad i = 1, \ldots, N_s. \end{aligned} \tag{3.43}$$

Furthermore, it is assumed that the Lewis number for the mixture fraction Le_Z, is equal to 1, and by using (1.17), $P_\perp^{i,alt}$ can be written as, cf. [17]

$$\begin{aligned} P_\perp^{i,alt} = &-\frac{\partial Y_i}{\partial Z}\left(\frac{1}{Le_i} - 1\right)\left[\frac{1}{4}\frac{\partial \rho\chi}{\partial Z} + \frac{1}{4}\frac{\chi}{D}\frac{\partial\left(\rho D\right)}{\partial Z}\right] + \\ &\sum_{k=1}^{N_s}\frac{1}{Le_k}\left[\frac{\rho\chi}{2}\frac{\partial^2 Y_k}{\partial Z^2}Y_i + \frac{1}{4}\frac{\partial\left(\rho\chi Y_i\right)}{\partial Z}\frac{\partial Y_k}{\partial Z} + \frac{1}{4}\frac{\chi}{D}\frac{\partial\left(\rho D Y_i\right)}{\partial Z}\frac{\partial Y_k}{\partial Z}\right] \\ &\text{for} \qquad i = 1, \ldots, N_s. \end{aligned} \tag{3.44}$$

Note that the first term is identical to the first term of $P_\perp^i$ (3.35). The second term arises due to the introduction of the correction velocity V^C. In the derivation of the preferential diffusion term $P_\perp^i$ of section 3.2.3, no correction velocity was introduced. Instead, mass conservation, i.e. $\sum_{k=1}^{N_s} Y_k V_k = 0$, is obeyed by using the following constraint for nitrogen

$$\sum_{k\neq N_2}^{N_s} Y_k V_k = -Y_{N_2} V_{N_2}. \tag{3.45}$$

If this approach is also followed here, the velocity correction terms will vanish from the $P_\perp^{i,alt}$ term. Then it is possible to express the preferential diffusion term $P_\perp^i$, from section 3.2.3, in terms of $P_\perp^{i,alt}$ as follows

$$\begin{aligned} P_\perp^i = P_\perp^{i,alt} + \frac{\partial Y_i}{\partial Z}\sum_{j=1}^{N_e}\sum_{k=1}^{N_s}\beta'_{jk}\frac{1}{Le_k}\left[\frac{\rho\chi}{2}\frac{\partial^2 Y_k}{\partial Z^2} + \frac{1}{4}\frac{\partial(\rho\chi)}{\partial Z}\frac{\partial Y_k}{\partial Z} + \frac{1}{4}\frac{\chi}{D}\frac{\partial(\rho D)}{\partial Z}\frac{\partial Y_k}{\partial Z}\right] \\ \text{for} \qquad i = 1, \ldots, N_s - 1, \end{aligned} \tag{3.46}$$

where the additional term with the double summation at the r.h.s. of (3.46) is the result of mixture fraction variations caused by preferential diffusion. These mixture fraction variations already appeared at the r.h.s. of the conservation equation of the mixture fraction (3.9). This means that if the same definition for Z is used as Peters and Pitsch use, i.e. equation (3.38), the preferential diffusion term $P_{\perp}^{i}$ equals $P_{\perp}^{i,alt}$.

3.3 Numerical analysis

In this section, a numerical analysis will be applied to calculate the order of magnitude of $P_{\perp}^{i}$, using CHEM1D [5]. Equation (3.35) will be evaluated with CHEM1D to calculate $P_{\perp}^{i}$. The flame used is a methane-air counterflow diffusion flame, which is a 2D geometry, see also figure 3.2. Fuel is flowing from the left side and air from the right side of the flame. The ambient pressure is 1 atm and the ambient temperature is 300 K. Furthermore it is assumed that the flame is stationary. To describe the 2D geometry with a 1D model, the flamelet equations (2.7)-(2.9) are solved in physical space, where the 2D effects are represented by the stretch term K, on the r.h.s. of these equations. This means that an additional equation for K has to be solved. This equation is a rewritten form of the momentum equation (1.7) in y-direction. The applied strain a is needed as a boundary condition to solve the equation for K, i.e. $K_{ox} = a$. Furthermore, ρK^2 at the oxidiser side is equal to ρK^2 at the fuel side, which leads to $K_{fu} = \sqrt{\frac{\rho_{ox}}{\rho_{fu}}} K_{ox}$. For additional information, see also [22]. Furthermore, it is assumed that there is no curvature, i.e. $\sigma = 1$. The reaction mechanism that is used is the Smooke mechanism [18]. The applied strain rate a was varied, i.e. $a = 100\ s^{-1}$, $a = 200\ s^{-1}$, $a = 300\ s^{-1}$ and $a = 400\ s^{-1}$. For the Lewis numbers, three cases are considered, $Le_i = 1$, $Le_i = 1.1$ and $Le_i = const$, see appendix A.

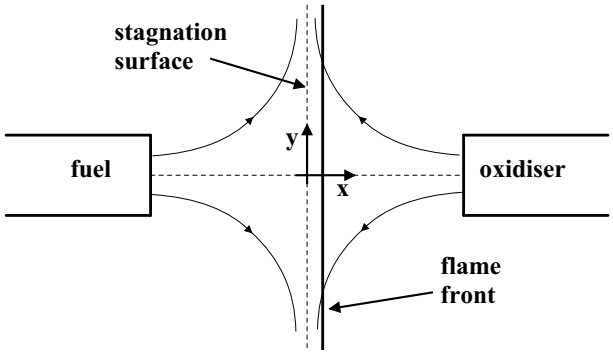

Fig. 3.2: Schematic representation of a diffusion counterflow geometry

1. Unity Lewis numbers for all species ($Le_i = 1$).

   This is not a very realistic case, but it will be used to obtain numerical results for the flamelet model derived in section 3.2.2. For this case it is obvious that equation (3.35) is equal to zero. Using the above assumptions, the r.h.s. of equations (3.5) and (1.23) then cancels, meaning that the element fractions and the enthalpy behave the same as the mixture fraction. This indicates that the element mass fractions and the mixture fraction should be linearly dependent on the mixture fraction.

2. All Lewis numbers are equal for all species ($Le_i = 1.1$).

   In this case there is only a difference between thermal conduction and mass diffusion. The mass diffusion is the same for all species and therefore it will have no contribution to the preferential mass diffusion term, see also equation (3.12). When all Lewis numbers are equal, equation (3.5) can be written analogous to equation (3.12), indicating that the element fractions behave the same way as the mixture fraction. The enthalpy equation (1.23) however, will have a source term on the r.h.s. of the equation. Because of this source term in the enthalpy equation, the enthalpy does not behave the same as the mixture fraction. This indicates that the element mass fractions again should be linearly dependent on the mixture fraction, while the enthalpy is not.

3. All Lewis numbers are constant, but different for all species ($Le_i = const$).

   This is a more realistic case, where all species have different Lewis numbers. These Lewis numbers can be found in appendix A. Now there is not only a difference between thermal conduction and mass diffusion, but all species experience a difference in diffusion as well. Now the r.h.s. of the equation for the element mass fractions (3.5) does not cancel. Generally, the r.h.s. of this equation will be different for each element. Because the mixture fraction is a linear combination of the element mass fractions, the element mass fractions are no longer linearly dependent on the mixture fraction. This is also true for the enthalpy.

3.3.1 Results for $Le_i = 1$

The assumption that all Lewis numbers are equal to $Le_i = 1$ is not very realistic, but this is the flamelet model that was derived by Peters. It will therefore be discussed here as a reference case for a non-preferential diffusion flame.

When all Lewis numbers are equal to 1, it follows from equation (3.35) that there is no preferential diffusion at all, see figure 3.3. The solid line represents the chemical source term, the dash-dotted line represents the diffusion term, and the dotted line is the preferential diffusion term. Furthermore, only two species are shown here. For the other species, the reader is referred to appendix B.1. Note that not the complete range of the mixture fraction domain is shown.

The flame is situated near $Z_{st} = 0.055$. All terms have been scaled according to $\tilde{\omega}_i = \dot{\omega}_i/\dot{\omega}_{i,max}$. The source term for CH_4 is negative, indicating that CH_4 is consumed, while the source term for H_2O is positive, meaning that H_2O is produced. The preferential diffusion term is equal to zero, not only for these two species, but for all species. This is exactly what is expected, because there is no preferability of mass diffusion between species. Hence, $P^i = 0$. The element mass fractions and the enthalpy are linearly dependent on the mixture fraction, and therefore will not be shown here. This figure, D.1, can be found in appendix D.1.

3.3.2 Results for $Le_i = 1.1$

When all Lewis numbers are equal to 1.1, equation (3.12) shows that there is only preferability of thermal conduction over mass diffusion. In figure 3.4 the scaled source terms and the preferential diffusion term for CH_4 (l) and for H_2O (r) can be seen.

The preferential diffusion term $P^i_\perp$ is still equal to zero, but this is also what is expected, because there is no preferability of mass diffusion between species, and hence, there is also

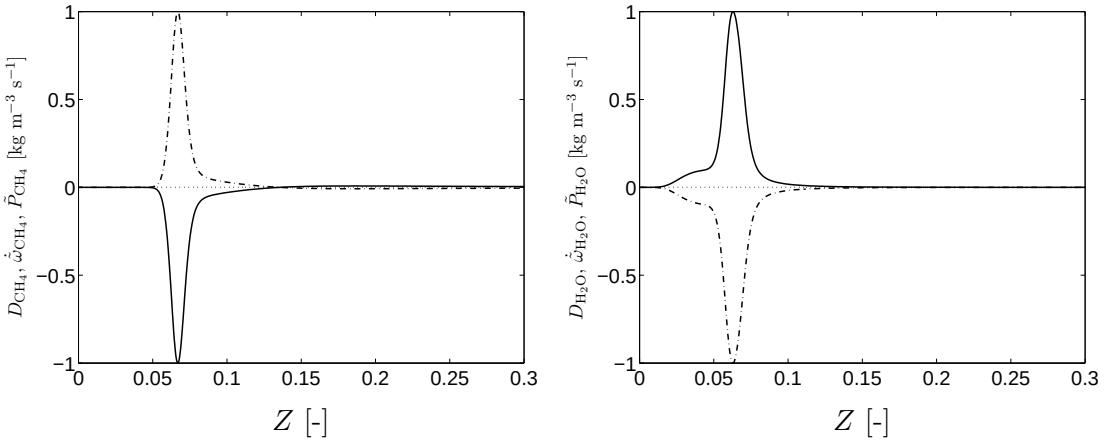

Fig. 3.3: Source term, preferential diffusion term and the diffusion term, as defined in (3.37), for CH_4 (l) and H_2O (r) as a function of the mixture fraction Z in a non-premixed counterflow flame with $Le_i = 1$ and $a = 100\ s^{-1}$. All terms are scaled with $\dot{\omega}_{i,max}$. Solid: scaled chemical source term; dash-dotted: diffusion term; dotted: preferential diffusion term.

no preferability of mass diffusion between species and the mixture fraction. The r.h.s. of the conservation equation the enthalpy (1.23), which represents enthalpy perturbations caused by preferential diffusion, does not reduce to zero. This indicates that the enthalpy is no longer linearly dependent on the mixture fraction, which can also be seen in figure 3.5. Here, the enthalpy can be seen for $Le_i = 1.1$ as a function of the mixture fraction. The enthalpy is scaled according to

$$\tilde{h} = \frac{h - h_{ox}}{h_{fu} - h_{ox}}. \tag{3.47}$$

The element mass fractions are still linearly dependent on the mixture fraction. This figure, D.2, can be found in appendix D.2.

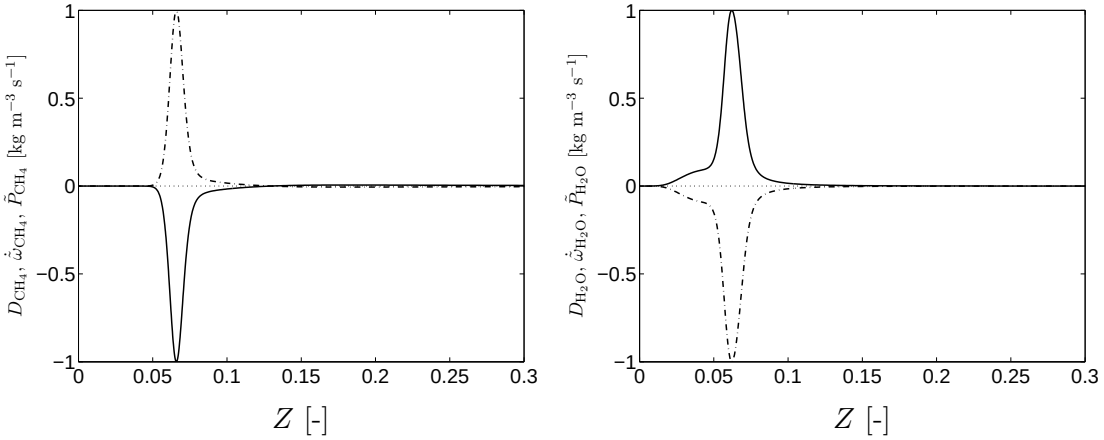

Fig. 3.4: Source term, preferential diffusion term and the diffusion term, as defined in (3.37), for CH_4 (l) and H_2O (r) as a function of the mixture fraction Z in a non-premixed counterflow flame with $Le_i = 1.1$ and $a = 100\ s^{-1}$. All terms are scaled with $\dot{\omega}_{i,max}$. Solid: scaled chemical source term; dash-dotted: diffusion term; dotted: preferential diffusion term.

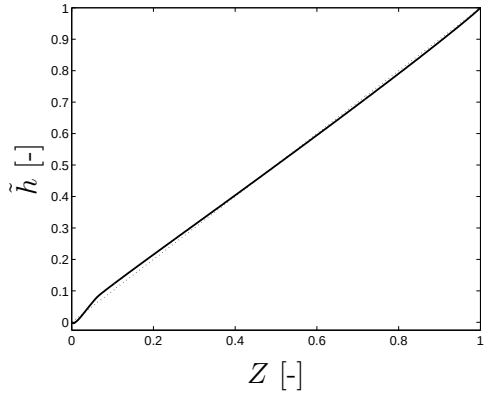

Fig. 3.5: Enthalpy, scaled according to (3.47). The dotted line represents the case that the enthalpy is linearly dependent on the mixture fraction.

3.3.3 Results for $Le_i = const$

A more realistic case is when all Lewis numbers are different, but constant, i.e. $Le_i = const$. The preferential mass diffusion is now described by equation (3.35). In figure 3.6 the chemical source term and preferential diffusion term are scaled according to $\tilde{\omega}_i = \dot{\omega}_i/\dot{\omega}_{i,max}$. Only 4 of the total 16 species are shown, i.e. CO_2 (top left), H_2O (top right) and two intermediate species, CH_3O (bottom left) and H_2 (bottom right). The profiles for the other species can be seen in appendix B. As can be seen, the preferential diffusion terms have their maximum value near the surface of stoichiometric mixture. This can be understood when considering that $\frac{\partial Y_i}{\partial Z}$ is at its maximum near Z_{st} for almost all species. In table 3.1, the ratios of the maximum value of the preferential diffusion terms and the maximum value of the chemical source terms can be seen. For $a = 100\ s^{-1}$, this ratio is about 14% for CO, while for CO_2 it is nearly 20%. For $a = 400\ s^{-1}$, the ratio of the maximum value of the preferential diffusion term and the maximum value of the chemical source term for CO is again about 14%, while for CH_3O and CO_2 it is up to 20%. For the remaining species this ratio remains below 10%.

Species	$P^i_\perp/\dot{\omega}_{i,max}$	**Species**	$P^i_\perp/\dot{\omega}_{i,max}$
CH_4	0.0508	H	0.0800
CH_3	0.0520	O_2	0.0001
CH_3O	0.0946	O	0.0113
CH_2O	0.0547	OH	0.0177
HCO	0.0449	HO_2	0.0002
CO_2	0.1825	H_2O	0.1141
CO	0.1422	H_2O_2	0.0001
H_2	0.0061	N_2	N.A.*

Species	$P^i_\perp/\dot{\omega}_{i,max}$	**Species**	$P^i_\perp/\dot{\omega}_{i,max}$
CH_4	0.0797	H	0.0744
CH_3	0.0849	O_2	0.0019
CH_3O	0.2002	O	0.0006
CH_2O	0.0887	OH	0.0033
HCO	0.0551	HO_2	0.0013
CO_2	0.2146	H_2O	0.0766
CO	0.1367	H_2O_2	0.0011
H_2	0.0097	N_2	N.A.*

Table 3.1: Ratio of the preferential diffusion term and the chemical source term of each species for a strain rate of $a = 100\ s^{-1}$ (l) and $a = 400\ s^{-1}$ (r).

In figure 3.7 the element mass fractions for carbon (tl), hydrogen (tr) and oxygen (bl) can be seen for $Le_i = const$, as well as the enthalpy (br). The enthalpy is again scaled according to (3.47), and the element mass fractions are scaled according to

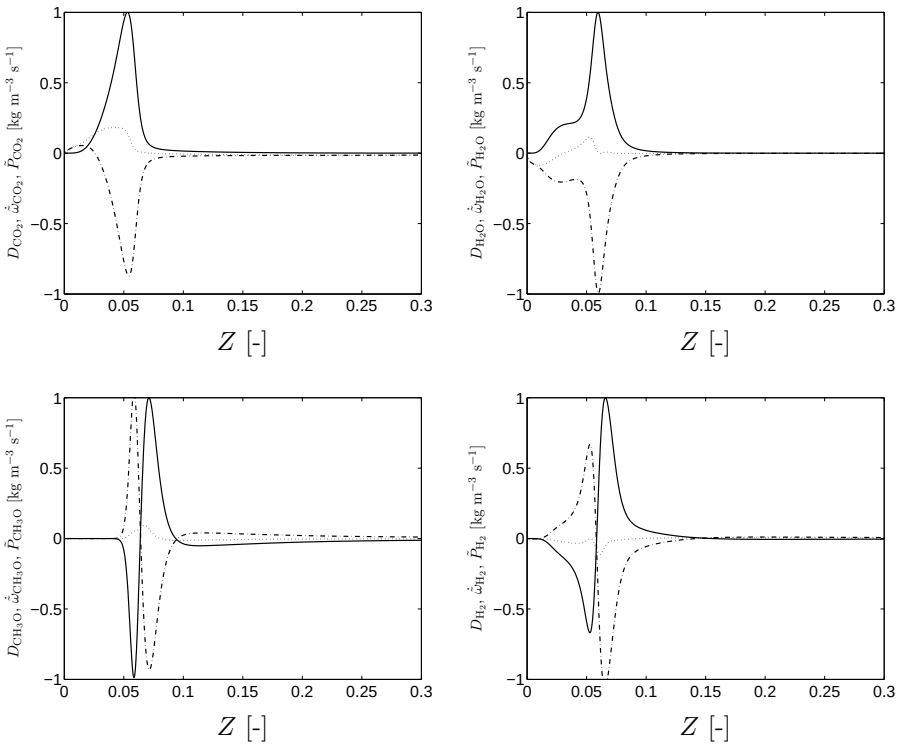

Fig. 3.6: Source term, preferential diffusion term and the diffusion term, as defined in (3.37) for CO_2 (tl), H_2O (tr), CH_3O (bl) and H_2 (br), as a function of the mixture fraction Z in a non-premixed counterflow flame with $Le_i = const$ and $a = 100\ s^{-1}$. All source terms and preferential diffusion terms are scaled with the maximum value of the source term. Solid: scaled chemical source term; dash-dotted: diffusion term; dotted: preferential diffusion term.

$$\tilde{Z}_j = \frac{Z_j - Z_{j,ox}}{Z_{j,fu} - Z_{j,ox}} \qquad \text{for} \qquad j = 1, \ldots, N_e. \tag{3.48}$$

Note that although there are preferential diffusion effects, Z is still continuously increasing. It must be noted however, that this is not generally the case. Now, the element mass fractions are no longer linearly dependent on the mixture fraction, see figure 3.7.

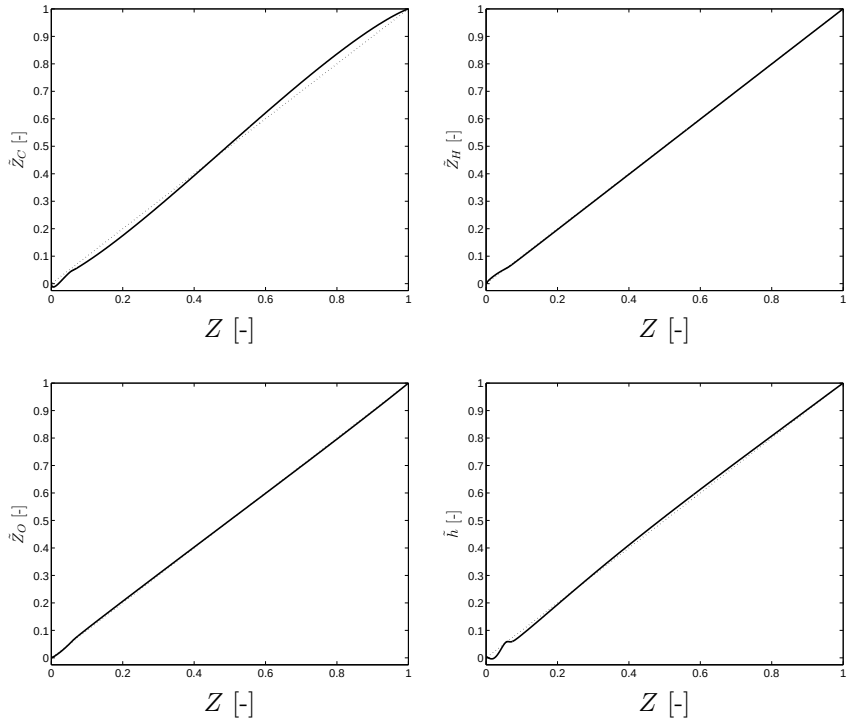

Fig. 3.7: Element mass fractions and enthalpy for $Le_i = const$. Shown here are carbon (tl), hydrogen (tr), oxygen (bl), which are scaled according to (3.48) and the enthalpy (br), scaled according to (3.47). The dotted line represents the case that the element mass fractions and the enthalpy are linearly dependent on the mixture fraction.

The actual effect of preferential diffusion on the diffusion flame structure, can be seen in figures 3.8 - 3.10. In these figures, the profiles for the mixture fraction (3.8), the temperature (3.9) and the scalar dissipation rate (3.10) are shown for two cases: the solid line represents the case without preferential diffusion and the dotted line is the case with preferential diffusion. The strain rates for these cases are $a = 100\ s^{-1}$ (l) and $a = 400\ s^{-1}$ (r). The difference in the mixture fraction profiles between the case without preferential diffusion and with preferential diffusion is about 2.51% for $a = 100\ s^{-1}$ and about 2.34% for $a = 400\ s^{-1}$. For the temperature, this difference between a flame without preferential diffusion and with preferential diffusion is 6.99% for $a = 100\ s^{-1}$, and for $a = 400\ s^{-1}$ this is also 6.36%, but this seems to be coincidental. The difference in the scalar dissipation rate between a flame without preferential diffusion and with preferential diffusion is about 22.8% for $a = 100\ s^{-1}$ and about 23.2% for $a = 400\ s^{-1}$. The maximum values of the profiles for the cases without preferential diffusion have been used as reference value. All these values, and also for $a = 200\ s^{-1}$ and $a = 300\ s^{-1}$ can be found in appendix C.

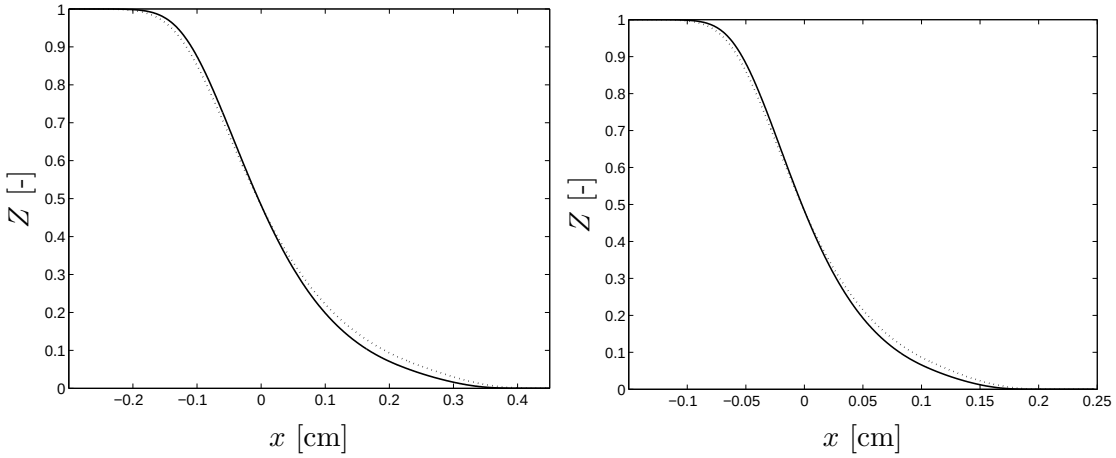

Fig. 3.8: The mixture fraction as a function of the position for two cases, i.e. $Le_i = 1$ and $Le_i = const$ with a strain rate of $a = 100\ s^{-1}$ (l) and $a = 400\ s^{-1}$ (r). Solid: no preferential diffusion; dotted: preferential diffusion.

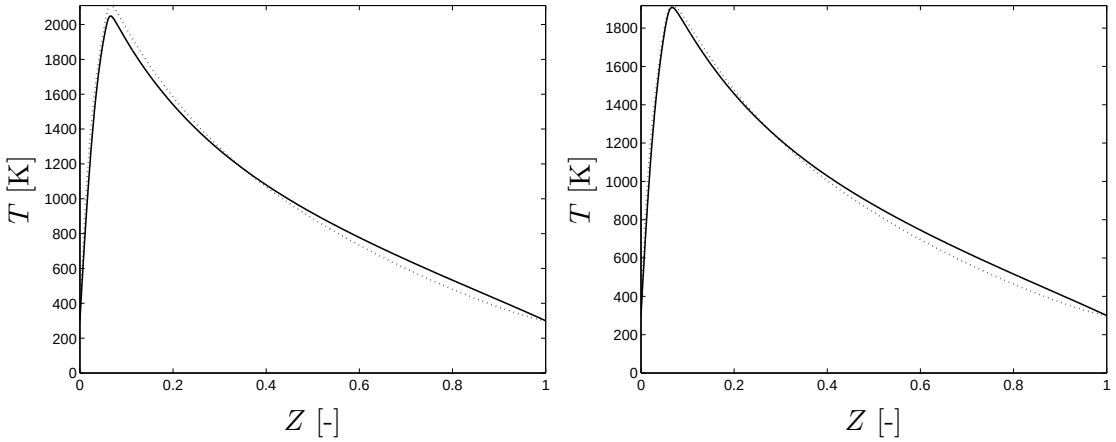

Fig. 3.9: The temperature as a function of the mixture fraction for two cases, i.e. $Le_i = 1$ and $Le_i = const$ with a strain rate of $a = 100\ s^{-1}$ (l) and $a = 400\ s^{-1}$ (r). Solid: no preferential diffusion; dotted: preferential diffusion.

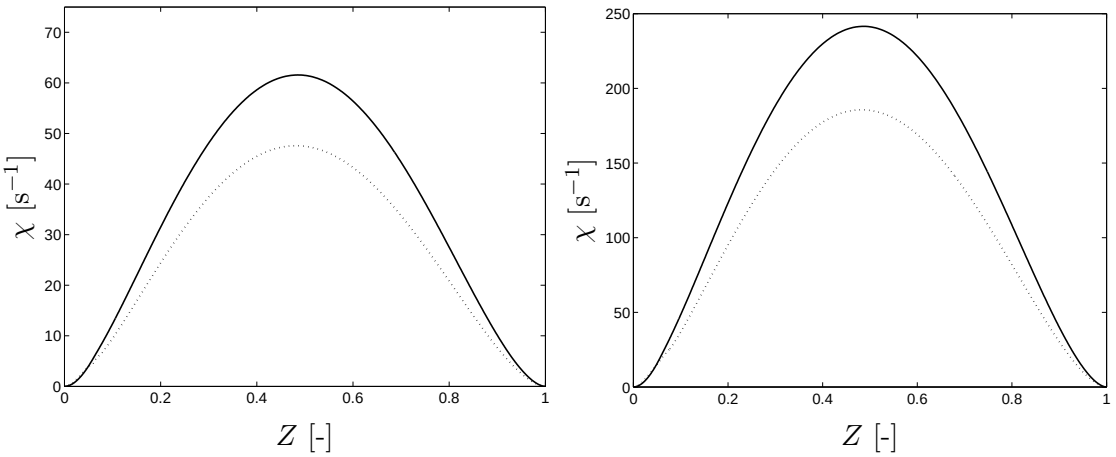

Fig. 3.10: The scalar dissipation rate as a function of the mixture fraction for two cases, i.e. $Le_i = 1$ and $Le_i = const$ with a strain rate of $a = 100\ s^{-1}$ (l) and $a = 400\ s^{-1}$ (r). Solid: no preferential diffusion; dotted: preferential diffusion.

3.4 Conclusions

In this chapter, first a flamelet model has been derived that does not include preferential diffusion, by assuming that $Le_i = 1$. The coordinate transformation discussed in this chapter has been used to write the conservation equations for species in a quasi-1D form (3.30). As a result, the spatial coordinate x_1 has been replaced by the mixture fraction coordinate Z. The resulting equation is a function of the mixture fraction Z and the scalar dissipation rate χ and can be used to construct a 2D flamelet database. This database can be used to find the flame structure that corresponds to certain values of Z and χ. This will be discussed in more detail in the next chapter.

Because the assumption that all Lewis numbers are unity is not very realistic, the coordinate transformation was repeated, only now, the $Le_i = 1$ assumption was not made, resulting in a flamelet model (3.37) that includes preferential diffusion terms, gathered in $P^i_\perp$.

An alternative approach to include preferential diffusion was introduced by Peters and Pitsch. They define the mixture fraction as a conserved variable, that obeys a transport equation that does not include preferential diffusion effects. Instead, the diffusion velocities of species i are defined as a combination of V^D_i and V^C, which are the diffusion velocity of species i and a correction velocity, respectively. The correction velocity V^C is used to preserve mass conservation. The resulting flamelet model also includes a preferential diffusion term, which shows a great similarity with the preferential diffusion term (3.35) derived in section 3.2.3. Differences are that $P^i_\perp$ contains a summation over all elements, while $P^{i,alt}_\perp$ does not. This is probably caused by the fact that the mixture fraction in section 3.2.3, was defined as a combination of element mass fractions. The mixture fraction of Peters and Pitsch on the other hand, is directly defined as a conserved variable, with a transport equation that does not include preferential diffusion effects. Furthermore, by defining the mixture fraction Z directly as a conserved variable, equation (3.38), Z will still be a continuously increasing variable. This may not be always the case when preferential diffusion is included and Z is based on species mass fractions. However, in the computations presented here, Z was found to be continuously increasing. If on the other hand, Z is no longer continuously increasing, it may no longer be used to construct a flamelet database.

In the final section of this chapter, the order of magnitude of $P^i_\perp$ and the effect of preferential diffusion on the density and the scalar dissipation rate have been calculated using the 1D solver CHEM1D. This has been done for 4 strain rates, of which only $a = 100s^{-1}$ and $a = 400s^{-1}$ were shown, because there was not much difference between these 4 strain rates. Furthermore, 3 different cases for the Lewis numbers have been considered, i.e. $Le_i = 1$, $Le_i = 1.1$ and $Le_i = const.$ As expected, $P^i_\perp = 0$ for the first two cases, which was also predicted by equations (3.11) and (3.12). The element mass fractions and the mixture fraction show a linear dependence for both $Le_i = 1$ and $Le_i = 1.1$. The enthalpy and the mixture fraction on the other hand, only have a linear dependency for $Le_i = 1$. When the Lewis numbers are different for all species and not equal to 1, there will be preferential diffusion, leading to a perturbation of the mixture fraction. In his paper, Peters [14] used the assumption that all Lewis numbers are equal to 1, which led to a flamelet model that excluded preferential diffusion effects. It has been shown in this chapter however, that when more realistic values for Lewis numbers are chosen, the preferential diffusion term for several species can be well over 10% of the chemical source term. Furthermore, differences can be seen in the mixture fraction profile, the temperature profile and the profile for the scalar dissipation rate. For $a = 100\ s^{-1}$, differences in the mixture fraction profiles are about 2.51%, differences in the

temperature profiles are about 6.99%, and for the scalar dissipation rate these differences are about 23% between the case with preferential diffusion and without preferential diffusion. This means that preferential diffusion effects cannot always be neglected. For $a = 400\ s^{-1}$, differences in the mixture fraction profiles, the temperature and scalar dissipation rate profiles are about the same as for $a = 100\ s^{-1}$.

Chapter 4

Diffusion flamelet database

During non-premixed flame calculations, the conservation equation for the mixture fraction, like (3.9) is solved, and the scalar dissipation rate is computed from equation (3.27). With the values for Z and χ, the flame structure can then be retrieved from the flamelet database. Such a diffusion flamelet database can be constructed by solving the 1D flamelet equations (3.37). If these equations are solved in mixture fraction space, the scalar dissipation rate, which is a function of spatial coordinates as defined by (3.27), cannot be solved. In order to close the set of equations, an analytical expression that relates χ only to Z has to be derived. This will be done in section 4.1. When diffusion flamelets are used to construct a database, commonly the mixture fraction Z and the stoichiometric value of scalar dissipation rate χ_{st} are used to parameterise a diffusion flame. The flamelet solutions that are stored in the database, are characterised by χ_{st}. During flame calculations, local values for the mixture fraction and the scalar dissipation rate, i.e. Z_l and χ_l are computed. The local value of the scalar dissipation rate χ_l, is generally not the same as its stoichiometric value χ_{st}. Therefore, the same analytical expression that is used as a closure model, will also be used to relate χ_l to χ_{st}. This will be explained in section 4.2. Using CHEM1D, the scalar dissipation rate has been calculated numerically as well. This numerical result will be compared with the theoretical scalar dissipation rate to analyse the accuracy of this approach, which will be done in section 4.3. Some conclusions will be drawn in section 4.4.

4.1 A theoretical model for the scalar dissipation rate

In this section a model describing the scalar dissipation rate for a counterflow configuration will be derived. Furthermore, a non-combusting system is assumed, meaning the density ρ and the diffusion constant D are constant.

A stationary counterflow geometry is considered, see figure 3.2. Furthermore, the system is assumed to be non-combusting, and only the velocity $\mathbf{u}$ is a function of both x and y, while the diffusion coefficient, the mixture fraction and the species mass fractions are a function of x only. Assuming that the density is constant, the conservation of mass equation (1.6) can be written as

$$\rho\frac{du}{dx} + \rho\frac{dv}{dy} = 0. \tag{4.1}$$

Assuming that the velocity in x-direction increases linear with x, i.e. $u = Ux$, equation (4.1)

indicates that the strain rate $\frac{dv}{dy} = a = -U$. The velocity u then becomes $u = -ax$. For the case that all Lewis numbers are unity, the equation for the mixture fraction (3.11) becomes

$$\frac{d}{dx}(\rho u Z) + \frac{d}{dy}(\rho v Z) - \frac{d}{dx}\left(\rho D \frac{dZ}{dx}\right) = 0. \tag{4.2}$$

This can also be written as

$$\rho u \frac{dZ}{dx} + \rho Z \frac{du}{dx} + \rho Z \frac{dv}{dy} - \frac{d}{dx}\left(\rho D \frac{dZ}{dx}\right) = 0. \tag{4.3}$$

Using (4.1) and $u = -ax$ equation (4.3) becomes

$$-\rho a x \frac{dZ}{dx} - \frac{d}{dx}\left(\rho D \frac{dZ}{dx}\right) = 0. \tag{4.4}$$

Note that for a non-combusting system, ρD is constant. Using the continuity equation, the above equation can be written as

$$-\rho a x \frac{dZ}{dx} = \rho D \frac{d^2 Z}{dx^2}, \tag{4.5}$$

Using the following substitution, $f = \frac{dZ}{dx}$, equation (4.5) becomes a first order differential equation

$$-\frac{a}{D} x dx = \frac{df}{f}. \tag{4.6}$$

The solution of equation (4.6) is

$$f = f_0 exp\left(-\frac{a}{2D}x^2\right). \tag{4.7}$$

The solution of the mixture fraction equation can be found by integration of equation (4.7), resulting in

$$Z(x) = \frac{1}{2}\sqrt{\frac{2\pi D}{a}} f_0 \text{ erf}\left(\frac{1}{2}\sqrt{\frac{2a}{D}}x\right) + C_0, \tag{4.8}$$

where 'erf' is known as the error-function. The boundary conditions are $Z(x \to -\infty) = 1$ and $Z(x \to \infty) = 0$. These boundary conditions are used to determine f_0 and C_0

$$f_0 = -\left(\sqrt{\frac{2\pi D}{a}}\right)^{-1},$$
$$C_0 = \frac{1}{2}.$$

Equation (4.8) can now be written as

$$Z(x) = \frac{1}{2}\text{erfc}\left(\frac{1}{2}\sqrt{\frac{2a}{D}}x\right), \tag{4.9}$$

with erfc the complementary error function, which is defined by $\text{erfc}(x) = 1 - \text{erf}(x)$. The inverse of equation (4.9) is

$$x = 2\left(\sqrt{\frac{2a}{D}}\right)^{-1} \text{erfc}^{-1}(2Z)\,. \tag{4.10}$$

Using equation (4.10) to replace x in equation (4.7) squared, leads to

$$f^2 = \left(\frac{dZ}{dx}\right)^2 = \frac{a}{2\pi D}\exp\left(-2\left[\text{erfc}^{-1}(2Z)\right]^2\right). \tag{4.11}$$

The model for the scalar dissipation rate χ_{m_1} can then be written as

$$\chi_{m_1} = \frac{a}{\pi}\exp\left(-2\left[\text{erfc}^{-1}(2Z)\right]^2\right), \tag{4.12}$$

where $\text{erfc}^{-1}(x)$ is the inverse of the complementary error function and not the reciprocal. Note that (4.12) is accurate only when there is a constant density.

4.2 Using the mixture fraction and the scalar dissipation rate as parameters

According to (3.37), the species mass fractions Y_i depend on the mixture fraction Z and the scalar dissipation rate χ. This allows for Z and χ to be used to construct a 2D manifold [16]. In a pre-processing step, flamelets are computed, where equation (4.12) is used as a closure model to calculate χ. Then, the flame structure is stored in a flamelet database as a function of Z and χ_{st}. Here, χ_{st} is the value the scalar dissipation rate has at the surface of stoichiometric mixture. During flame calculations, only Z and χ need to be calculated [16]. With these two values, equation (4.12) is used again, but now to relate the local value of χ to its stoichiometric value as follows

$$\frac{\chi}{\chi_{st}} = \frac{\chi_{m_1}}{\chi_{m_1,st}}, \tag{4.13}$$

where it is assumed that the scalar dissipation rate as described by the analytical model has the same shape as the actual scalar dissipation rate. Figure 4.1 shows the scalar dissipation rate as a function of the mixture fraction for an applied strain rate of $a = 100\ s^{-1}$.

Suppose that during flame calculations, the local value that is found for the scalar dissipation rate is the value that is denoted by $(Z_l,\ \chi_l)$. Equation (4.13) is then used to find the corresponding stoichiometric value for the scalar dissipation rate, denoted by $(Z_{st},\ \chi_{st})$. The stoichiometric value for χ can then be used to identify which flamelet solution from the flamelet database represents the local flow conditions that arise during flame calculation. Figure 4.2 shows the mass fractions of several species as a function of the mixture fraction, for two values of χ_{st}, i.e. $\chi_{st} = 4.19\ s^{-1}$ (l) and $\chi_{st} = 8.52\ s^{-1}$ (r). Generally, the value of χ_l does not match values of χ_{st} stored in the flamelet database. If, for instance, the value of χ_l is equal to $6.23\ s^{-1}$, there are two flamelets that closely describe the flamelet that corresponds to $\chi_l = 6.23\ s^{-1}$. As can be seen in figure 4.2 these are the flamelets that correspond to $\chi_{st} = 4.19\ s^{-1}$ (l) and $\chi_{st} = 8.52\ s^{-1}$ (r), respectively. Because the mixture fraction is also

known, the flame structures can now be retrieved from the flamelet database for these two flamelets. By way of interpolation, the correct flame structure can be determined.

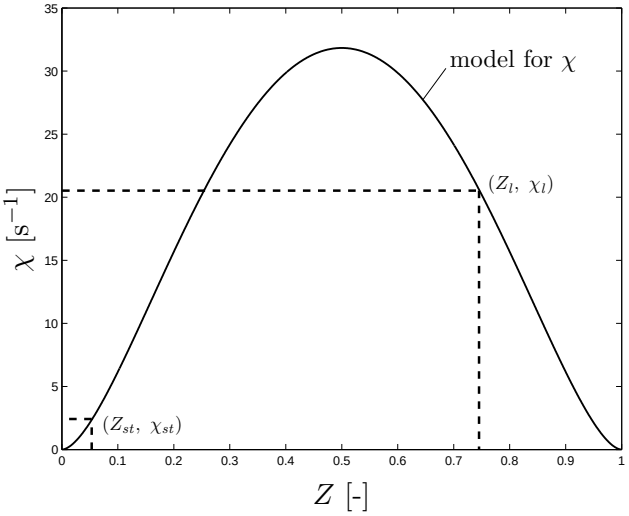

Fig. 4.1: A model for the scalar dissipation rate as defined by (4.12), which is used to relate the local value of the scalar dissipation rate, $(Z_l,\ \chi_l)$, to its stoichiometric value, $(Z_{st},\ \chi_{st})$.

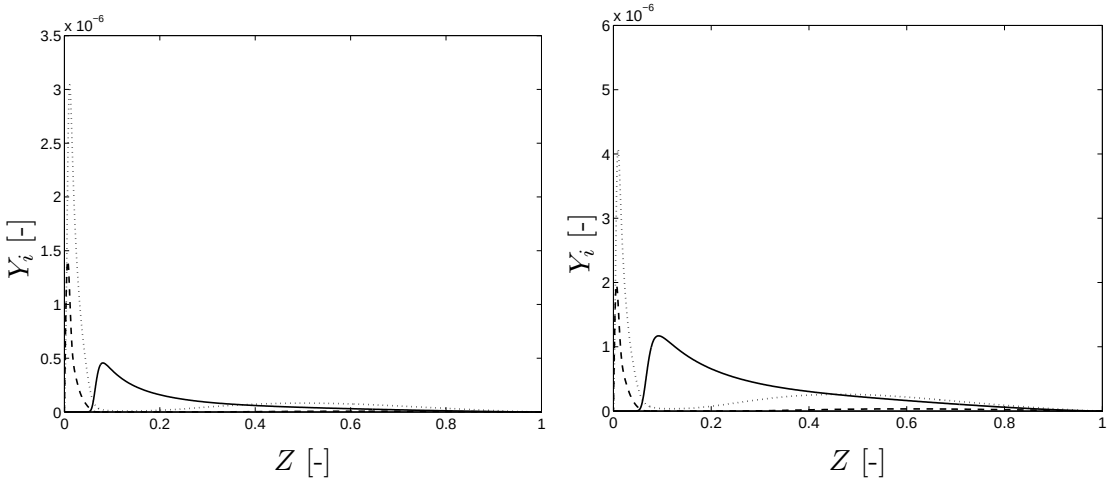

Fig. 4.2: Species mass fractions for two different values of χ_{st}, i.e. $\chi_{st} = 4.19\ s^-$ (l) and $\chi_{st} = 8.52\ s^-$ (r). The value of χ_{st} is used to identify the flamelet solution from the flamelet database that represents flow conditions that occur locally during flame calculations. When the local value of the scalar dissipation rate χ_l, lies between two values of χ_{st}, the flame structure can be found by using interpolation techniques. Solid: $Y_{\mathrm{CH_3O}}$; dotted: $Y_{\mathrm{HO_2}}$; dashed: $Y_{\mathrm{H_2O_2}}$.

4.3 Evaluation of the scalar dissipation rate model, using a numerical analysis

During the derivation of χ_{m_1}, the system was assumed to be non-combusting. Therefore, two non-combusting solutions has been calculated with CHEM1D, and the computed scalar dissipation rate χ_c will be compared with the modeled scalar dissipation rate χ_{m_1}. The first is a non-combusting solution of a non-premixed system, where the density at the fuel side differs from the density at the oxidiser side. This can be seen in figure 4.3 (r). This figure shows that there is still a relatively large difference with the model, because the density is not completely constant. In order to have (almost) equal densities at both sides, oxidiser has been added to the fuel side, and vice versa. This resulted in the following composition: $Y_{CH_4} = 0.61$, $Y_{O_2} = 0.19$, $Y_{N_2} = 0.20$ at the fuel side, and $Y_{CH_4} = 0.59$, $Y_{O_2} = 0.21$, $Y_{N_2} = 0.20$ at the oxidiser side of the flame. Because the left-side composition is not exactly the same as the right-side composition, it is still possible to use the mixture fraction Z to describe the system. This does imply that the value of Z_{st} will be different from the one used throughout this report. However, this is not of importance here, because only the influence of the density is studied here. This can be seen in figure 4.3 (l), where the scalar dissipation rate computed with CHEM1D χ_c, nicely matches the modeled scalar dissipation rate χ_{m_1} as expected.

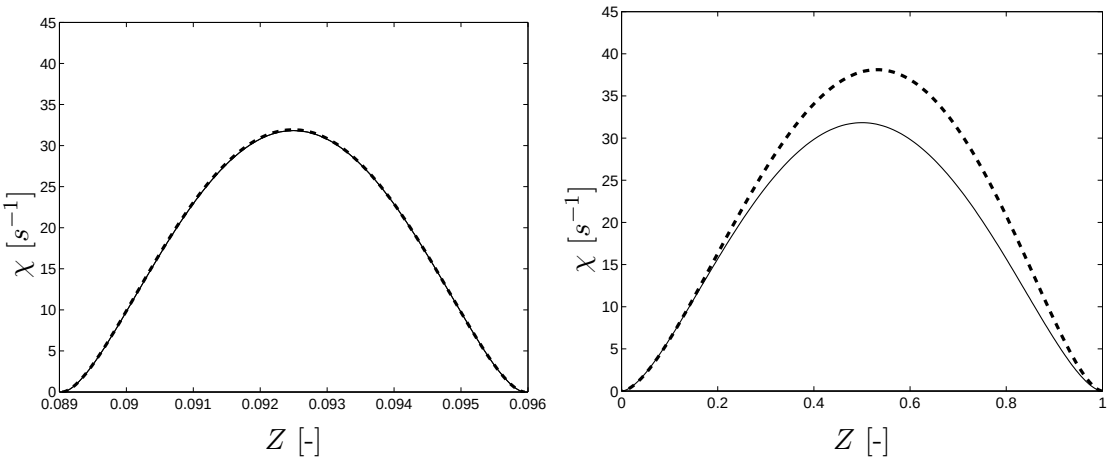

Fig. 4.3: Scalar dissipation rate for two non-reacting gas flows, with a constant density (l), and a non-constant density (r). The mixture that has a constant density has a different composition than the non-premixed flames used throughout this report, meaning that Z_{st} will have a different value. However, this is not of importance here, because only the influence of the density is shown here.

The assumption that the density is constant, is not valid for a combustion system. This will result in larger differences between χ_{m_1} and χ_c. In figures 4.4 and 4.5, a comparison between χ_{m_1} and the one computed with CHEM1D χ_c, can be seen. Both the computed scalar dissipation rate χ_c and the modeled scalar dissipation rate χ_{m_1} have been scaled according to equation 4.13, making both equal to 1 at Z_{st}. Two strain rates are shown, i.e. $a = 100\ s^{-1}$ and $a = 400\ s^{-1}$. The theoretical scalar dissipation rate is symmetrical with respect to $Z = 0.5$, whereas the scalar dissipation rate computed with CHEM1D is not. This is caused by the difference in density at the oxidiser side and at the fuel side of the flame. As can be seen, the maximum, relative differences, i.e. $(\chi_c - \chi_{m_1})/\chi_{m_1}$, are not very large for $Le_i = 1$. For $a = 100\ s^{-1}$ this difference is about 8.3%, while for $a = 400\ s^{-1}$ it is about 7.8%. These

differences become larger when more realistic Lewis numbers are used, i.e. $Le_i = const$, i.e. 15.6% for $a = 100\ s^{-1}$ and 18.5% for $a = 400\ s^{-1}$. The other values can be seen in table 4.1.

To account for variable density effects, the following theoretical scalar dissipation rate can be used [17]

$$\chi_{m_2} = \frac{a_{ox}}{4\pi} \frac{3\left(\sqrt{\frac{\rho_{ox}}{\rho}} + 1\right)^2}{2\sqrt{\frac{\rho_{ox}}{\rho}} + 1} \exp\left(-2\left[\mathrm{erfc}^{-1}\left(2Z\right)\right]^2\right). \tag{4.14}$$

Note that for this model, there is a dependence on the density ρ. Analogous to (4.12), equation (4.14) can be used to relate the local value of the scalar dissipation rate to its stoichiometric value as follows

$$\frac{\chi}{\chi_{st}} = \frac{\chi_{m_2}}{\chi_{m_2,st}}, \tag{4.15}$$

where ρ_{st} is local the density at the stoichiometric mixture fraction. In figure 4.6, χ_{m_2} has been compared with χ_{m_1} and χ_c. As can be seen, the second model for the scalar dissipation rate, χ_{m_2} is better than the first model, χ_{m_1} for the case that $Le_i = const$. In appendix F, the relative maximum difference between χ_{m_1} and χ_c, and between χ_{m_2} and χ_c can be found. Note that in order to evaluate equation (4.15), the profile of the density has to be known. However, it was stated that during the computation of flamelets in Z-space, χ is used as an independent parameter, which seems not to be possible when (4.15) is used, because the density profile is not known. The density profiles were obtained by computing flamelets with CHEM1D. While this is not the way to do it, it does give an idea of the accuracy of equation (4.15). If however, equation (4.15) is used in combination with (3.37) to compute flamelets, then the density has to be computed by other means, which would be very interesting to study.

4.4 Conclusions

When diffusion flamelets are used to model diffusion flames, the characteristic parameters are the mixture fraction Z and the scalar dissipation rate at stoichiometric value χ_{st}. During complex flame calculations, the local values Z_l and χ_l are used in equation (4.12) to find the stoichiometric value for χ. This stoichiometric value can then be used to find the correct flamelet in the database. After that, using Z, the composition of the mixture can be determined. Using CHEM1D, it has been shown in this chapter that there is a significant difference between the numerical and theoretical values of χ_{st}. This is because it was assumed that the density is constant, while this is clearly not the case when combustion is taking place. By using equation (4.12), it is assumed that χ and χ_{st} have the same dependence as χ_{m_1} and $\chi_{m_1,st}$. It has been shown that this is reasonable for the case that $Le_i = 1$, however, for $Le_i = const$ this is not the case. Differences between these profiles have been shown to be about 15% for an applied strain of $a = 100\ s^{-1}$ and about 18% for an applied strain of $a = 400\ s^{-1}$. The local value of the scalar dissipation rate χ_l, is related to its stoichiometric value by way of an analytical model. Differences between the modeled stoichiometric scalar dissipation rate χ_{m_1} and the scalar dissipation rate as computed with CHEM1D χ_c have been shown to be up to 18%. This can also lead to inaccurate results when this value for χ_{st} is used as a lookup parameter in the diffusion flamelet method. It would therefore be interesting

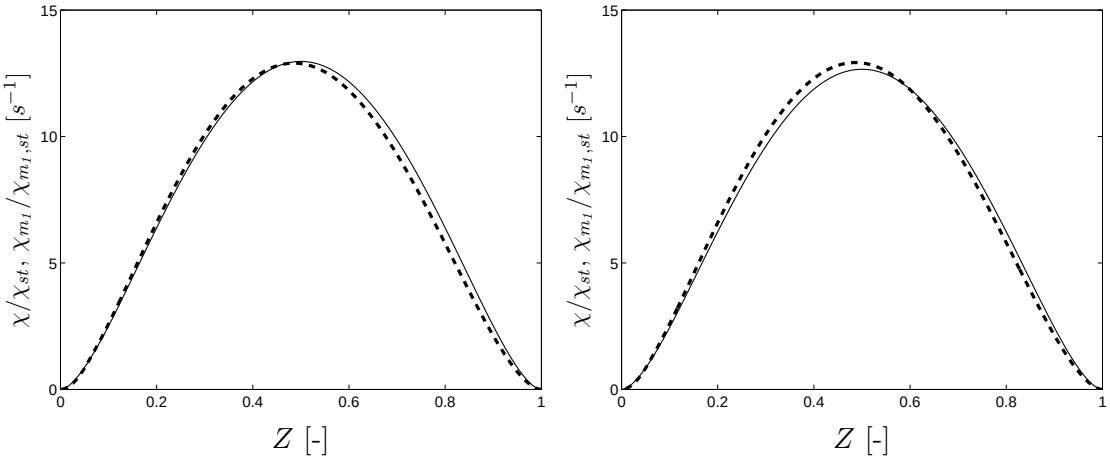

Fig. 4.4: Comparison of the modeled scalar dissipation rate χ_{m_1} and the scalar dissipation rate as computed with CHEM1D for $Le_i = 1$. The two strain rates are $a = 100\ s^{-1}$ (l) and $a = 400\ s^{-1}$ (r). Solid: model (4.12); dotted: CHEM1D.

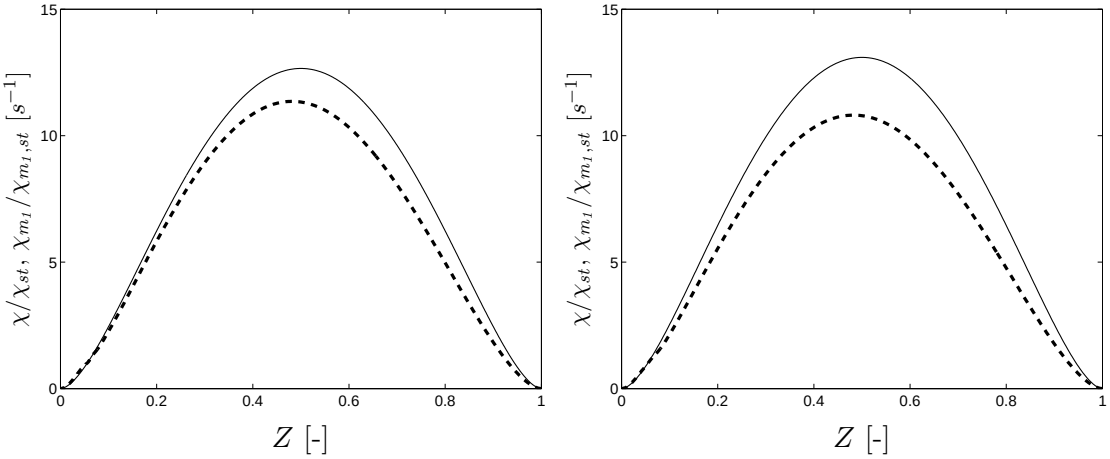

Fig. 4.5: Comparison of the modeled scalar dissipation rate χ_{m_1} and the scalar dissipation rate as computed with CHEM1D for $Le_i = const$. The two strain rates are $a = 100\ s^{-1}$ (l) and $a = 400\ s^{-1}$ (r). Solid: model (4.12); dotted: CHEM1D.

Applied strain	$\Delta\chi/\chi_{m_1,st}$
$a = 100\ s^{-1}$	0.083763
$a = 200\ s^{-1}$	0.080739
$a = 300\ s^{-1}$	0.078856
$a = 400\ s^{-1}$	0.077568

Applied strain	$\Delta\chi/\chi_{m_1,st}$
$a = 100\ s^{-1}$	0.074339
$a = 200\ s^{-1}$	0.073816
$a = 300\ s^{-1}$	0.072095
$a = 400\ s^{-1}$	0.070869

Applied strain	$\Delta\chi/\chi_{m_1,st}$
$a = 100\ s^{-1}$	0.156102
$a = 200\ s^{-1}$	0.170330
$a = 300\ s^{-1}$	0.180136
$a = 400\ s^{-1}$	0.184809

Table 4.1: The maximum difference between the model for the scalar dissipation rate and the scalar dissipation rate computed with CHEM1D for $Le_i = 1$ (l), $Le_i = 1.1$ (c) and $Le_i = const$ (r).

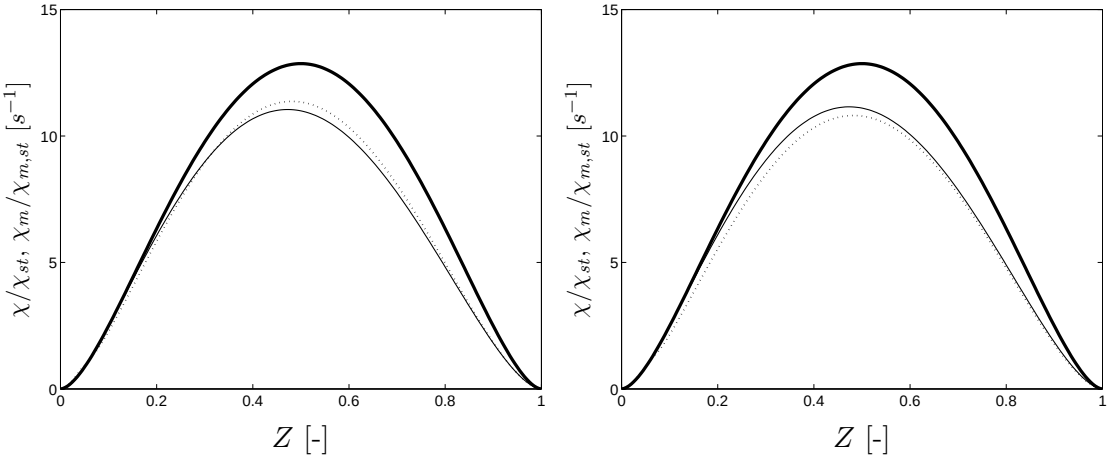

Fig. 4.6: Comparison of 2 models for the scalar dissipation rate, i.e. χ_{m_1} and χ_{m_2}, and the scalar dissipation rate as computed with CHEM1D for $Le_i = const.$ The two strain rates are $a = 100\ s^{-1}$ (l) and $a = 400\ s^{-1}$ (r). Thick solid: model 1 (4.12); thin solid: model 2 (4.14); dotted: CHEM1D.

to investigate the magnitude of the errors that arise in the flame structure when the value of χ_{st} is not predicted accurately. If however, an improved model for χ_m that also takes density effects that arise in a non-combusting system, is included, the model becomes more accurate.

Chapter 5

Conclusions and recommendations

5.1 Conclusions

This report serves as a starting point in the development of a reduction technique that is based on a diffusion flamelet model, analogous to the Flamelet Generated Manifolds or Phase-Space Intrinsic Low-Dimensional Manifolds methods for (partially) premixed flames. Ultimately, a systematic reduction method based on a **unified** flamelet model, applicable to both premixed and non-premixed flames, may be developed. The goal of the report is to study the diffusion flamelet model, and the underlying assumptions, as introduced by Peters. Both the flamelet model itself and the way a diffusion flamelet database is used is studied in this report.

The first step is to study and compare the existing reduction techniques. Therefore, a brief overview has been given of various reduction methods in chapter 2. It can be concluded that there are reduction methods that can be applied to both premixed and non-premixed flames, like the Conventional Reduction Method and the Intrinsic Low-Dimensional Manifolds method. However, these reduced mechanisms are based on chemistry only, which may lead to inaccuracies in colder flame regions. Other methods like the Flamelet Generated Manifolds method and the Phase-Space Intrinsic Low-Dimensional Manifolds method, based on a premixed flamelet model, overcome this problem. With the FGM method, a manifold is constructed by solving premixed flamelets, which include convection and diffusion, and storing the solutions in a database. With the PS-ILDM method, a time-scale analysis is applied to the reactive-diffusive system, which is derived from premixed flamelet equations. Including convection and diffusion in the manifolds gives more accurate results for (partially) premixed flames. However, their applicability to diffusion flames remains questionable.

Therefore, a reduction technique based on a diffusion flamelet model should be developed, analogous to the FGM method. Before such a new reduction method can be developed, an initial study into a diffusion flamelet model has been done in chapter 3. The diffusion flamelet model that was studied, was first introduced by Peters [14], and it was assumed that $Le_i = 1$. This means that preferential diffusion effects are neglected. To evaluate the effect of this assumption, the flamelet model was extended to include preferential diffusion. When for this model, $Le_i = 1$ is chosen, this model reduces to Peters' original flamelet model. If $Le_i = const$, where $Le_i \neq Le_k$, is chosen, the mixture fraction as defined in the flamelet model that includes preferential diffusion is no longer guaranteed to be continuously increasing. Therefore, another diffusion flamelet model, developed by Peters and Pitsch, was presented. It was shown that this alternative flamelet model, which also includes preferential

diffusion, has great similarities with the preferential diffusion flamelet model that was derived in this report. For the preferential diffusion flamelet model derived in this report, the order of magnitude of the preferential diffusion terms has been calculated and compared to the order of magnitude of the chemical source terms. It was shown that the preferential diffusion terms for several species can be about 20% of the chemical source terms. By comparing the profiles of the mixture fraction, the temperature and the scalar dissipation rate for $Le_i = 1$ with the profiles for $Le_i = const$, the effect of preferential diffusion can be further quantified. The differences for the mixture fraction profile have been shown to be 2.51% for $a = 100\ s^{-1}$ and 2.34% for $a = 400\ s^{-1}$. For the temperature, this difference is 6.99% for $a = 100\ s^{-1}$ and 6.36% for $a = 400\ s^{-1}$, and for the scalar dissipation rate this difference is 22.8% for $a = 100\ s^{-1}$, and for $a = 400\ s^{-1}$ this is 23.2%.

When diffusion flamelets are used to construct a flamelet library, commonly the mixture fraction and the stoichiometric value of the scalar dissipation rate are used as lookup parameters. During complex flame calculations, only the conservation equation for the mixture fraction is solved. The scalar dissipation rate is calculated with equation (3.27). The local value of χ will most likely not be the stoichiometric value, which means that the local value of χ first has to be related to its stoichiometric value. This can be achieved by using an analytical model, where χ is expressed as a function of Z. In chapter 4, such a model for the scalar dissipation rate was derived, where it was assumed that the profile of the scalar dissipation rate as computed with CHEM1D has the same shape as the profile of the modeled scalar dissipation rate. It has been shown that this is reasonable for the case that $Le_i = 1$. However, for $Le_i = const$ this is not the case. Differences between these profiles have been shown to be about 15% for an applied strain of $a = 100\ s^{-1}$ and about 18% for an applied strain of $a = 400\ s^{-1}$.

Using an analytical expression to relate the local value of the scalar dissipation rate to its stoichiometric value, combined with the $Le_i = 1$ assumption can lead to errors in the flamelet database. During flame calculations, a flamelet database is used to retrieve the flame structure, where χ_{st} is used as a lookup parameter in the diffusion flamelet method. It would therefore be interesting to investigate the magnitude of the errors that arise in the flame structure when the value of χ_{st} is not accurately predicted.

5.2 Recommendations

In this section, recommendations for future research will be given. First, recommendations will be given on how to further test the diffusion flamelet model that was developed by Peters, which was presented in chapter 3. This will be done in section 5.2.1. After that, in section 5.2.2, recommendations will be given on how a reduction method that is based on a diffusion flamelet model may be developed. There are several directions that can be followed, and they will be discussed briefly. And finally, a general outline and initial ideas on how to develop a unified flamelet theory will be given in section 5.2.3.

5.2.1 Further testing of the diffusion flamelet model

In order to get a more complete overview of the accuracy of the existing, standard diffusion flamelet model, several additional tests need to be done. As mentioned in chapter 3, it would be interesting to calculate the order of magnitude of the tangential transport $R^i_{\|}$ and

tangential preferential diffusion $P^i_{\parallel}$, and compare them with the chemical source terms or with the preferential diffusion terms $P^i_{\perp}$. This can be tested by using a 2D flame geometry. It would be also interesting to apply the coordinate transformation of De Goey and Ten Thije Boonkkamp [6] to derive a diffusion flamelet model, and to see if there is a difference between the tangential terms of that flamelet model compared to the tangential terms of the flamelet model derived by Peters.

Deriving a diffusion flamelet model that is based on the coordinate transformation of De Goey and Ten Thije Boonkkamp will now be briefly discussed. First a kinematic equation, like (2.4), for the mixture fraction will be introduced as follows

$$\frac{dZ}{dt} \equiv \frac{\partial Z}{\partial t} + \mathbf{u}_f \cdot \nabla Z = 0, \tag{5.1}$$

which means that a point on a $Z = const$ surface stays on this surface for all t, and describes the movement of the flame. Furthermore, the velocity S_C is introduced according to $\mathbf{u}_f = \mathbf{u} + S_C\mathbf{n}$. Here, $\mathbf{u}$ is the local fluid velocity and $\mathbf{u}_f$ is the velocity of flame-surface, see figure 5.1 for a schematic representation of a curvilinear coordinate system attached to iso-surfaces of a non-premixed flame. The local normal vector is defined as

$$\mathbf{n} = -\frac{\nabla Z}{|\nabla Z|}, \tag{5.2}$$

directed to the oxidiser side of the flame. The velocity S_C will be very similar to the burning velocity S_L of premixed flames, at least its definition. The physical interpretation of this velocity is still unclear for diffusion flames and has to be studied in detail. With the definition of the consumption velocity S_C, equation (5.1) can be written as

$$\frac{\partial Z}{\partial t} + \mathbf{u} \cdot \nabla Z = S_C |\nabla Z|, \tag{5.3}$$

which is similar to the so-called G-equation. The next step is to introduce a coordinate transformation that describes the flamelet equations in a flame adapted coordinate system, with spatial coordinates, that is locally orthogonal, and with the axes adapted to the iso-surfaces of Z as in figure 5.1. The main difference with the approach that Peters followed is that Peters attaches the coordinate system only to the surface of the stoichiometric mixture fraction. This means that the coordinate system is only orthogonal at the surface of stoichiometric mixture. The equations that describe conservation of mass, species mass fractions and enthalpy are given by the set of equations (2.7)-(2.9). It is likely that the tangential terms $R^i_{\parallel}$ and $P^i_{\parallel}$, as defined in this report are different from the tangential terms of equations (2.7)-(2.9), and it would be interesting to evaluate these terms, using a 2D flame geometry. The 1D flamelet equations can be computed with CHEM1D and compared for both coordinate transformations as well.

The continuity equation can be written such that all perturbations from 1D flame behaviour are gathered in the so-called stretch-rate K on the r.h.s. of the equation, and curvature effects are represented by the flame-surface σ. The next step would be to introduce a conservation equation for the scalar variable Z, which is similar to the conservation equation for the mixture fraction as introduced by Peters and Pitsch. Combining the rearranged continuity equation, the kinematic and the conservation equations for Z, a quasi-1D equation for the mixture fraction can be found. Assuming a flat 1D flame with no curvature, i.e. $K = 0$ and $\sigma = 1$, leads to a set of 1D non-premixed flamelet equations.

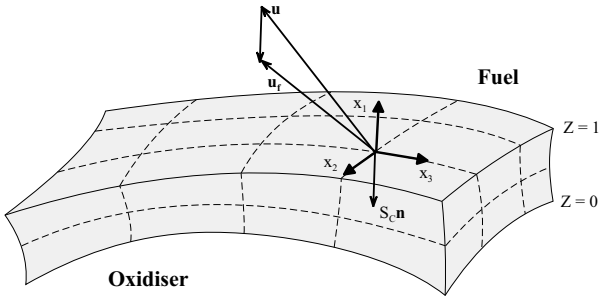

Fig. 5.1: Curvilinear coordinate system attached to a non-premixed flame

The mixture fraction for the diffusion flamelet model that was derived in section 3.2.3, is no longer guaranteed to be always continuously increasing. Therefore, another diffusion flamelet model has to be used to construct a diffusion flamelet database. Such a model was developed by Peters and Pitsch, and has been briefly discussed in this report. However, a more extensive study of that diffusion flamelet model has to be done as well. For that model, the mixture fraction has been directly defined as a conserved variable. While this ensures that the mixture fraction is continuously increasing, the mixture fraction is no longer coupled with the local composition.

Although the order of magnitude of the preferential diffusion effects has been calculated, it remains to be seen what the effect of preferential diffusion is, when a diffusion flamelet model is used to construct a diffusion flamelet database according to Peters [16]. An interesting test case would be to construct two diffusion flamelet databases, one with preferential diffusion effects and one without. To construct these diffusion flamelet databases, different flamelets can be solved with CHEM1D for a counterflow diffusion flame geometry. These diffusion flamelet databases can then be used to retrieve the flame structure during complex flame computations, using Z and χ_{st} as lookup parameters. The results generated with the database that includes preferential diffusion will likely differ from the results generated with the database that does not contain preferential diffusion effects.

For the scalar dissipation rate, several assumptions have been made. One of these assumptions is that the scalar dissipation profile as computed with CHEM1D can be described by a profile that corresponds to an analytical model. This assumption has been tested in chapter 4 of this report. Furthermore, by relating the local value of the scalar dissipation rate χ_l to the stoichiometric value by using the same analytical model, it is also assumed that the profiles of the scalar dissipation rate of complex 3D flame structures, can be described by this model as well. The validity of this assumption can be tested by doing complex 3D flame computations. The profile of the scalar dissipation rate can then be extracted by reconstructing flamelets from the 3D computations. After identifying iso-surfaces of the mixture fraction, Z is known as a function of the position. The scalar dissipation rate, which is defined by equation (3.27), can now be determined and compared to the profile of the modeled scalar dissipation rate.

When diffusion flamelets are used to construct a database, using an analytical expression to relate the local value of the scalar dissipation rate to its stoichiometric value may lead to inaccurate results. This still has to be tested, which can be done by constructing a flamelet database using the diffusion counterflow geometry. The mixture fraction and the stoichiometric value of the scalar dissipation rate are used as lookup variables. If it is shown that there are significant inaccuracies, then an improved model for the scalar dissipation rate should be

used. One of the improvements could be to include density variations in the model. Such a model is already available, i.e. equation (4.14), but this model has not been thoroughly tested in this report.

5.2.2 Development of a reduction method based on a diffusion flamelet model

When a reduction technique is developed based on diffusion flamelets, the goal is to capture multiple time-scales in the manifold. Traditionally the scalar dissipation rate has been used in the diffusion flamelet approach [16]. The question is whether the scalar dissipation rate is a suitable controlling variable when a reduced mechanism is constructed. When species mass fractions are used to include more time-scales in the manifold, the dimension of the manifold can be increased, whereas this is not straightforward when the stoichiometric value of the scalar dissipation rate is used to parameterise a diffusion flamelet database. To this end, a comparison of a database using Z and χ_{st} has to be made with a database using Z and Y_{cv}, where Y_{cv} can be a species mass fraction or a linear combination of species mass fractions.

The reduction technique that will be based on a diffusion flamelet model, describing the inner structure of a diffusion flame, will have its roots in the flamelet approach. The implementation on the other hand, which is to include multiple time-scales, is similar to reduction techniques, as is the case with FGM and PS-ILDM. Therefore, it may be better to use species mass fractions, or linear combinations of species mass fractions, as lookup parameters instead of χ_{st}. When species mass fractions are used as a lookup parameter, it has to be ensured that flamelet solutions are uniquely parameterised.

The next step would be the developmednt of a systematic reduction technique analogous to the Flamelet Generated Manifolds method or the Phase-Space Intrinsic Low-Dimensional Manifolds method for diffusion flames. Like the FGM method, a diffusion flamelet model can be used to compute a whole range of different flamelets, which can then be stored as a diffusion flamelet manifold. These flamelets can be parameterised by the mixture fraction, and species mass fractions may be used as additional controlling variables. Another possibility would be the development of a reduction method analogous to the PS-ILDM method, which can be done by using the existing, standard non-premixed flamelet model of Peters, or by deriving a new non-premixed flamelet model by applying the coordinate transformation of De Goey and Ten Thije Boonkkamp [6]. The choice of which non-premixed flamelet model will be used, can be based on the outcome of the additional study of the non-premixed flamelet models as outlined in section 5.2.1. The construction of the manifold can then be done by performing a time-scale analysis of the reactive-diffusive system, analogous to the PS-ILDM method.

5.2.3 Development of a unified flamelet theory

When a reduction technique that is based on a non-premixed flamelet models has been derived and tested, a reduction method based on a unified flamelet model may be developed. First a **unified flamelet model** has to be derived, after which a **unified reduction technique** can be developed.

The idea behind a unified flamelet model is that the same equations that describe premixed flamelets can be used to describe diffusion flamelets. Furthermore, the idea is that differences between premixed and non-premixed systems may only lead to different boundary conditions. If that is the case, a so-called unified reduction technique can be developed analogous to

either the FGM method or PS-ILDM method. It cannot yet be said which approach should be followed. This unified reduction method could be used to construct a manifold that encompasses both premixed and non-premixed compositions. There are applications, where during complex flame calculations, the complete range between premixed and non-premixed compositions are encountered. The manifold found with the unified reduction technique can then be used to retrieve the local composition. The so-called triple flame, as described in [22] would be a suitable configuration to test the unified reduction technique, because this flame contains both regions that can be considered a premixed flame, as well as regions that are more like diffusion flames.

List of symbols

Roman

a	strain rate	s^{-1}
a_{jk}	number of elements j in species k	-
C_0	integration constant	-
c_p	specific heat	$\mathrm{J\ kg^{-1}\ K^{-1}}$
c_{p_i}	partial specific heat	$\mathrm{J\ kg^{-1}\ K^{-1}}$
$\boldsymbol{\mathcal{D}}$	binary mass diffusion coefficient	$\mathrm{m^2\ s^{-1}}$
D	diffusion coefficient	$\mathrm{m^2\ s^{-1}}$
D_{im}	mixture-average diffusion coefficient	$\mathrm{m^2\ s^{-1}}$
f	substitution variable	$\mathrm{m^{-1}}$
$\mathbf{g}$	gravitational acceleration	$\mathrm{m\ s^{-2}}$
h	enthalpy density	$\mathrm{J\ kg^{-1}}$
h_i	enthalpy density of species i	$\mathrm{J\ kg^{-1}}$
h_i^*	enthalpy density of formation	$\mathrm{J\ kg^{-1}}$
$\boldsymbol{\mathcal{I}}$	unit tensor	-
$\mathbf{J}$	Jacobian	$\mathrm{s^{-1}}$
K	stretch rate	$\mathrm{s^{-1}}$
Le_i	Lewis number	-
Le_Z	mixture fraction Lewis number	-
$\bar{M}$	mean molar mass	$\mathrm{kg\ mol^{-1}}$
M_i	molar mass of species i	$\mathrm{kg\ mol^{-1}}$
m	mass burning rate	$\mathrm{kg\ m^{-2}\ s^{-1}}$
N_r	number of reactions	-
N_s	number of species	-
N_{ss}	number of steady-state species	-
$\mathbf{n}$	normal vector	-
n	molar concentration	$\mathrm{mol\ m^{-3}}$
n_i	molar concentration of species i	$\mathrm{mol\ m^{-3}}$
$\boldsymbol{\mathcal{P}}$	stress tensor	$\mathrm{kg\ m^{-1}\ s^{-2}}$
P^i	preferential diffusion term	$\mathrm{kg\ m^{-3}\ s^{-1}}$
$P^{i,alt}$	alternative preferential diffusion term	$\mathrm{kg\ m^{-3}\ s^{-1}}$
p	hydrostatic pressure	Pa
p_i	partial pressure	Pa
Q_i	transport of species i along the flame surface	$\mathrm{kg\ m^{-3}\ s^{-1}}$
Q_h	transport of enthalpy along the flame surface	$\mathrm{J\ m^{-3}\ s^{-1}}$
$\mathbf{q}$	heat flux	$\mathrm{J\ m^{-2}\ s^{-1}}$

R	universal gas constant	J mol^{-1} K^{-1}
R^i	transport tangent to flame surface	kg m^{-3} s^{-1}
r_j	reaction rate	mol m^{-3} s^{-1}
S_C	consumption velocity	m s^{-1}
S_L	burning velocity	m s^{-1}
s	arc length	m
T	temperature	K
t	time	s
$\mathbf{u}$	average flow velocity	m s^{-1}
$\mathbf{u}_f$	local velocity of the flame surface	m s^{-1}
$\mathbf{u}_i$	particular velocity of species i	m s^{-1}
u	velocity in x-direction	m s^{-1}
$\mathbf{V}_i$	diffusion velocity of species i	m s^{-1}
V^C	diffusion correction velocity	m s^{-1}
V_i^D	species diffusion velocity	m s^{-1}
v	velocity in y-direction	m s^{-1}
w	velocity in z-direction	m s^{-1}
w_{jk}	mass fraction of elements j in species k	-
X_i	species mole fraction	-
x	space coordinate	m
$\boldsymbol{\mathcal{Y}}$	progress variable	-
Y_i	species mass fraction	-
y	space coordinate	m
Z	mixture fraction	-
Z^*	unscaled mixture fraction	mol kg^{-1}
Z_j	element mass fraction	-
z	space coordinate	m

Greek

β_j	specific stoichiometric factor of element j	mol kg^{-1}
$\beta_{jk}^{'}$	stoichiometric factor of element j in species k	-
$\boldsymbol{\Theta}$	vector containing source terms of Y_i and ψ_i	-
λ	heat conductivity	J K^{-1} m^{-1} s^{-1}
λ_i	eigenvalue	s^{-1}
μ	dynamic viscosity	kg m^{-1} s^{-1}
ν	kinematic viscosity	m^2 s^{-1}
ν_{ij}	stoichiometric coefficient	-
ρ	mass density	kg m^{-3}
ρ_i	mass density of species i	kg m^{-3}
σ	surface	m^2
$\boldsymbol{\tau}$	viscous stress tensor	Pa
χ	scalar dissipation rate	s^{-1}
ψ_i	diffusive flux of species i	kg m^{-2} s^{-1}
ψ_h	diffusive flux of enthalpy	J kg^{-1} m^{-1}
$\boldsymbol{\Omega}$	vector containing Y_i, h, ψ_i and ψ_h	-

$\dot{\omega}_i$	chemical source term	kg m^{-3} s^{-1}

Subscripts

$\perp$	perpendicular direction
$\parallel$	tangential direction
b	burnt
c	value computed with CHEM1D
co	correction
cv	controlling variable
fu	fuel
h	enthalpy based
i	species index
j	element index
k	species index
l	local value from detailed computation
m	mixture index
max	maximum value
m_1	model 1
m_2	model 2
ox	oxidiser
pd	preferential diffusion
r	reaction index
ss	steady state
st	stoichiometric
u	unburnt
x	x-component
y	y-component
z	z-component
η	tangential component

Superscripts

0	initial state
$\tilde{}$	scaled quantity
$*$	reference state
$\bar{}$	mean quantity
alt	alternative model

Appendix A

Species Lewis numbers for the case that $Le_i = const$

Species	Le_i	**Species**	Le_i
CH_4	0.7796	H	0.1750
CH_3	0.9671	O_2	1.0796
CH_3O	1.2858	O	0.6992
CH_2O	1.2649	OH	0.7148
HCO	1.2568	HO_2	1.0663
CO_2	1.3354	H_2O	0.8226
CO	1.0880	H_2O_2	1.0693
H_2	0.2988	N_2	N.A.*

Table A.1: Species Lewis numbers for $Le_i = const$.

Appendix B

Individual contributions of $\dot{\omega}_i$, $P_\perp^i$ and the diffusion term

B.1 $Le_i = 1$

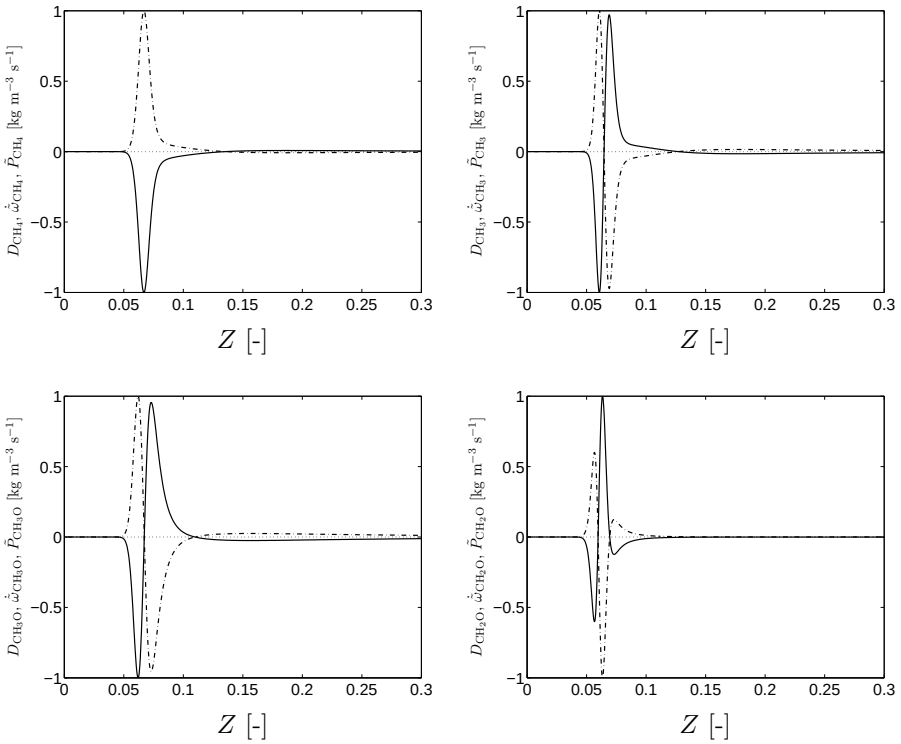

Fig. B.1: Source term, diffusion term and preferential diffusion term for CH_4 (tl), CH_3 (tr), CH_3O (bl) and CH_2O (br) as a function of the mixture fraction Z in a non-premixed counterflow flame with $Le_i = 1$ and $a = 100\ s^{-1}$. All terms are scaled with $\dot{\omega}_{i,max}$. Solid: scaled chemical source term; dash-dotted: diffusion term; dotted: preferential diffusion term.

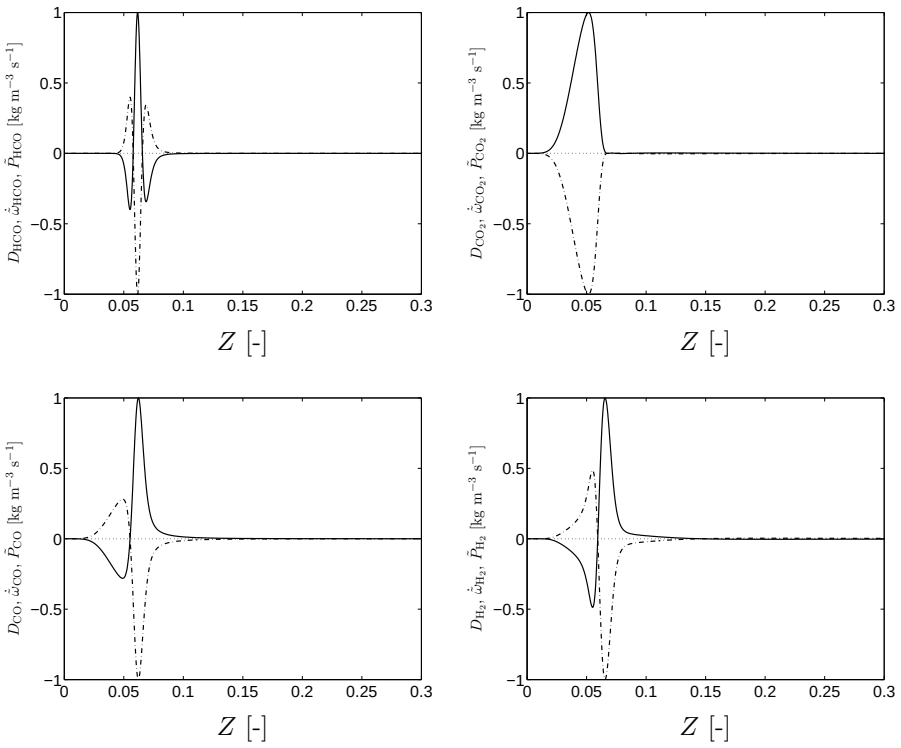

Fig. B.2: Source term, diffusion term and preferential diffusion term for HCO (tl), CO_2 (tr), CO (bl) and H_2 (br) as a function of the mixture fraction Z in a non-premixed counterflow flame with $Le_i = 1$ and $a = 100\ s^{-1}$. All terms are scaled with $\dot{\omega}_{i,max}$. Solid: scaled chemical source term; dash-dotted: diffusion term; dotted: preferential diffusion term.

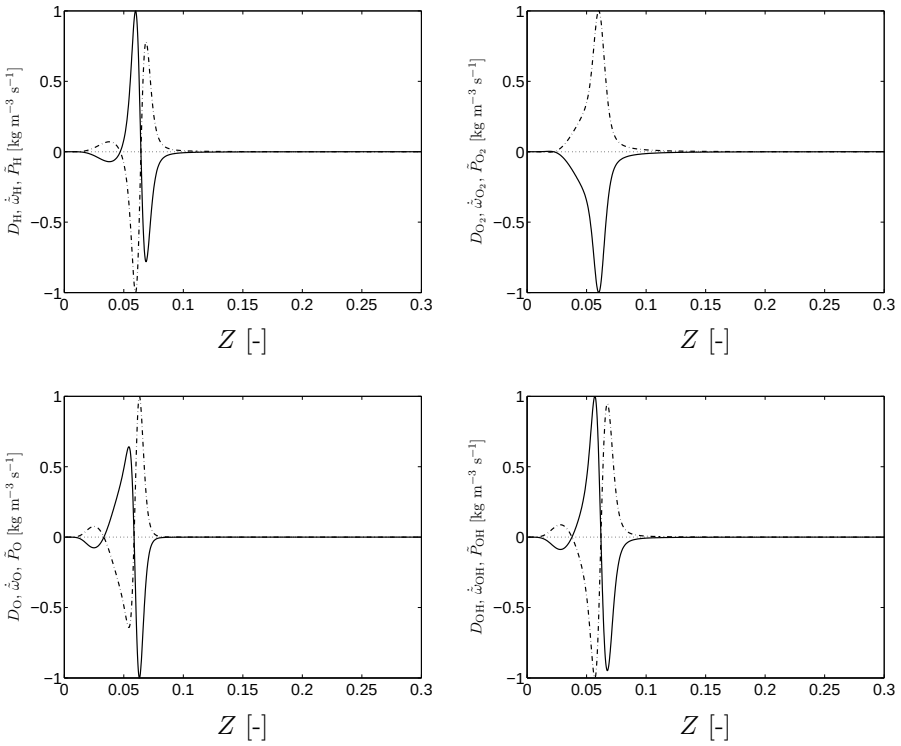

Fig. B.3: Source term, diffusion term and preferential diffusion term for H (tl), O_2 (tr), O (bl) and OH (br) as a function of the mixture fraction Z in a non-premixed counterflow flame with $Le_i = 1$ and $a = 100\ s^{-1}$. All terms are scaled with $\dot{\omega}_{i,max}$. Solid: scaled chemical source term; dash-dotted: diffusion term; dotted: preferential diffusion term.

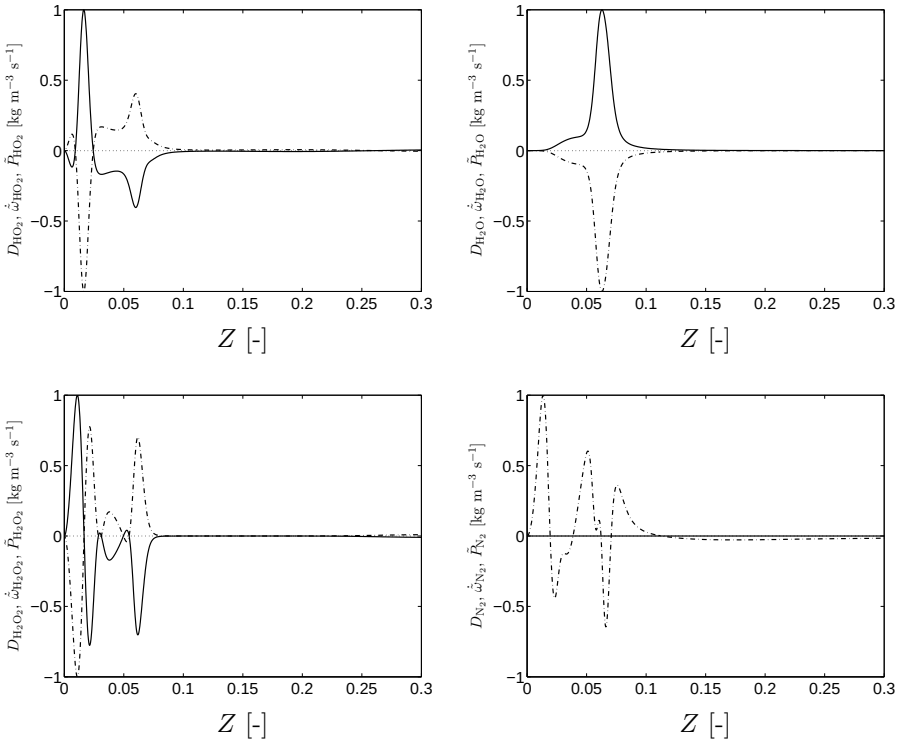

Fig. B.4: Source term, diffusion term and preferential diffusion term for HO_2 (tl), H_2O (tr), H_2O_2 (bl) and N_2 (br) as a function of the mixture fraction Z in a non-premixed counterflow flame with $Le_i = 1$ and $a = 100\ s^{-1}$. All terms are scaled with $\dot{\omega}_{i,max}$. Note that for N_2 the following equation was used: $\sum_{k \neq N_2}^{N_s} Y_k V_k = -Y_{N_2} V_{N_2}$. Solid: scaled chemical source term; dash-dotted: diffusion term; dotted: preferential diffusion term.

B.2 $Le_i = 1.1$

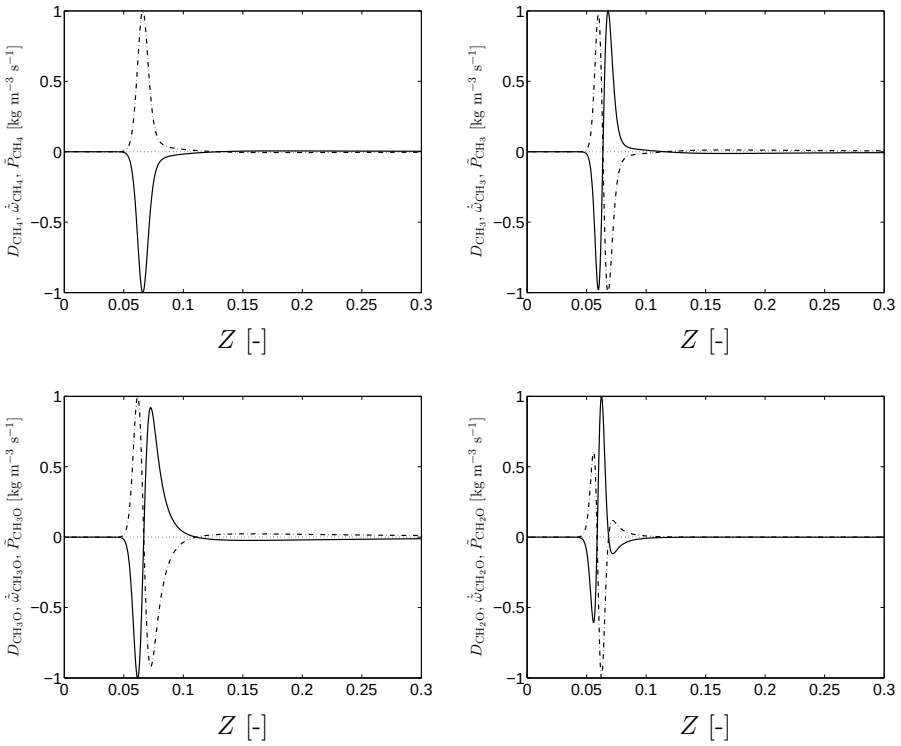

Fig. B.5: Source term, diffusion term and preferential diffusion term for CH_4 (tl), CH_3 (tr), CH_3O (bl) and CH_2O (br) as a function of the mixture fraction Z in a non-premixed counterflow flame with $Le_i = 1.1$ and $a = 100\ s^{-1}$. All terms are scaled with $\dot{\omega}_{i,max}$. Solid: scaled chemical source term; dash-dotted: diffusion term; dotted: preferential diffusion term.

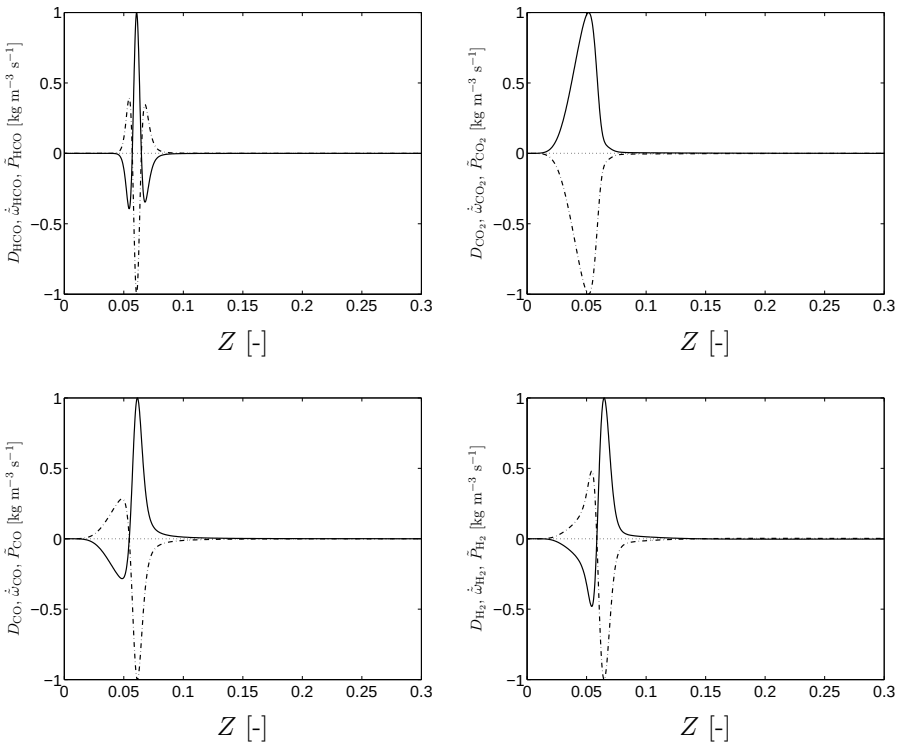

Fig. B.6: Source term, diffusion term and preferential diffusion term for HCO (tl), CO_2 (tr), CO (bl) and H_2 (br) as a function of the mixture fraction Z in a non-premixed counterflow flame with $Le_i = 1.1$ and $a = 100\ s^{-1}$. All terms are scaled with $\dot{\omega}_{i,max}$. Solid: scaled chemical source term; dash-dotted: diffusion term; dotted: preferential diffusion term.

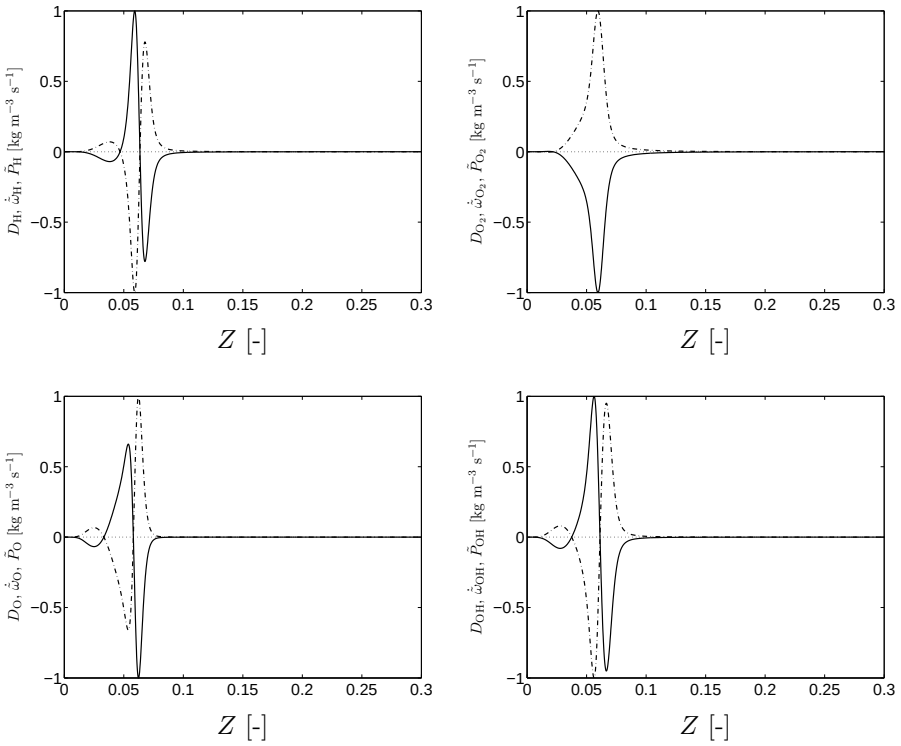

Fig. B.7: Source term, diffusion term and preferential diffusion term for H (tl), O_2 (tr), O (bl) and OH (br) as a function of the mixture fraction Z in a non-premixed counterflow flame with $Le_i = 1.1$ and $a = 100\ s^{-1}$. All terms are scaled with $\dot{\omega}_{i,max}$. Solid: scaled chemical source term; dash-dotted: diffusion term; dotted: preferential diffusion term.

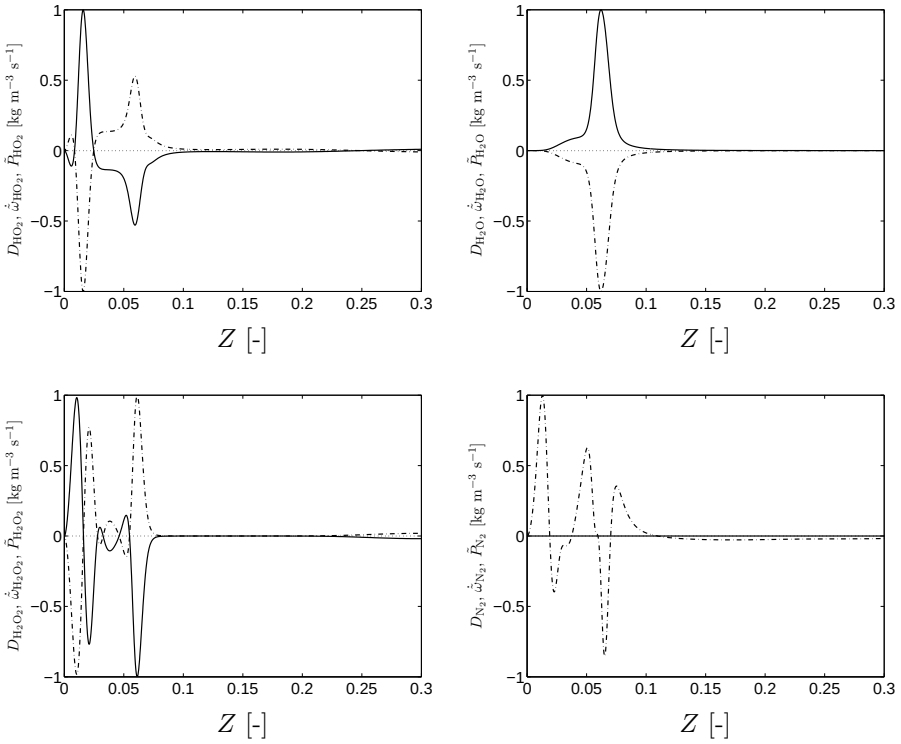

Fig. B.8: Source term, diffusion term and preferential diffusion term for HO_2 (tl), H_2O (tr), H_2O_2 (bl) and N_2 (br) as a function of the mixture fraction Z in a non-premixed counterflow flame with $Le_i = 1.1$ and $a = 100\ s^{-1}$. All terms are scaled with $\dot{\omega}_{i,max}$. Note that for N_2 the following equation was used: $\sum_{k \neq N_2}^{N_s} Y_k V_k = -Y_{N_2} V_{N_2}$. Solid: scaled chemical source term; dash-dotted: diffusion term; dotted: preferential diffusion term.

B.3 $Le_i = const$

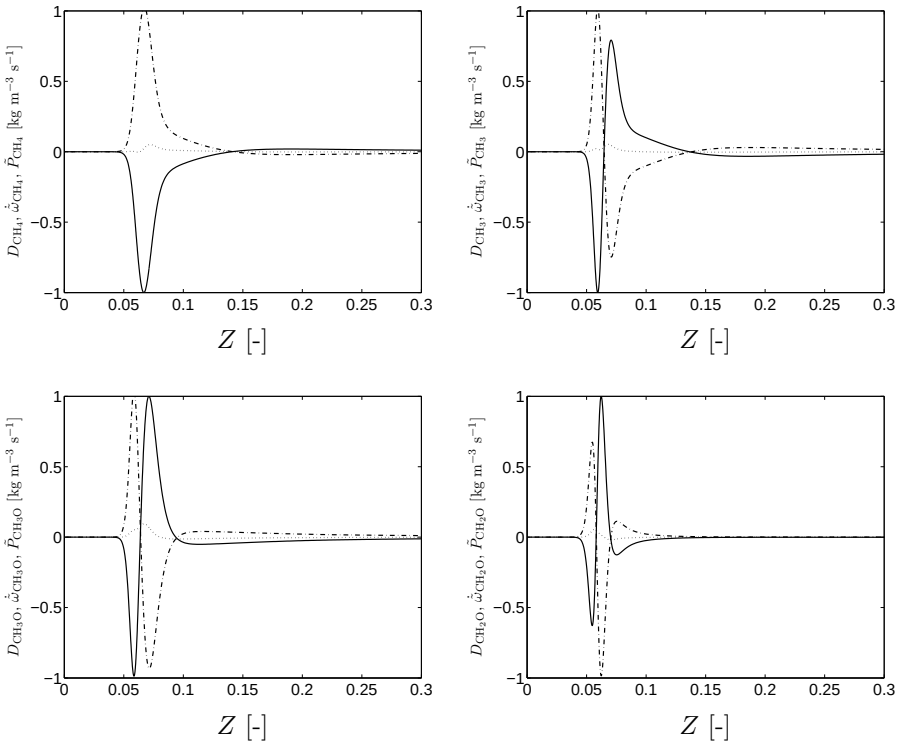

Fig. B.9: Source term, diffusion term and preferential diffusion term for CH_4 (tl), CH_3 (tr), CH_3O (bl) and CH_2O (br) as a function of the mixture fraction Z in a non-premixed counterflow flame with $Le_i = const$ and $a = 100\ s^{-1}$. All terms are scaled with $\dot{\omega}_{i,max}$. Solid: scaled chemical source term; dash-dotted: diffusion term; dotted: preferential diffusion term.

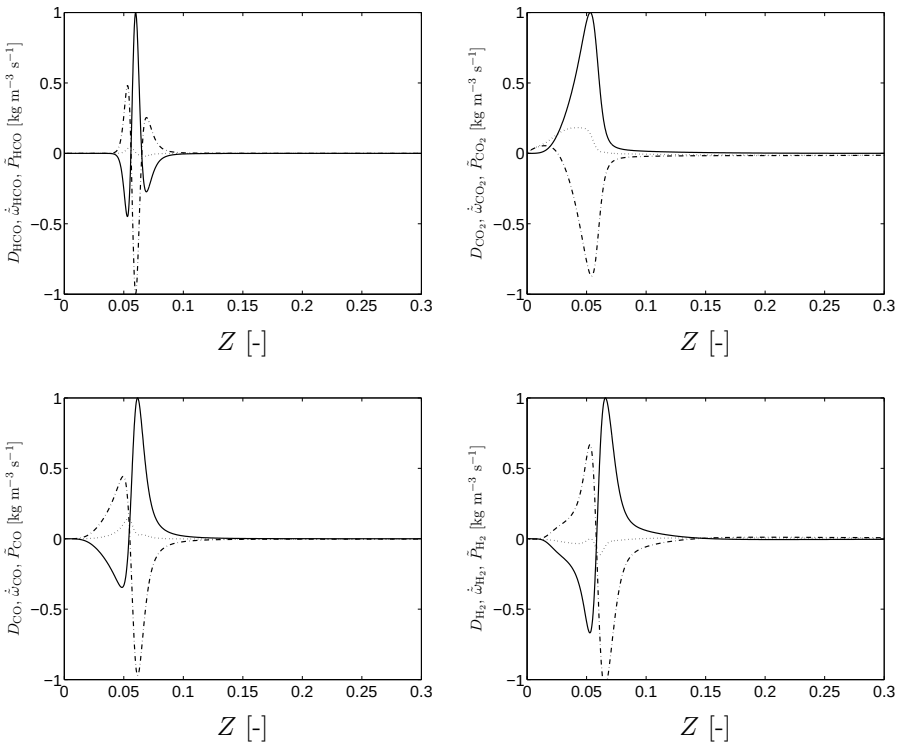

Fig. B.10: Source term, diffusion term and preferential diffusion term for HCO (tl), CO_2 (tr), CO (bl) and H_2 (br) as a function of the mixture fraction Z in a non-premixed counterflow flame with $Le_i = const$ and $a = 100\ s^{-1}$. All terms are scaled with $\dot{\omega}_{i,max}$. Solid: scaled chemical source term; dash-dotted: diffusion term; dotted: preferential diffusion term.

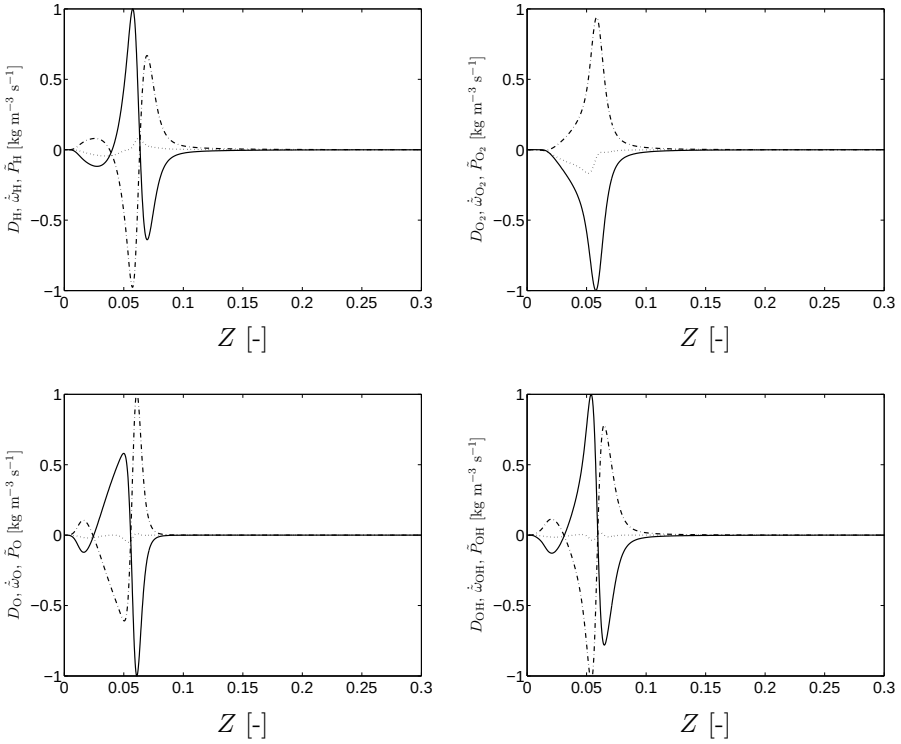

Fig. B.11: Source term, diffusion term and preferential diffusion term for H (tl), O_2 (tr), O (bl) and OH (br) as a function of the mixture fraction Z in a non-premixed counterflow flame with $Le_i = const$ and $a = 100\ s^{-1}$. All terms are scaled with $\dot{\omega}_{i,max}$. Solid: scaled chemical source term; dash-dotted: diffusion term; dotted: preferential diffusion term.

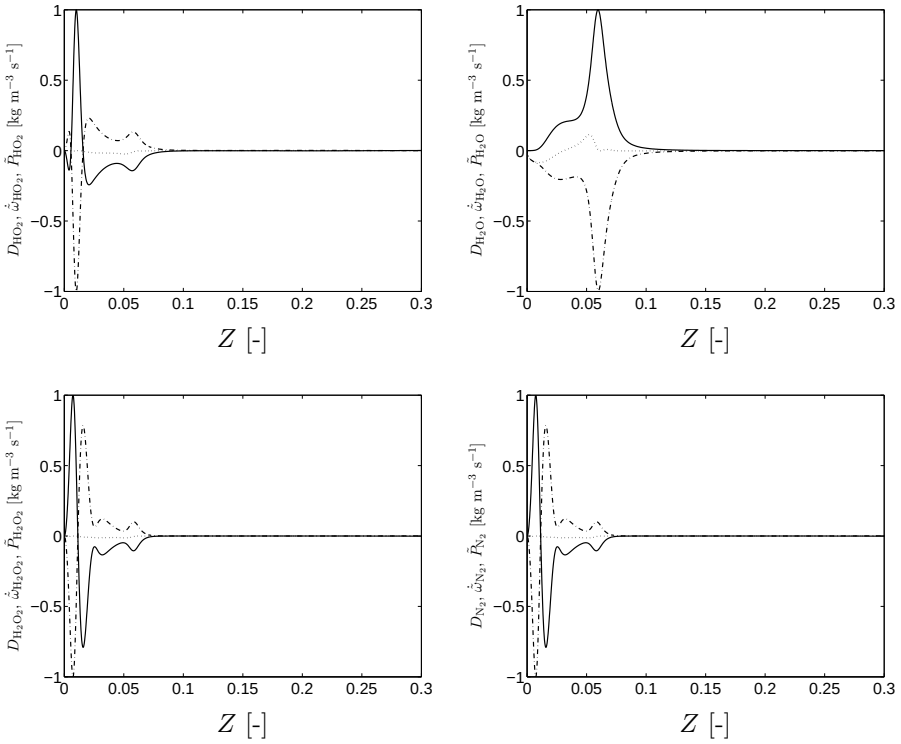

Fig. B.12: Source term, diffusion term and preferential diffusion term for HO_2 (tl), H_2O (tr), H_2O_2 (bl) and N_2 (br) as a function of the mixture fraction Z in a non-premixed counterflow flame with $Le_i = const$ and $a = 100\ s^{-1}$. All terms are scaled with $\dot{\omega}_{i,max}$. Note that for N_2 the following equation was used: $\sum_{k \neq N_2}^{N_s} Y_k V_k = -Y_{N_2} V_{N_2}$. Solid: scaled chemical source term; dash-dotted: diffusion term; dotted: preferential diffusion term.

Appendix C

Ratios between various quantities for $Le_i = 1$ and $Le_i = const$

Applied strain	$\Delta_{max}Z$ / Z_{max}	x-position
$a = 100\ s^{-1}$	0.0251	0.1400
$a = 200\ s^{-1}$	0.0252	0.0980
$a = 300\ s^{-1}$	0.0248	0.0790
$a = 400\ s^{-1}$	0.0234	0.0670

Table C.1: The relative maximum difference between the mixture fraction profiles for $Le_i = 1$ and $Le_i = const$.

Applied strain	$\Delta_{max}T$ / T_{max}	Z value
$a = 100\ s^{-1}$	0.0699	0.0170
$a = 200\ s^{-1}$	0.0671	0.0200
$a = 300\ s^{-1}$	0.0682	0.0150
$a = 400\ s^{-1}$	0.0636	0.0140

Table C.2: The relative maximum difference between the temperature profiles for $Le_i = 1$ and $Le_i = const$.

Applied strain	$\Delta_{max}\chi$ / χ_{max}	Z value
$a = 100\ s^{-1}$	0.2276	0.5000
$a = 200\ s^{-1}$	0.2278	0.5000
$a = 300\ s^{-1}$	0.2289	0.5000
$a = 400\ s^{-1}$	0.2318	0.5000

Table C.3: The relative maximum difference between the scalar dissipation profiles for $Le_i = 1$ and $Le_i = const$.

* Here, the reference state is the $Le_i = 1$ case.

Appendix D

Element mass fractions and enthalpy

D.1 $Le_i = 1$

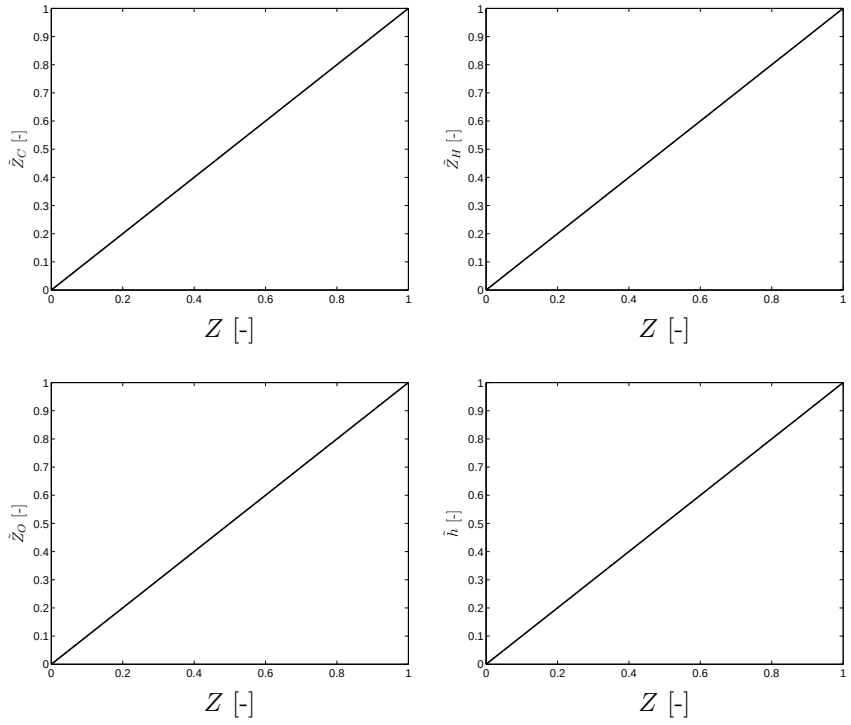

Fig. D.1: Element mass fractions and enthalpy for $Le_i = 1$. Shown here are carbon (tl), hydrogen (tr), oxygen (bl), which are scaled according to (3.48) and the enthalpy (br), scaled according to (3.47). The dotted line represents the case that the element mass fractions and the enthalpy are linearly dependent on the mixture fraction.

D.2 $Le_i = 1.1$

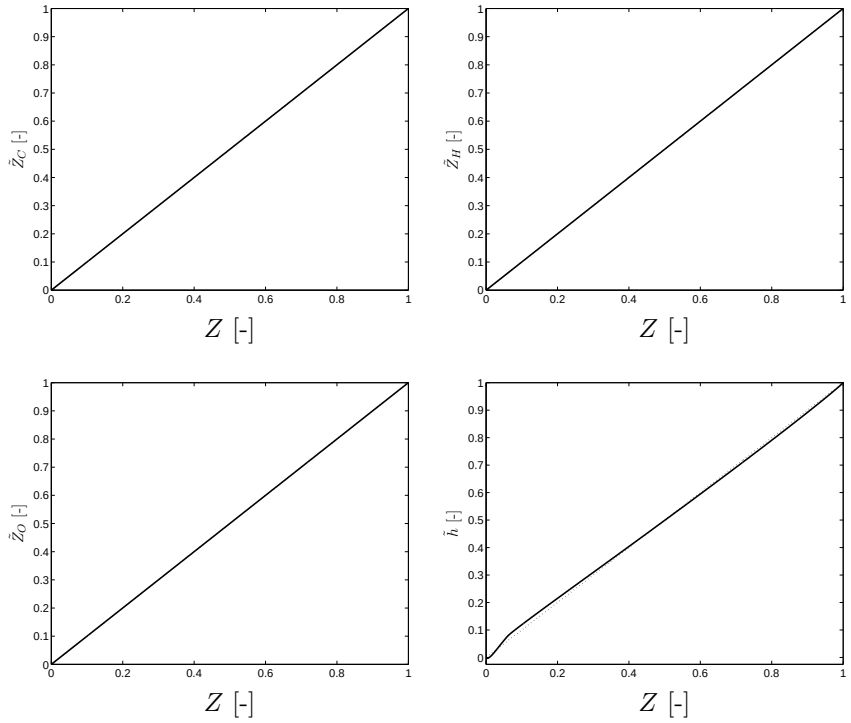

Fig. D.2: Element mass fractions and enthalpy for $Le_i = 1.1$. Shown here are carbon (tl), hydrogen (tr), oxygen (bl), which are scaled according to (3.48) and the enthalpy (br), scaled according to (3.47). The dotted line represents the case that the element mass fractions and the enthalpy are linearly dependent on the mixture fraction.

D.3 $Le_i = const$

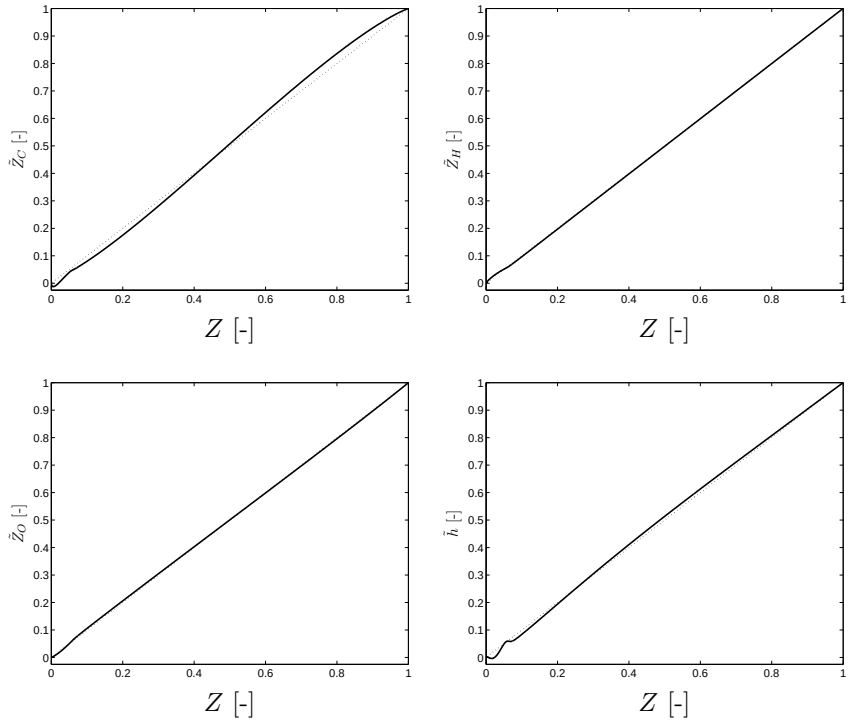

Fig. D.3: Element mass fractions and enthalpy for $Le_i = const$. Shown here are carbon (tl), hydrogen (tr), oxygen (bl), which are scaled according to (3.48) and the enthalpy (br), scaled according to (3.47). The dotted line represents the case that the element mass fractions and the enthalpy are linearly dependent on the mixture fraction.

Appendix E

Ratio between $P_{\perp}^{i}$ and $\dot{\omega}_{i,max}$

Species	$P_{\perp}^{i}/\dot{\omega}_{i,max}$	**Species**	$P_{\perp}^{i}/\dot{\omega}_{i,max}$
CH_4	0.0508	H	0.0800
CH_3	0.0520	O_2	0.0001
CH_3O	0.0946	O	0.0113
CH_2O	0.0547	OH	0.0177
HCO	0.0449	HO_2	0.0002
CO_2	0.1825	H_2O	0.1141
CO	0.1422	H_2O_2	0.0001
H_2	0.0061	N_2	N.A.*

Species	$P_{\perp}^{i}/\dot{\omega}_{i,max}$	**Species**	$P_{\perp}^{i}/\dot{\omega}_{i,max}$
CH_4	0.0797	H	0.0744
CH_3	0.0849	O_2	0.0019
CH_3O	0.2002	O	0.0006
CH_2O	0.0887	OH	0.0033
HCO	0.0551	HO_2	0.0013
CO_2	0.2146	H_2O	0.0766
CO	0.1367	H_2O_2	0.0011
H_2	0.0097	N_2	N.A.*

Table E.1: Ratio of the preferential diffusion term and the chemical source term of each species for a strain rate of $a = 100\ s^{-1}$ (l) and $a = 400\ s^{-1}$ (r).

* Because nitrogen is in abundance, N_2 was not considered.

Appendix F

Ratio between between 2 models for χ and χ computed with CHEM1D

Applied strain	$\Delta\chi_{max}$ / χ_{m1}	$\Delta\chi$ / χ_{m2}
$a = 100\ s^{-1}$	0.083763	0.157567
$a = 200\ s^{-1}$	0.080739	0.155588
$a = 300\ s^{-1}$	0.078856	0.154051
$a = 400\ s^{-1}$	0.077568	0.152512

Table F.1: The relative maximum difference between the 2 models the for the scalar dissipation rate, χ_{m1} and χ_{m2}, and the scalar dissipation rate computed with CHEM1D for $Le_i = 1$.

Applied strain	$\Delta\chi_{max}$ / χ_{m1}	$\Delta\chi$ / χ_{m2}
$a = 100\ s^{-1}$	0.074339	0.153934
$a = 200\ s^{-1}$	0.073816	0.151866
$a = 300\ s^{-1}$	0.072095	0.150141
$a = 400\ s^{-1}$	0.070869	0.148776

Table F.2: The relative maximum difference between the 2 models the for the scalar dissipation rate, χ_{m1} and χ_{m2}, and the scalar dissipation rate computed with CHEM1D for $Le_i = 1.1$.

Applied strain	$\Delta\chi_{max}$ / χ_{m1}	$\Delta\chi$ / χ_{m2}
$a = 100\ s^{-1}$	0.156102	0.038920
$a = 200\ s^{-1}$	0.170330	0.071991
$a = 300\ s^{-1}$	0.180136	0.074510
$a = 400\ s^{-1}$	0.184809	0.076265

Table F.3: The relative maximum difference between the 2 models the for the scalar dissipation rate, χ_{m1} and χ_{m2}, and the scalar dissipation rate computed with CHEM1D for $Le_i = const$ (r).

List of Figures

Bibliography

[1] World Energy Assessment, *Energy and the challenge of sustainability*, United Nations Development Programme, New York.

[2] R.W. Bilger, *The structure of turbulent non-premixed flames*, Proc. Combust. Inst. **22** (1988), 475–488.

[3] H Bongers, *personal communication*.

[4] H. Bongers, J. A. van Oijen, and L.P.H. de Goey, *Intrinsic low-dimensional manifold method extended with diffusion*, Proc. Combust. Inst. **29** (2002).

[5] CHEM1D, *a package for the simulation of one-dimensional flames*, Eindhoven University of Technology, 2002, http://www.combustion.tue.nl.

[6] L. P. H. de Goey and J. H. M. ten Thije Boonkkamp, *A flamelet description of premixed laminar flames and the relation with flame stretch*, Combust. Flame **119** (1999), 253–271.

[7] A.L. de Lavoisier, *Réflexions sur le phlogistique*, Mémoires de l'Académie des sciences, année 1783, 505-538, 1783.

[8] L.P.H. de Goey, *personal communication*.

[9] G.R.A. Groot, *Modelling of propagating spherical and cylindrical premixed flames*, Ph.D. thesis, Eindhoven University of Technology, http://www.combustion.tue.nl, 2004.

[10] R.J. Kee and J.A. Miller, *A structured approach to the computational modeling of chemical kinetics and molecular transport in flowing systems*, Springer Series in Chemical Physics **47** (1986), 196.

[11] Pijush K. Kundu, *Fluid mechanics*, Academic Press, Inc., 1990.

[12] U. Maas and S. B. Pope, *Symplifying chemical kinetics: Intrinsic low-dimensional manifolds in composition space*, Combust. Flame **88** (1992), 239–264.

[13] A. Majda and K.G. Lamb, *Simplified equations for low mach number combustion with strong heat release*, The IMA Volumes in Mathematics and its Applications **35** (1991), 167–211.

[14] N. Peters, *Laminar diffusion flamelet models in non-premixed turbulent combustion*, Prog. Energy Combust. Sci. **10** (1984), 319–339.

[15] N. Peters, *Reducing mechanisms*, Lecture Notes in Physics (M.D. Smooke, ed.), vol. 384, Springer-Verlag, Berlin, 1991, pp. 48–85.

[16] N. Peters, *Turbulent combustion*, Cambridge University Press, 2000.

[17] N. Peters and H. Pitsch, *A consistent flamelet formulation for non-premixed combustion considering differential diffusion effects*, Combust. Flame. **114** (1998), 26–40.

[18] M. D. Smooke and V. Giovangigli, *Formulation of the premixed and nonpremixed test problems*, Reduced kinetic mechanisms for asymptotic approximations for methane-air flames (M.D. Smooke, ed.), Lecture Notes in Physics 384, Springer-Verlag, Berlin, 1991, pp. 1–28.

[19] J. A. van Oijen and L. P. H. de Goey, *Modelling of premixed laminar flames using flamelet-generated manifolds*, Combust. Sci. and Techn. **161** (2001), 113–137.

[20] J. A. van Oijen and L. P. H. de Goey, *Modeling of premixed counterflow flames using the flamelet-generated manifold method*, Combust. Theory and Modelling. **6** (2002), 463–478.

[21] J. A. van Oijen, F. A. Lammers, and L. P. H. de Goey, *Modeling of complex premixed burner systems using flamelet-generated manifolds*, Combust. Flame **127** (2001), 2124–34.

[22] J.A. van Oijen, *Flamelet-generated manifolds: Development and application to premixed laminar flames*, Ph.D. thesis, Eindhoven University of Technology, http://www.combustion.tue.nl, 2002.

[23] F. A. Williams, *Turbulent combustion*, The Mathematics of Combustion (1985), 97–131.